

Ultra-cold atoms as quantum simulators for relativistic phenomena

Ralf Schützhold^{a,b,*}

^a*Helmholtz-Zentrum Dresden-Rossendorf, Bautzner Landstraße 400, 01328 Dresden, Germany*

^b*Institut für Theoretische Physik, Technische Universität Dresden, 01062 Dresden, Germany*

Abstract

The goal of this article is to review developments regarding the use of ultra-cold atoms as quantum simulators. Special emphasis is placed on relativistic quantum phenomena, which are presumably most interesting for the audience of this journal. After a brief introduction into the main idea of quantum simulators and the basic physics of ultra-cold atoms, relativistic quantum phenomena of linear fields are discussed, including Hawking radiation, the Unruh effect, cosmological particle creation, the Gibbons-Hawking and Ginzburg effects, super-radiance, Sauter-Schwinger and Breit-Wheeler pair creation, as well as the dynamical Casimir effect. After that, the focus is shifted to phenomena of non-linear fields, such as the sine-Gordon model, the Kibble-Zurek mechanism, false-vacuum decay, and quantum back-reaction. In order to place everything into proper context, the basic underlying mechanisms of these phenomena are briefly recapitulated before their simulators are discussed. Even though effort is made to provide a review as fair as possible, there can be no claim of completeness and the selection as well as the relative weights of the topics may well reflect some personal bias.

Keywords: quantum analogues, quantum simulations, Bose-Einstein condensates, optical lattices, particle creation

*Corresponding author

Email address: r.schuetzhold@hzdr.de (Ralf Schützhold)

Contents

1	Introduction	4
1.1	Quantum simulators	4
1.1.1	Sequential quantum algorithms	4
1.1.2	Quantum ground-state algorithms	5
1.1.3	Quantum simulators for physical systems	7
1.2	Ultra-cold atoms	9
1.2.1	Many-body Hamiltonian	9
1.2.2	Measurement schemes	10
1.2.3	Hubbard Hamiltonians	11
1.2.4	Dirac Hamiltonian	12
1.2.5	Scalar field	14
1.2.6	Gauge fields	15
2	Linear fields	18
2.1	Curved space-time analogues (a.k.a. analogue gravity)	18
2.2	Hawking radiation	20
2.2.1	Black hole analogues	23
2.2.2	Hawking radiation as tunneling?	25
2.3	Unruh effect	26
2.3.1	Analogue of Unruh effect	27
2.4	Cosmological particle creation	29
2.4.1	Analogue Universe in condensate at rest	30
2.4.2	Expanding condensates	32
2.5	Gibbons-Hawking effect	33
2.5.1	Analogue of Gibbons-Hawking effect in expanding condensate	34
2.6	Ginzburg effect	34
2.7	Super-radiance and Penrose process	35
2.7.1	Quantum vortices in Bose-Einstein condensates	36
2.7.2	Quasi-normal modes	37
2.8	Electromagnetic fields: Sauter-Schwinger and Breit-Wheeler effect	38
2.8.1	Sauter-Schwinger effect	38
2.8.2	Breit-Wheeler effect	41
2.8.3	Quantum simulator for Sauter-Schwinger and Breit-Wheeler effect	42
2.9	Dynamical Casimir effect	43
3	Non-linear fields	45
3.1	Sine-Gordon model	45
3.1.1	Analogues for the sine-Gordon model	46
3.2	Kibble-Zurek mechanism	47

3.3	False-vacuum decay	50
3.4	Back-reaction and cosmological constant	53
3.4.1	Cosmological constant problem	53
3.4.2	Back-reaction in fluids and Bose-Einstein condensates	54
3.4.3	Quantum fluid dynamics	56
4	Summary and outlook	58
4.1	Lessons (to be) learned	58
4.2	Outlook	60

1. Introduction

Let us start by setting the stage. Unless explicitly noted for illustrative purposes, natural units with

$$\hbar = c = \varepsilon_0 = \mu_0 = 1 \quad (1.1)$$

will be used throughout. Note that the elementary charge q could then be expressed in terms of a dimensionless number via the QED fine structure constant $\alpha_{\text{QED}} = q^2/(4\pi\varepsilon_0\hbar c) \approx 1/137$ but we shall not do this here and keep the charge q explicitly. Furthermore, since we are dealing with ultra-cold atoms instead of ions¹, for example, the real charge q will typically be replaced by an effective charge q_{eff} for the quantum simulators. Similarly, the real speed of light c will also be replaced by an effective speed of light c_{eff} , typically the propagation velocity of the relevant quasi-particles, in most of the quantum simulators. The fact that this effective speed of light c_{eff} is often much smaller than c renders the experimental realization of the quantum phenomena under consideration typically far easier.

As another interesting option, one could consider replacing the Planck constant \hbar by an effective value \hbar_{eff} . This could correspond to modeling the quantum fluctuations (governed by \hbar) by classical fluctuations, for example, such that \hbar_{eff} is bigger than \hbar . However, such a replacement would probably be no longer considered a quantum simulator and thus we do not discuss this option here.

Four vectors such as k_μ are defined with respect to the Minkowski metric $g_{\mu\nu}^{\text{Min}}$ in flat space-time (or a general metric $g_{\mu\nu}$ in curved space-time) for which we use the signature in the “particle-physics convention” $(+1, -1, -1, -1)$. The cases where we go to Euclidean space will be mentioned explicitly.

1.1. Quantum simulators

Before turning to ultra-cold atoms, it is probably helpful to specify the term “quantum simulators” and the main ideas behind it, see, e.g., [10, 11, 12, 13]. To this end, let us take a small detour into the field of quantum computation, see, e.g., [14], where we start with the standard scenario of a sequential quantum algorithm, see also Fig. 1.1.

1.1.1. Sequential quantum algorithms

Without loss of generality, we may assume that the initial state $|\psi_{\text{in}}\rangle$ is one of the computational basis states, say $|\psi_{\text{in}}\rangle = |00\dots00\rangle$. Then, in order to execute the quantum algorithm, we apply a series of gate operations to the state, where the first gate could be a Hadamard gate \mathfrak{H}_1 acting on the first qubit

$$|\psi_{\text{in}}\rangle = |00\dots00\rangle \rightarrow \mathfrak{H}_1 |00\dots00\rangle = \frac{|00\dots00\rangle + |10\dots00\rangle}{\sqrt{2}}. \quad (1.2)$$

Then we apply the second gate (for example, a Hadamard gate \mathfrak{H}_2 acting on the second qubit) and so on, see Fig. 1.1. After applying a number of gates comparable to the number n of qubits, the quantum state is turned into a superposition of a huge number (possibly even all $N = 2^n$) of computational basis states (“quantum parallelism”). If the quantum state would only contain a small number of computational basis states, one could simulate the quantum algorithm efficiently on a classical computer, i.e., there would be no real quantum advantage.

Towards the end of the quantum algorithm, however, this superposition of a huge number of computational basis states should be focused into a smaller set of possible solutions states. For example, in the case of the Grover search

¹This would open up a completely new field [1], see, e.g., [2, 3, 4, 5, 6, 7, 8, 9] for a few examples out of many more.

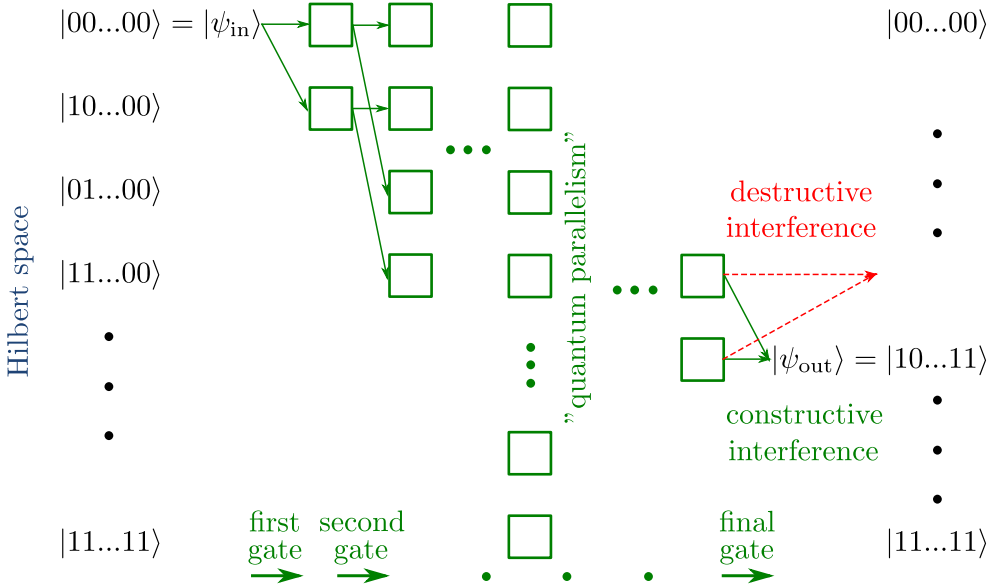


Figure 1.1: Sketch of a sequential quantum algorithm.

algorithm [15] with only one possible solution, the final state $|\psi_{\text{out}}\rangle$ would be (to a very good approximation) one of the computational basis states, such as $|\psi_{\text{out}}\rangle = |10\dots11\rangle$. The way this works is that we have constructive interference for the paths leading to this desired final state $|\psi_{\text{out}}\rangle$ whereas the paths leading to all other (unwanted) output states interfere destructively and thus their amplitudes are suppressed, as indicated in Fig. 1.1.

Obviously, the interference necessary for such a quantum algorithm to work is prone to decoherence and other imperfections. Especially the relative phase between contributions from computational basis states which differ in many qubits is quite vulnerable since the environment could induce a small phase shift (or other error) at each qubit. Furthermore, the quantum algorithm contains a significant number of quantum gates (typically scaling polynomially with the number n of qubits) such that the errors can accumulate. Thus, making such a quantum algorithm work for a significant number of qubits (such that it can solve problems which are intractable on a classical computer) would require significant error correction – which in turn, necessitates very low decoherence rates for the gates and qubits. This is probably the main obstacle for actually realizing such quantum computers.

1.1.2. Quantum ground-state algorithms

One idea to avoid or at least reduce the problem of decoherence mentioned above could be to replace the scheme of sequential quantum algorithms by another approach where one constructs a Hamiltonian \hat{H}_{problem} such that the ground state of this Hamiltonian \hat{H}_{problem} encodes the solution to the problem one is interested in. This ground state should then be quite robust to decoherence – especially if there is a sizable gap to the excited state(s). Actually, constructing such a Hamiltonian \hat{H}_{problem} is possible for the problems (e.g., factoring large numbers [16]) usually discussed in connection with quantum computing – and even for some more problems (e.g., the traveling salesman problem) for which no sequential quantum algorithm offering a strong speed-up is known.

However, even after constructing such a Hamiltonian \hat{H}_{problem} , there is still the task of actually finding the ground state. For problem Hamiltonians \hat{H}_{problem} which are supposed to answer interesting questions, the potential landscape typically contains many local minima (like a glassy system) and thus going to the global minimum is difficult since the system is likely to get stuck in one of the local minima. Thus, just starting in some initial state $|\psi_{\text{in}}\rangle$ and cooling the

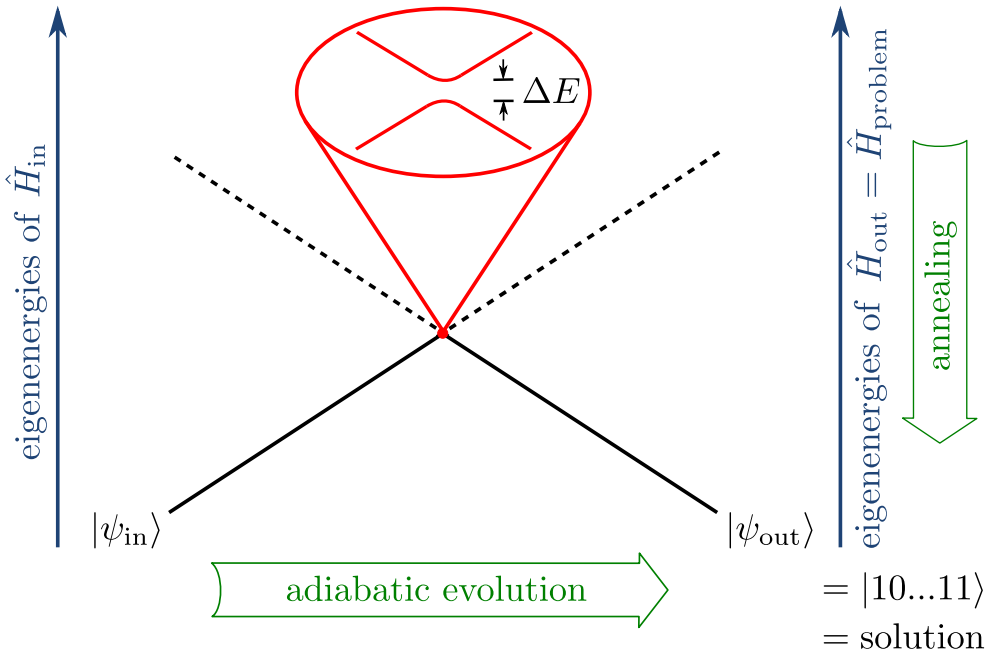


Figure 1.2: Sketch of a quantum ground-state (e.g., adiabatic) algorithm.

system does probably not work within a reasonable time. One idea to go down in energy is to use annealing techniques where thermal or quantum fluctuations are used to overcome the potential barriers and thus to “rescue” the system from a local minimum, see, e.g., [17].

As another idea, one could start with an initial Hamiltonian \hat{H}_{in} which can easily be realized experimentally and whose ground state $|\psi_{in}\rangle$ is known, has a sufficiently large energy gap to the excited states, and can be prepared experimentally. Then the initial Hamiltonian \hat{H}_{in} is slowly deformed into the final problem Hamiltonian \hat{H}_{problem} , see, e.g., [18, 19]. The most simple way would be a linear interpolation scheme with a run-time T

$$\hat{H}(t) = \frac{T-t}{T} \hat{H}_{in} + \frac{t}{T} \hat{H}_{\text{problem}}, \quad (1.3)$$

but more involved schemes are conceivable as well, see, e.g., [20]. If this deformation is performed slowly enough (i.e., T is large enough), the adiabatic theorem demands that we indeed end up in the desired ground state of \hat{H}_{problem} . Thus, this scheme is referred to as adiabatic quantum computing. How slow is slow enough is then mainly determined by the energy gap $\Delta E(t)$ as each instant of time t between the instantaneous ground state of $\hat{H}(t)$ and the first excited state(s), see, e.g., [21].

Unfortunately, the “law of the conservation of difficulty” strikes here again, since this energy gap $\Delta E(t)$ typically becomes extremely small at some time t (or even at multiple times), see Fig. 1.2. As an intuitive picture, one can use the analogy to a Landau-Zener transition where the system has to tunnel from the initial minimum of the potential landscape to the final minimum (quite analogous to false vacuum decay discussed in Sec. 3.3 below) which takes some time and the small tunneling rate is related to the energy gap ΔE , see Fig. 1.3. This point where the energy gap ΔE becomes very small corresponds to the analogue of a first-order phase transition (for a large but finite system). Carrying this analogy a bit further, one could expect that a second-order phase transition (where the system does not have to tunnel from one minimum to another) might actually be advantageous, see also [22, 23] and Fig. 1.3.

Apart from the long run-time T required by the adiabatic theorem, such an avoided level crossing with a small energy gap ΔE may also be especially prone to decoherence, see, e.g., [24, 25, 26]. In summary, although adiabatic quantum

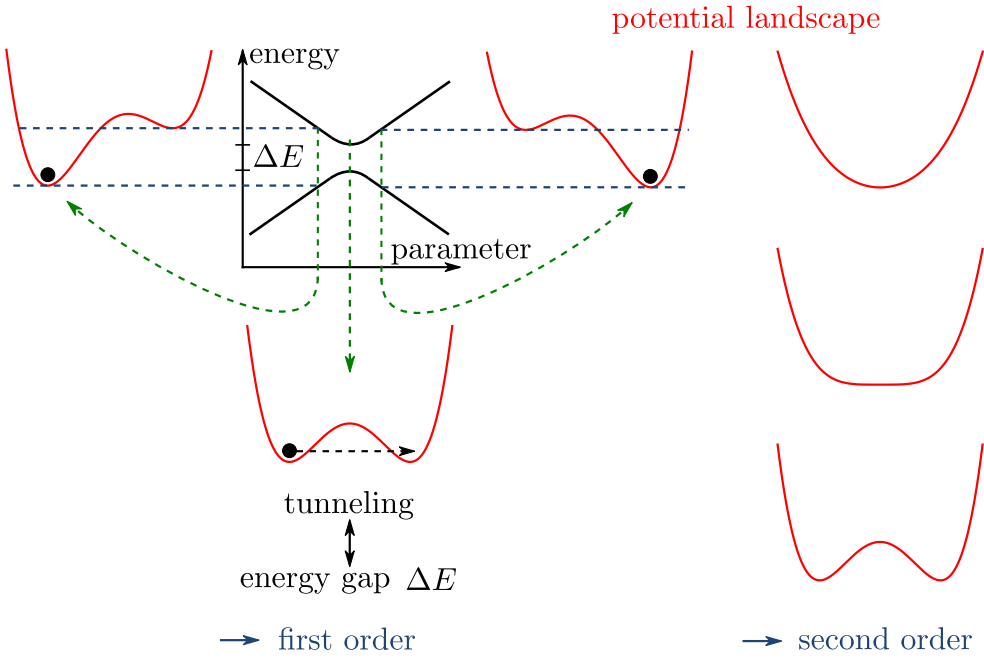


Figure 1.3: Left: Landau-Zener transition and associated effective potential landscape, which corresponds to a first-order phase transition. Right: effective potential landscape for a symmetry-breaking (top to bottom) or symmetry-restoring (bottom to top) second-order phase transition. Such a symmetry-breaking phase transition will be relevant for the Kibble-Zurek mechanism discussed in Sec. 3.2. The potential landscape on the right-hand side, on the other hand, is analogous to the false-vacuum decay discussed in Sec. 3.3.

algorithms or, more generally, quantum ground-state algorithms might offer some advantages in comparison to sequential quantum algorithms, their potential for solving real computational problems is still an open question. However, as it became evident above, we see more and more analogies to physical systems, such as glassy behaviour and many local minima in the potential landscape, first-order and second-order phase transitions, and Landau-Zener tunneling etc.

1.1.3. Quantum simulators for physical systems

Apart from solving classical problems such as factoring large numbers, quantum computers should also be able to simulate quantum systems much better than classical computers. Actually, this was one of the main motivations for Feynman [27, 28] who referred to quantum computers as “universal quantum simulators.” A typical question here is the following: given an initial state $|\psi_{\text{in}}\rangle$ and a possibly time-dependent physical Hamiltonian $\hat{H}_{\text{phys}}(t)$, what is the resulting final state $|\psi_{\text{out}}\rangle = \hat{U}(T)|\psi_{\text{in}}\rangle$ after a period of time T . More precisely, quantum computers do not provide the full information about this quantum state $|\psi_{\text{out}}\rangle$ (such as all the amplitudes in front of the basis states) but properties of this state, i.e., observables. This is related to the problem of how to measure relevant observables in such a quantum simulator – which will be discussed below in Sec. 1.2.2.

Provided that this Hamiltonian $\hat{H}_{\text{phys}}(t)$ has reasonable properties (see, e.g., [14]), the above problem can be mapped to a sequential quantum algorithm as described above, e.g., by discretizing the time t and approximating the small time steps of the quantum evolution $\hat{U}(t)$ by the Trotter formula. Depending on the structure of $\hat{H}_{\text{phys}}(t)$, there are quite efficient schemes for doing that. However, since the problem of decoherence described above prevented us from constructing such universal quantum computers (which allow the implementation of arbitrary sequential quantum algorithms) with many qubits, the direct application of this scheme is not possible with present technology – at least for large numbers of qubits, see also [29].

As a way out, one could instead construct a specific quantum system (i.e., a quantum simulator) such that its Hamiltonian $\hat{H}_{\text{sim}}(t)$ can be mapped to the physical Hamiltonian $\hat{H}_{\text{phys}}(t)$ to be simulated, in the sense that it reproduces its essential features. Examples of this idea will be discussed below – basically, in the whole rest of this review.

Now, one could object that the problem of decoherence (which was a huge problem for the ideas above) would also spoil this approach. One of the main points is that this objection is not necessarily correct: Provided that the similarity between $\hat{H}_{\text{sim}}(t)$ and $\hat{H}_{\text{phys}}(t)$ is close enough, one would expect that all decoherence channels and small imperfections which could apply to the quantum simulator $\hat{H}_{\text{sim}}(t)$ should also be possible for the real physical system $\hat{H}_{\text{phys}}(t)$. Thus, one would expect that these decoherence channels do not pose a very serious problem – or, if they do, one would also like to know about it. For example, if the real physical system $\hat{H}_{\text{phys}}(t)$ displays some properties such as Hawking radiation (see Sec. 2.2) or high-temperature superconductivity (see Sec. 1.2.3), but small imperfections or perturbations in $\hat{H}_{\text{sim}}(t)$ destroy these features, then one would expect that analogous imperfections or perturbations in the real physical system $\hat{H}_{\text{phys}}(t)$ would have a similar effect. Turning this argument around, the robustness of the phenomena under consideration (e.g., Hawking radiation or high-temperature superconductivity) is one of the important points one can study using these quantum simulators (see also Sec. 4). Quite generally, one would expect that physical phenomena which we can observe should be robust against small enough imperfections or perturbations because all Hamiltonians $\hat{H}_{\text{phys}}(t)$ we do calculations with are approximations. Thus, such physical phenomena which are robust should also be observable in a suitable quantum simulator.

So far, we have mainly discussed quantum simulators in analogy to sequential quantum algorithms in Sec. 1.1.1, but very similar arguments apply to the ground-state case discussed in Sec. 1.1.2. If the Hamiltonian \hat{H}_{phys} (or, equivalently, \hat{H}_{sim} provided that they are similar enough) has many local minima in its potential landscape where the system is likely to get stuck then it would be important to know this. Moreover, in such a case the precise structure of the true ground state may not be so important for our physical understanding (since it is never reached anyway), instead the typical structure of the low-lying local minima would determine the characteristic (e.g., glassy) behaviour of this system. Similar arguments apply to cases where the ground state is very vulnerable to small imperfections or perturbations.

For the transition scenario as in Eq. (1.3) between two physically relevant Hamiltonians, it would also be interesting to know whether there is a point where the energy gap becomes extremely small (i.e., the analogue of a phase transition) and where that critical point is. As explained above, traversing this point can easily result in non-adiabatic behaviour, which is basically the underlying mechanism for the Kibble-Zurek effect discussed in Sec. 3.2.

Here, we follow the route described above and consider quantum simulators for specific physical systems instead of universal quantum computers. More explicitly, the term “quantum simulators” is meant to refer to laboratory systems (in our case ultra-cold atoms) whose relevant degrees of freedom can be described by the Hamiltonian $\hat{H}_{\text{sim}}(t)$ which reproduces essential features of the Hamiltonian $\hat{H}_{\text{phys}}(t)$ of another physical quantum system we want to simulate. Clearly, this is most relevant for investigating (or reproducing) quantum effects – but in several cases it can also be interesting to study their classical analogues. It should be mentioned here that this notation is by no means unique. For example, sometimes also the terms “analogue quantum simulators” or “analogue quantum simulations” are used, where “analogue” could refer to an analogy or to the opposite of “digital” (i.e., based on bits or qubits, see, e.g., [29]) or both.

1.2. Ultra-cold atoms

Ultra-cold atoms are very promising candidates for quantum simulators since our experimental capabilities for manipulation, control and read out are very advanced, see, e.g., [30, 31, 32, 33, 34, 35, 36, 37, 38]. One can combine different species of atoms (e.g., bosonic and fermionic) with the desired properties or exploit their internal states. The associated energy scales are quite low and thus the resulting time scales are rather long (in the millisecond regime or even longer) such that it is easy to manipulate ultra-cold atoms fast enough to reach non-equilibrium conditions. Characteristic length scales in the micrometer regime and above are also much longer than those in other areas (such as solid state or particle physics) and thus can be resolved by optical means. It is possible to tune the strength and the geometry of the external potential felt by the atoms as well as their interaction among each other. Furthermore, these atoms can be well isolated from the environment and cooled down to extremely low temperatures below one nano-Kelvin, which is the lowest temperature reachable in the laboratory so far – allowing us to reach quantum degeneracy. Actually, in view of the temperature of the cosmic microwave background radiation of about 2.7 Kelvin², these systems have been called “the coldest systems in the Universe.” Note, however, that this low temperature is – strictly speaking – only an effective temperature since ultra-cold atomic vapor is a meta-stable state and not the true ground state. For typical examples such as Rubidium or Sodium atoms, the real ground state would be a metallic solid. Their vaporized state can live quite long if they are very dilute. In this case, almost all collisions are two-body collisions, where the atoms cannot “clump together” and form molecules due to energy-momentum conservation. Molecule formation is thus only possible in three-body collisions where the third atom carries away the excess energy. However, in dilute systems (possibly in combination with suitable potentials such as optical lattices) these three-body collisions are very rare events. Nevertheless, these three-body losses results in decoherence – even at arbitrary low temperatures and for nearly perfect isolation from any environment – which pose ultimate limits on the quantum properties of these simulators, see, e.g., [39, 40].

1.2.1. Many-body Hamiltonian

Neglecting these three-body losses, ultra-cold atoms can be described by the general Hamiltonian

$$\hat{H} = \int d^3r \left(\sum_a \frac{(\nabla \hat{\psi}_a^\dagger) \cdot (\nabla \hat{\psi}_a)}{2m_a} + \sum_{ab} V_{ab} \hat{\psi}_a^\dagger \hat{\psi}_b \right) + \int d^3r d^3r' \sum_{abcd} W_{abcd}(\mathbf{r}, \mathbf{r}') \hat{\psi}_a^\dagger(\mathbf{r}) \hat{\psi}_b^\dagger(\mathbf{r}') \hat{\psi}_c(\mathbf{r}') \hat{\psi}_d(\mathbf{r}). \quad (1.4)$$

Since the ultra-cold atoms are naturally quite slow, the non-relativistic description above is typically sufficient. The many-particle field operators $\hat{\psi}_a$ and $\hat{\psi}_a^\dagger$ annihilate or create atoms, which could be bosons or fermions or a mixture, where a labels the different atomic species (different atoms or isotopes, spin states or internal states etc.) which could also have different masses m_a .

The potential term $V_{ab} \hat{\psi}_a^\dagger \hat{\psi}_b$ is typically generated by external electromagnetic fields. For example, off-resonant optical laser fields, blue or red detuned, may generate diagonal terms $V_{aa} \hat{\psi}_a^\dagger \hat{\psi}_a$ corresponding to repulsive or attractive potentials for the atoms, respectively. Resonant or near-resonant optical laser fields could induce transitions corresponding to off-diagonal terms $V_{ab} \hat{\psi}_a^\dagger \hat{\psi}_b$ with $a \neq b$ if the labels a and b distinguish the internal atomic states. As another possibility, a static magnetic field B in x -direction can induce such an off-diagonal term $\hat{\psi}_\uparrow^\dagger \hat{\psi}_\downarrow$ if the labels a and b correspond to the spin of the fermionic atoms (with $s = 1/2$) in z -direction. These potentials can be used to confine the atomic cloud or to

²Even lower temperatures of approximately one Kelvin might exist in the Boomerang Nebula, which indicates that this system has not equilibrated with its surroundings yet. However, this is still far above the temperature of the ultra-cold atoms.

form an optical lattice (or a combination of both).

As another interesting possibility, one could depart from the treatment of the photon field as an external field and take the photonic degrees of freedom as dynamical variables into account – for example, after enhancing the coupling to certain photon modes via enclosing the ultra-cold atoms by a cavity, see, e.g., [41].

Finally, $W_{abcd}(\mathbf{r}, \mathbf{r}')$ describes the interactions between the atoms. As explained above, we neglect processes involving three or more atoms which would correspond to the product of six or more many-particle field operators $\hat{\psi}_a$ and $\hat{\psi}_a^\dagger$. For ultra-cold atoms, mainly three interaction types are relevant. Interactions or collisions with ranges much shorter than all other relevant length scales can be approximated by contact interactions $W_{abcd}(\mathbf{r}, \mathbf{r}') \approx g_{abcd} \delta^3(\mathbf{r} - \mathbf{r}')$ with the coupling constants or scattering cross sections being encoded in g_{abcd} . In most cases, they will be the same for all atomic species $g_{abcd} = g \delta_{ad} \delta_{bc}$ but one can obtain additional interesting effects if the inter-species and the intra-species coupling differ, see also Sec. 2.4. As a further step, one could also imagine interaction-induced transitions which would correspond to off-diagonal elements, but we shall not consider them here. Other important examples are the (magnetic) dipole-dipole interaction which is of finite range and behaves as $W_{abcd}(\mathbf{r}, \mathbf{r}') \sim 1/|\mathbf{r} - \mathbf{r}'|^3$ for fixed dipole moments, see, e.g., [42, 43]. If the dipole moments are not fixed but fluctuating, one can still obtain an interaction of the van-der-Waals type, which behaves as $1/|\mathbf{r} - \mathbf{r}'|^6$. These interactions can be amplified strongly using Rydberg atoms, i.e., atoms in high-lying excited states, see, e.g., [44, 45, 46, 47, 48, 49, 50, 51, 52, 53]. This option does also offer more knobs for manipulation and control because the interaction properties of those Rydberg atoms strongly depend on their quantum numbers.

1.2.2. Measurement schemes

Of course, realizing the Hamiltonian which allows us to simulate the phenomenon under consideration is not the end of the story, we also need a read-out scheme in order to measure the observables we are interested in. For ultra-cold atoms, the majority of the schemes relies on measuring the positions of the atoms³ or the position-dependent number or density of atoms in some way, e.g., by taking pictures or by sending the atoms into an atom detector, see, e.g., [56]. Obviously, the former method can be less destructive than the latter and thus could be repeated several times during the course of evolution. However, one should keep in mind that such a non-destructive measurement is never “interaction-free”. According to the laws of quantum theory, such a measurement changes the quantum state of the system (unless it happens to be in an atom number eigen-state) and thus perturbs it. This perturbation can be small (e.g., in the case of weak measurements) but it cannot be avoided completely.

In some cases, the observables under consideration are directly related to the number of atoms depending on their position, such as the various lattice sites (see, e.g., [57]), or the density profile of the atoms or their density-density correlations (see, e.g., [58, 59, 60, 61, 62]) which can be extracted by repeating the experiments many times. In these cases, the detection scheme is usually referred to as *in situ* and can be non-destructive (as discussed above). In other cases, the trick is to translate the observables of interest to the number or density of atoms. As one example, if we consider different atomic species (e.g., hyperfine states) and start with atoms of one species only, suitable light-induced resonant transitions could be used to translate the number of phonons (i.e., excitation quanta) to the number of atoms in a different species. Then, with resonant light which strongly couples to the latter species but basically not to the former, one can measure the number of atoms in that species and thereby infer the original number of phonons [63].

³However, alternative ideas are conceivable as well, see, e.g., [54, 55].

For measuring observables which are canonically conjugate to the atom numbers or densities, one can apply methods and ideas from quantum state tomography: After the actual quantum simulation itself, one could add periods of suitable unitary evolutions of varying delay times which rotate the canonically conjugate variables into each other. By measuring the atom numbers or densities after varying time delays, one can also infer their canonically conjugate variables (i.e., phases), see, e.g., [64]. A related concept is the *time-of-flight* technique, where the trap confining the atoms is switched off after the quantum simulation. If the interactions between the atoms are sufficiently weak (dilute-gas limit) and the (initial) confining potential is sufficiently strong, the atoms basically start to move according to their momenta at the switch-off time. Then, letting the atomic cloud expand until it is much larger than its initial size, a snap-shot of the atomic cloud allows us to infer the momentum distribution at the switch-off time – in contrast to an *in situ* measurement of the position distribution. As another difference, such a *time-of-flight* measurement is obviously destructive while an *in situ* measurement can be non-destructive.

1.2.3. Hubbard Hamiltonians

Even though Hubbard Hamiltonians belong more to condensed-matter or solid-state physics than to relativistic particle physics, let us briefly discuss them – possible relations will hopefully become more evident below. Focusing on bosons for a moment, we may expand the field operators $\hat{\psi}_a(\mathbf{r})$ into a complete set of orthonormal basis functions $f_a^I(\mathbf{r})$ via

$$\hat{\psi}_a(\mathbf{r}) = \sum_I \hat{b}_I f_a^I(\mathbf{r}). \quad (1.5)$$

Insertion of this expansion into the general form (1.4) yields

$$\hat{H} = - \sum_{IJ} T_{IJ} \hat{b}_I^\dagger \hat{b}_J + \sum_{IJKL} U_{IJKL} \hat{b}_I^\dagger \hat{b}_J^\dagger \hat{b}_K \hat{b}_L, \quad (1.6)$$

where the T_{IJ} are determined by the matrix elements of the differential operator in Eq. (1.4) between the basis functions $f_a^I(\mathbf{r})$ and $f_b^J(\mathbf{r})$. Similarly, the interaction terms U_{IJKL} represent convolutions of the interaction kernel $W_{abcd}(\mathbf{r}, \mathbf{r}')$ in Eq. (1.4) with four basis functions. The diagonal terms T_{II} can be identified with the single-particle energies per mode I and the off-diagonal terms T_{IJ} as the tunneling or hopping matrix between the modes I and J . This form (1.6) is still quite general, but let us now apply some specifications. First, we assume a periodic potential such as an optical lattice and choose the basis set $f_a^I(\mathbf{r})$ to be the associated Wannier functions. Second, this lattice potential is supposed to be sufficiently deep such that the different bands are well separated in energy and we may focus on the lowest Wannier band. In addition, for deep lattice potentials, the Wannier states in this lowest band are strongly localized. Third, we consider only one atomic species and short-range interactions. With these assumptions and approximations, we arrive at the Bose-Hubbard Hamiltonian [65] with the number operator $\hat{n}_I = \hat{b}_I^\dagger \hat{b}_I$ for the lattice site I

$$\hat{H} \approx - \sum_{IJ} T_{IJ} \hat{b}_I^\dagger \hat{b}_J + U \sum_I \hat{n}_I (\hat{n}_I - 1). \quad (1.7)$$

Due to the strong localization of the Wannier states (for deep lattice potentials), it is sufficient if we keep the tunneling matrix elements T_{IJ} between neighboring lattice sites I and J only.

A renowned phenomenon of the Bose-Hubbard Hamiltonian (1.7) is the super-fluid–Mott transition, see, e.g., [66]. For small interactions U , the ground state is a super-fluid (i.e., a Bose-Einstein condensate) as characterized by a long-range order parameter $\langle \hat{b}_I^\dagger \hat{b}_J \rangle$. For large on-site repulsion U , however, the character of the ground state changes. Assuming unit filling $\langle \hat{n}_I \rangle = 1$, we have essentially one atom per lattice site and the large energy penalty U prevents them from hopping

to the next lattice site. As a result, the ground state is insulating and separated by a finite gap (the Mott gap) from the excited states. In this case, the coherence $\langle \hat{b}_I^\dagger \hat{b}_J \rangle$ essentially vanishes for $I \neq J$.

Applying the same approximations for fermionic atoms in optical lattices, we arrive at the Fermi-Hubbard Hamiltonian

$$\hat{H} \approx - \sum_{IJs} T_{IJ} \hat{c}_{Is}^\dagger \hat{c}_{Js} + U \sum_I \hat{n}_I^\uparrow \hat{n}_I^\downarrow, \quad (1.8)$$

which is even more famous than the bosonic version (1.7). Naturally, this system has also been realized experimentally, see, e.g., [57, 67, 68, 69] as well as [70, 71]. Due to the additional spin degree $s \in \{\uparrow, \downarrow\}$, its dynamics is more involved and less well understood. Nevertheless, for large U , the ground state does also become a Mott insulator in the case of half filling $\langle \hat{n}_I^\uparrow \rangle = \langle \hat{n}_I^\downarrow \rangle = 1/2$. For small U , on the other hand, the state would be metallic (in more than one dimension), i.e., conducting. In the Mott insulator state, conduction requires the generation of quasi-particle excitations in the form of doublons (i.e., doubly occupied lattice sites) or holons (i.e., empty lattice sites). The proper description of their dynamics, including the interactions among each other (see, e.g., [72] and references therein) is an open question and might also be relevant for our understanding of high-temperature superconductivity.

1.2.4. Dirac Hamiltonian

After this detour to the non-relativistic Hubbard Hamiltonians, let us now turn our attention to the Dirac Hamiltonian

$$\hat{H} = \int d^3r \hat{\Psi}^\dagger (-i\boldsymbol{\alpha} \cdot \boldsymbol{\nabla} + m\beta) \hat{\Psi} = \int d^3r \hat{\Psi}^\dagger (-i\gamma^0 \boldsymbol{\gamma} \cdot \boldsymbol{\nabla} + m\gamma^0) \hat{\Psi}, \quad (1.9)$$

where we first consider in 3+1 dimensions. For the γ^μ matrices (or, equivalently, for the $\boldsymbol{\alpha} = \gamma^0 \boldsymbol{\gamma}$ and $\beta = \gamma^0$ matrices), we use the Dirac basis

$$\gamma^0 = \begin{pmatrix} \mathbf{1} & 0 \\ 0 & -\mathbf{1} \end{pmatrix}, \quad \gamma^1 = \begin{pmatrix} 0 & \sigma_x \\ -\sigma_x & 0 \end{pmatrix}, \quad \gamma^2 = \begin{pmatrix} 0 & \sigma_y \\ -\sigma_y & 0 \end{pmatrix}, \quad \gamma^3 = \begin{pmatrix} 0 & \sigma_z \\ -\sigma_z & 0 \end{pmatrix}, \quad (1.10)$$

where σ_x , σ_y and σ_z are the usual Pauli spin matrices. Other basis sets, such as the Weyl basis or the Majorana basis (with purely imaginary Dirac matrices) can also be used. The bi-spinor field operators $\hat{\Psi}$ and $\hat{\Psi}^\dagger$ have four components encoding the two spin degrees of freedom as well as the particle and anti-particle components.

After spatial discretization $\hat{\Psi}(\mathbf{r}) \rightarrow \hat{c}_{Is}$, the above Hamiltonian (1.9) can in principle be cast into a form $T_{IJ}^{ss'} \hat{c}_{Is}^\dagger \hat{c}_{Js'}$ similar to the Hubbard Hamiltonian (1.8) with vanishing interaction $U = 0$, but realizing such a hopping matrix $T_{IJ}^{ss'}$ experimentally may be a bit involved, see also [73].

Fortunately, many phenomena such as the Sauter-Schwinger effect discussed in Sec. 2.8 do not necessarily require 3+1 dimensions but can already be observed in 2+1 or even 1+1 dimensions. Thus, let us simplify the problem and consider the Dirac Hamiltonian in 1+1 dimensions (again $s = 1/2$) with $\gamma^0 = \sigma_z$ and $\gamma^1 = i\sigma_x$

$$\hat{H} = \int dx \hat{\Psi}^\dagger (i\sigma_y \partial_x + m\sigma_z) \hat{\Psi}. \quad (1.11)$$

Here, 2×2 Dirac matrices are sufficient and thus we only have two components for $\hat{\Psi}$ and $\hat{\Psi}^\dagger$. Note that these two components describe the particle and anti-particle components, but not the spin degree of freedom.

As it turns out, this form (1.11) admits a quite simple lattice representation, see, e.g., [74, 75, 76]. For example, we may encode the upper and lower components of $\hat{\Psi}$ in the even and odd lattice sites I . (Corresponding to the remark above, we consider the spin of the fermionic atoms to be fixed, e.g., by a strong magnetic field.) Then, the spatial derivative $\partial_x \hat{\Psi}$ at the position of the lattice site I can be represented by $(\hat{c}_{I+1} - \hat{c}_{I-1})/(2\Delta x)$ where Δx is the distance between the lattice

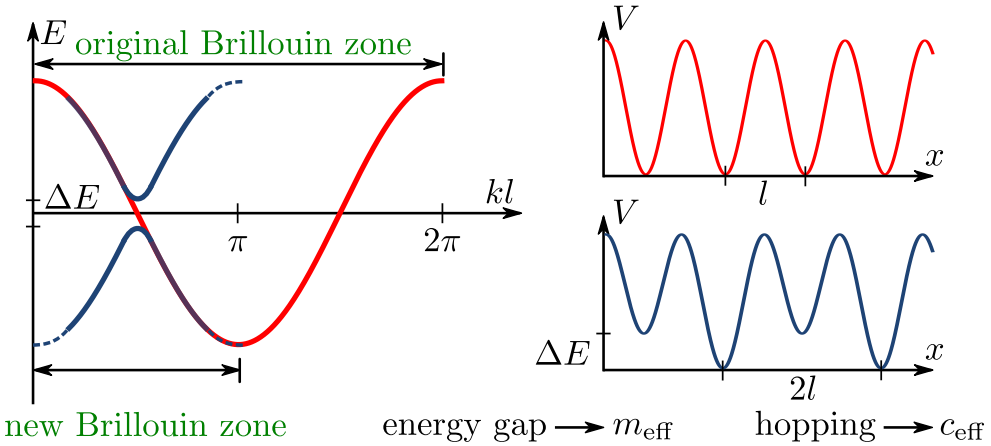


Figure 1.4: Sketch of the dispersion relations (left) for the original (top) and the bi-chromatic (bottom) optical lattices (right).

sites. As a result, the kinetic term in Eq. (1.11) becomes a sum of simple hopping terms $\pm(\hat{c}_I^\dagger \hat{c}_{I\pm1} + \text{h.c.})$. The alternating signs \pm in front of these hopping terms can be eliminated by local phase shifts. For example, we may go through the one-dimensional lattice from left to right, i.e., with increasing I . Wherever such a hopping term $(\hat{c}_I^\dagger \hat{c}_{I+1} + \text{h.c.})$ comes with the “wrong” sign, we may “repair” this by applying a phase shift $\hat{c}_{I+1} \rightarrow -\hat{c}_{I+1}$ to the right lattice site.

Note that this ability to “repair” the phases (which would also work for more general complex phases $e^{i\varphi_I}$) is a peculiarity of a one-dimensional lattice, which has the same number of lattice sites and links (between neighboring lattice sites). In general higher-dimensional lattices, such as a square lattice in two dimensions, the number of lattice sites is smaller than the number of lattice links (even if only links between neighboring lattice sites are considered) and thus the number of possible phase shifts (i.e., lattice sites) is not sufficient to “repair” all the possible relative phases (at the links). This problem has to be taken into consideration when trying to realize lattice versions of higher-dimensional theories, such as the Hamiltonian (1.9) with the matrices (1.10). The issue becomes even more relevant for the implementation of gauge fields discussed in Sec. 1.2.6 where phase accumulated along a closed path (i.e., a Wilson loop) can be non-trivial, e.g., if a magnetic field is present.

Coming back to our 1+1 dimensional system (1.11) and its lattice realization, the hopping strength determines the effective speed of light c_{eff} which is naturally much slower than the real speed of light c , see Sec. 1. The mass term $m\sigma_z$ corresponds to a local (on-site) potential shift which is alternating, i.e., positive for the upper component of $\hat{\Psi}$ on the even sites and negative for the lower component of $\hat{\Psi}$ on the odd sites. As a result, we get a bi-chromatic lattice where the even sites have a higher energy than the odd sites, see Fig. 1.4.

The emergence of quasi-relativistic behaviour in such a lattice can also be understood on the level of the dispersion relations, see Fig. 1.4. Without the off-set between the even and odd lattice sites representing the mass term $m\sigma_z$, the lattice reproduces the standard cosine dispersion relation if we focus on the lowest Wannier band. Since we are going to distinguish odd and even sites by the off-set, we take our elementary cell to contain two lattice sites, such that our Brillouin zone in the reciprocal lattice is cut in half. Thus, we have to fold the usual cosine dispersion relation which can be done by taking both signs into account, i.e., mirroring it at the k -axis, see Fig. 1.4. Now, adding a small off-set basically turns the crossing of the two branches of the cosine dispersion relation at its zero into an avoided level crossing. In the vicinity of this avoided level crossing, the dispersion relation now has the quasi-relativistic form $\pm\sqrt{c_{\text{eff}}^2 k^2 + m_{\text{eff}}^2 c_{\text{eff}}^4}$.

To conclude this section, let us briefly discuss the Dirac Hamiltonian in 2+1 dimensions. Using the Dirac matrices $\gamma^0 = \sigma_z$, $\gamma^1 = i\sigma_x$ and $\gamma^2 = i\sigma_y$, it can also be realized via a two-component spinor $\hat{\Psi}$. On the one hand, this is a

great simplification when it comes to constructing a quantum simulator, but, on the other hand, this implies that some of the concepts known from the 3+1 dimensional case (1.9) and (1.10) cannot be applied here. Apart from the fact that the spin degree of freedom is not captured (as already mentioned above), there is no γ^5 matrix (as an independent matrix) here, i.e., one cannot apply the concept of chirality in the same way as in 3+1 dimensions⁴. One of the simplest ways to actually realize a lattice version of this 2+1 dimensional Dirac Hamiltonian is to have fermionic atoms in a hexagonal or honeycomb lattice, i.e., the same structure as graphene. In this case, a quasi-relativistic dispersion relation $\omega \approx c_{\text{eff}} |\mathbf{k} - \mathbf{k}_{\text{Dirac}}|$ without a mass gap arises naturally in the vicinity of the two Dirac points $\mathbf{k}_{\text{Dirac}}$ where $\omega = 0$, see, e.g., [77]. The fact that we obtain two inequivalent Dirac points (further Dirac points in the Brillouin zone are related via symmetries to these two) is related to the fermion doubling problem: When directly discretizing the Dirac Hamiltonian on a lattice, one typically obtains multiple copies of the original fermions in the low-energy sector. This should also be taken into account when constructing quantum simulators, e.g., by focusing on (or coupling to) one of these copies only – or by actually using these different copies for representing different fermion species of the original problem.

1.2.5. Scalar field

In the previous section, the original atomic field operators $\hat{\psi}_a(\mathbf{r})$ and the quasi-relativistic Dirac field operators $\hat{\Psi}(\mathbf{r})$ to be simulated were related by a simple linear transformation such as Eq. (1.5) plus the discretization on a lattice. In this section, let us consider a different scheme where the motional degrees of freedom of the atoms are mapped to the quasi-relativistic field to be simulated, in this case the scalar field $\hat{\phi}$. An alternative approach based on the phonon field in Bose-Einstein condensates will be discussed in Sec. 2.1.

To this end, we consider a chain (or array) of atoms with spin zero which are strongly localized in the x and y directions by suitable potentials (e.g., a deep optical lattice) such that they stay in the lowest quantum well states in those directions, see Fig. 1.5. Thus, we may focus on their motion in the remaining z direction where we assume that we have one atom in each lattice site I . Denoting the position of the atom with mass m in the lattice site I by q_I , this motion in z direction is influenced by the potential $V(q_I)$ which is supposed to be much weaker than the confining potentials in the x and y directions. Furthermore, we assume that the lattice sites are close enough that we may have a strong coupling (e.g., by having Rydberg atoms) between the lattice sites $W(q_{I+1} - q_I)$ where we neglect the coupling between next to nearest neighbors, see Fig. 1.5. Together with the usual kinetic term, the Lagrangian for this system reads

$$L = \sum_I \left(\frac{m}{2} \dot{q}_I^2 - V(q_I) - W(q_{I+1} - q_I) \right). \quad (1.12)$$

If we assume that the interaction $W(q_{I+1} - q_I)$ is quite strong and attractive, it tends to align the atoms, i.e., to make the difference $q_{I+1} - q_I$ quite small (e.g., much smaller than the lattice spacing). Thus, we may Taylor expand this interaction around its minimum at $q_{I+1} = q_I$ with the curvature κ (effective spring constant)

$$L \approx \sum_I \left(\frac{m}{2} \dot{q}_I^2 - V(q_I) - \frac{\kappa}{2} (q_{I+1} - q_I)^2 \right). \quad (1.13)$$

In addition, again using that the difference $q_{I+1} - q_I$ is quite small, we may go to the continuum limit with the identification $q_I(t) \rightarrow \phi(t, x)$ where the lattice site I is replaced by the coordinate $x = I\Delta x$ with the lattice spacing Δx . In this limit,

⁴Obviously, one can have circular motion in this case, but this is not really the same as chirality – even though the two concepts are sometimes mixed up a bit.

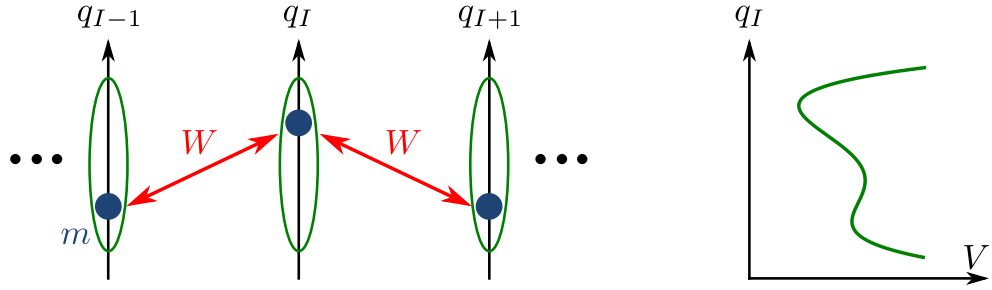


Figure 1.5: Sketch of the simulator for the scalar-field Lagrangian (1.14).

the difference $q_{I+1} - q_I$ becomes the spatial derivative $(q_{I+1} - q_I)/\Delta x \rightarrow \partial_x \phi$ and the sum over all lattice sites I turns into an integral $\Delta x \sum_I \dots \rightarrow \int dx \dots$. As a result, we arrive at the Lagrangian density for a scalar field

$$\mathcal{L} = \frac{1}{2} \dot{\phi}^2 - \frac{c_{\text{eff}}^2}{2} (\partial_x \phi)^2 - \mathcal{V}(\phi), \quad (1.14)$$

where the effective speed of light is set by the spring constant κ , see also Sec. 1. The on-site potential $\mathcal{V}(\phi)$ can be adjusted by suitably shaped laser beams, for example. For a purely parabolic potential $\mathcal{V}(\phi)$, we would simulate a free massive scalar field, but more involved potentials could be used to study the sine-Gordon model, see Sec. 3.1, the Kibble-Zurek mechanism, see Sec. 3.2, or the analogue of false-vacuum decay, see Sec. 3.3. Note that the experimentally available potentials and interaction strengths (e.g., using Rydberg atoms) are large enough to simulate the ground state properties of these theories at nano-Kelvin temperatures. Obviously, the above concept can be generalized to 2+1 dimensions in a quite straightforward manner, while a 3+1 dimensional version requires more effort.

1.2.6. Gauge fields

After having discussed the Dirac field (1.11) and the scalar field (1.14), let us now turn to vector fields A_μ . Here, it is important to carefully distinguish several levels of the incorporation of those fields A_μ , see also [78]. At the lowest level, one can consider external fields A_μ which can depend on space and time, but are fixed, i.e., treated as classical background fields. For example, one could have the quantum Dirac field $\hat{\Psi}$ as in Eq. (1.11), but propagating within the background of an external electromagnetic field A_μ . In 1+1 dimensions, the vector potential $A_\mu = (A_0, A_1)$ can be simplified by a gauge transformation $A_\mu \rightarrow A_\mu + \partial_\mu \chi$, e.g., by gauging the spatial part away $A_1 = 0$ such that only the potential $A_0 = \Phi$ remains. Note that this gauge transformation is related to the phase shift discussed above in Sec. 1.2.4 since the associated gauge transformation for the Dirac field just reads $\Psi \rightarrow \exp\{iq\chi\}\Psi$. After this gauge transformation, the interaction Hamiltonian reads

$$\hat{H}_{\text{int}} = q \int dx \hat{\Psi}^\dagger \hat{\Psi} A_0 = q \int dx \hat{\Psi}^\dagger \hat{\Psi} \Phi. \quad (1.15)$$

In the lattice representation in Fig. 1.4, such a term can simply be modeled by an additional optical laser with suitably shaped intensity profile (which is determined by Φ). As another option, a spatially homogeneous force $F(t)$ (representing a purely time-dependent electric field) can also be applied by accelerating (e.g., shaking) the lattice.

Going to higher dimensions – as also explained above in Sec. 1.2.4 – the situation becomes more complicated, i.e., more interesting. In addition to the homogeneous force $F(t)$ generated by accelerating the lattice, one could also imagine a rotating lattice such that the Coriolis force corresponds to the Lorentz force in the presence of a magnetic field. More involved gauge fields can be modeled by suitable phase imprints on the hopping matrix elements T_{IJ} such that a particle

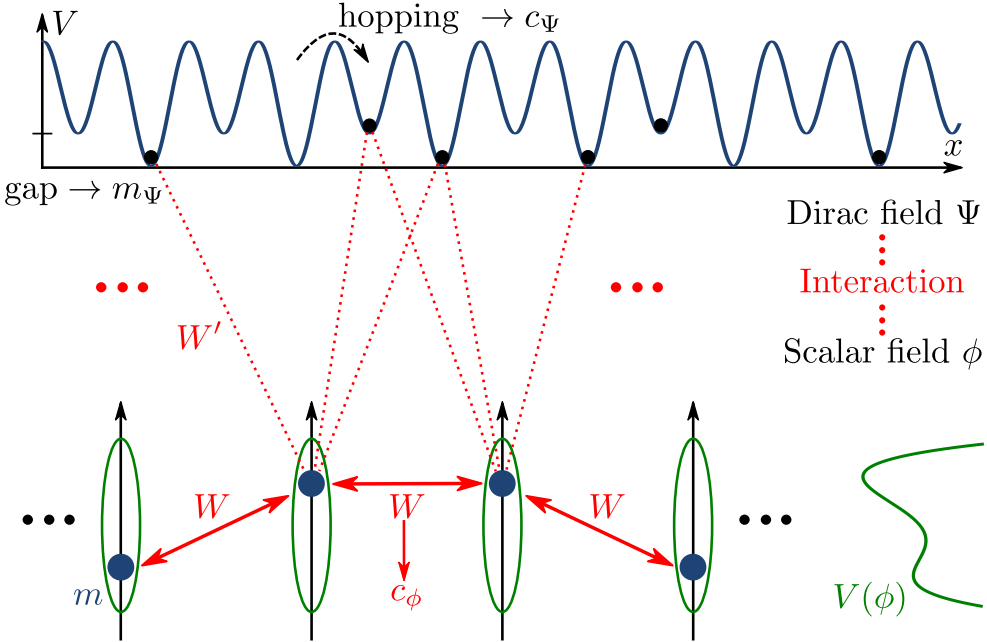


Figure 1.6: Sketch of the simulator for the Dirac field (1.11) coupled to the scalar-field (1.14).

hopping from one lattice site to another acquires a phase. For ultra-cold atoms in optical lattices, such phases can be induced in driven systems, e.g., by applying suitable time-dependent electromagnetic fields. In this way, the atoms evolve (in the continuum limit) as if they were under the influence of an effective field A_μ , which is referred to as a synthetic gauge field or an artificial gauge field, see, e.g., [49, 79, 80, 81, 82, 83, 84, 85, 86, 87, 88].

Going one step beyond external fields, one could also include the interaction between the atoms. However, since the dipolar or van-der-Waals interactions between the atoms display a distance dependence which is different⁵ from the Coulomb interactions between Dirac particles such as electrons and positrons, for example, one would typically obtain a qualitative instead of a quantitative analogy. Still, such a qualitative analogy would allow us to tackle interesting questions, such as the back-reaction (due to the Coulomb interaction between electrons and positrons) onto the Sauter-Schwinger effect, see Sec. 2.8. On the qualitative level, these investigations could also shed light on other phenomena, such as string breaking in Quantum Chromodynamics (QCD).

The next level would be a fully dynamical treatment of the gauge fields (instead of dipolar or van-der-Waals interactions where the interaction kernels $\propto 1/|\mathbf{r} - \mathbf{r}'|^3$ or $\propto 1/|\mathbf{r} - \mathbf{r}'|^6$ are fixed). In this case, one should also have quantized degrees of freedom modeling those gauge fields, see, e.g., [70, 89, 90, 91, 92, 93, 94, 95, 96]. As a very simple illustration, one could consider combining the simulator for the Dirac field (1.11) in Fig. 1.4 with that for the scalar field (1.14) in Fig. 1.5, which is sketched in Fig. 1.6. This simulator is realized via a one-dimensional bi-chromatic lattice half filled with fermionic atoms which represent the Dirac field (1.11). They do not interact with each other but can hop from one lattice site to the next, such that the hopping strength determines the effective speed of light c_Ψ for the Dirac field. The effective mass m_Ψ in the Dirac equation is generated by the energy difference between the even and odd sites (as in Fig. 1.4). The simulator for the scalar field as in Fig. 1.5 is then placed parallel to this one-dimensional fermionic lattice in the same plane, i.e., such that the motion q_I of those atoms changes their distance to the fermionic atoms, i.e., impacts their interaction W' , e.g., via having Rydberg atoms in the simulator for the scalar field. They do interact among each other and the associated

⁵This would not be the case for ions, but they are not considered here.

interaction W generates the effective speed of light c_ϕ for the scalar field, as in Fig. 1.5. In the continuum limit, this combination gives rise to the effective Lagrangian

$$\mathcal{L} = \Psi^\dagger (i\partial_t - ic_\Psi \sigma_y \partial_x - m_\Psi c_\Psi^2 \sigma_z + g_{\text{eff}} \phi) \Psi + \frac{1}{2} \dot{\phi}^2 - \frac{c_\phi^2}{2} (\partial_x \phi)^2 - \mathcal{V}(\phi), \quad (1.16)$$

where the effective coupling strength g_{eff} between the Dirac and the scalar field is determined by the interaction W' between the fermionic and the Rydberg atoms. As a result, although the fermionic atoms do not directly interact with each other, they acquire an indirect interaction, which is mediated via the dynamical and quantized scalar field $\hat{\phi}$. For example, if we assume a parabolic potential $\mathcal{V}(\phi) \propto \phi^2$ for the scalar field (i.e., an effective mass term m_ϕ), this field would mediate a one-dimensional Yukawa type interaction $\propto \exp\{-m_\phi c_\phi |x - x'|\}$ in the static limit. For large masses m_ϕ , this interaction would become very short range and could be approximated by an effective local four-Fermion interaction $\propto (\Psi^\dagger \Psi)^2$, similar to the U term in the Fermi-Hubbard model (1.8) or the Thirring model discussed in Sec. 3.1.

Already this simple example (1.16) indicates the complexity required for quantum simulators of dynamical gauge fields (e.g., the QCD Lagrangian), see, e.g., [70, 89, 90, 91, 92, 93, 94, 95, 96], especially when they should also be coupled to fermionic fields (e.g., representing the quarks). Nevertheless, one can make progress using results of lattice gauge field theory, e.g., by using the plaquette formulation.

2. Linear fields

To start our discussion, let us first focus on linear fields, i.e., quantum fields which obey linear evolution equations (to the level of approximation we are considering). Still, such fields can lead to highly non-trivial phenomena if we study their evolution under the influence of external (i.e., classical) background fields, such as gravitational or electromagnetic fields.

In most of these cases, it is sufficient to consider the simple example of a mass-less and minimally coupled scalar field ϕ propagating in a curved space-time with metric $g^{\mu\nu}$ as described by the Klein-Fock-Gordon equation

$$\square\phi = \nabla_\mu \nabla^\mu \phi = \frac{1}{\sqrt{-g}} \partial_\mu (\sqrt{-g} g^{\mu\nu} \partial_\nu \phi) = 0, \quad (2.1)$$

where g is the determinant of the metric $g_{\mu\nu}$. Later on, we will also study the Dirac field in the presence of an external electromagnetic field in Sec. 2.8. Of course, the phenomena discussed below (such as Hawking radiation or cosmological particle creation [97]) do also occur for other fields, such as the quantized electromagnetic (i.e., photon) field \hat{A}_μ .

2.1. Curved space-time analogues (a.k.a. analogue gravity)

As we have seen in Sec. 1.2.5, one option to simulate a scalar field is to arrange atoms with finite-range interactions in an optical lattice. In the following, let us take a different route and consider an atomic cloud in the form of a Bose-Einstein condensate, where we assume only one species of atoms with contact interactions. Then, the evolution equation for the scalar (non-relativistic) field operator $\hat{\psi}$ (in the Heisenberg picture) following from the Hamiltonian (1.4) reads

$$i\hbar \frac{\partial \hat{\psi}}{\partial t} = \left(-\frac{\hbar^2}{2m} \nabla^2 + V + g_s \hat{\psi}^\dagger \hat{\psi} \right) \hat{\psi}, \quad (2.2)$$

where g_s denotes the contact (s -wave scattering) interaction strength. In a Bose-Einstein condensate, almost all atoms occupy the same quantum state as described by condensate wave function $\psi_c(t, \mathbf{r})$ which can be time-dependent in general, see, e.g., [98]. Thus, we may apply the mean-field approximation $\hat{\psi}(t, \mathbf{r}) \approx \psi_c(t, \mathbf{r})$ where the many-particle field operator $\hat{\psi}(t, \mathbf{r})$ is effectively replaced by a c-number valued function $\psi_c(t, \mathbf{r})$. Note that this approximation $\hat{\psi}(t, \mathbf{r}) \approx \psi_c(t, \mathbf{r})$ is a strongly simplified picture. For example, in a state with a definite number of atoms

$$\hat{N} = \int d^3r \hat{\psi}^\dagger \hat{\psi} = \int d^3r \hat{\rho}, \quad (2.3)$$

we would have $\langle \hat{\psi} \rangle = 0$ which contradicts the mean-field approximation $\hat{\psi}(t, \mathbf{r}) \approx \psi_c(t, \mathbf{r})$. This contradiction can be repaired by a refined mean-field approximation $\hat{\psi}(t, \mathbf{r}) \approx \hat{A} \hat{N}^{-1/2} \psi_c(t, \mathbf{r})$ where \hat{A}^\dagger and \hat{A} are suitable creation and annihilation operators for the total number of atoms in the cloud $\hat{N} = \hat{A}^\dagger \hat{A}$, see, e.g., [99, 100, 101]. More refined expansion schemes such as $\hat{\psi}(t, \mathbf{r}) \approx \hat{A} \hat{N}^{-1/2} [\psi_c(t, \mathbf{r}) + \hat{\chi}(t, \mathbf{r})]$ can also include the quantum or thermal corrections $\hat{\chi}$ or fluctuations around this mean field or even higher-order corrections, see, e.g., [102].

Inserting the mean-field approximation into the evolution equation (2.2) yields the Gross-Pitaevskii equation

$$i\hbar \frac{\partial \psi_c}{\partial t} = \left(-\frac{\hbar^2}{2m} \nabla^2 + V + g_s |\psi_c|^2 \right) \psi_c. \quad (2.4)$$

To interpret this equation, let us apply the Madelung split of the condensate wave function ψ_c into the condensate density $\rho_c = |\psi_c|^2$ and a remaining phase (in analogy to the eikonal ansatz)

$$\psi_c = \sqrt{\rho_c} \exp\{iS/\hbar\}. \quad (2.5)$$

After inserting this split (2.5) into the Gross-Pitaevskii equation (2.4), the real part yields the evolution equation for the phase S which is very similar to the Hamilton-Jacobi equation in classical mechanics

$$\dot{S} + V + g_s \rho_c + \frac{(\nabla S)^2}{2m} = \frac{\hbar^2}{2m} \frac{\nabla^2 \sqrt{\rho_c}}{\sqrt{\rho_c}}, \quad (2.6)$$

apart from the additional “quantum pressure” term or “quantum potential” on the right-hand side. Originally, the term “quantum potential” stems from the Bohm formulation of quantum mechanics, but we may just use it to refer to the quantum corrections to the classical Hamilton-Jacobi equation (2.6) on the left-hand side.

The imaginary part of the Gross-Pitaevskii equation (2.4) yields the equation of continuity $\dot{\rho}_c + \nabla \cdot (\rho_c \mathbf{v}_c) = 0$ with the condensate velocity $\mathbf{v}_c = \nabla S/m$. Thus, the phase S is proportional to the velocity potential with $\mathbf{v}_c = \nabla S/m = \nabla \phi_c$ and the above equation (2.6) turns into the Bernoulli equation $\dot{\phi}_c + V/m + g_s \rho_c/m + \mathbf{v}_c^2/2 = 0$ if we neglect the “quantum pressure” term on right-hand side. From this Bernoulli equation, we may read off the internal pressure $p = g \rho_c^2/(2m)$ due to the contact interaction g_s between the atoms. As a result, the condensate supports sound waves, which we may describe by linearizing the Bernoulli and continuity equations around a given background profile $\phi_c = \phi_c^0 + \delta\phi_c$ and $\rho_c = \rho_c^0 + \delta\rho_c$. Combining these two first-order (in ∂_t) equations into one second-order equation, we find the wave equation for those sound waves

$$\left[(\partial_t + \nabla \cdot \mathbf{v}_c^0) \frac{m}{g_s} (\partial_t + \mathbf{v}_c^0 \cdot \nabla) - \nabla \cdot (\rho_c^0 \nabla) \right] \delta\phi_c = 0, \quad (2.7)$$

where all differential operators act on everything on their right. Here we may directly read off the speed of sound $c_s = \sqrt{g_s \rho_c^0/m}$, typically on the order of millimeter per second. As explained in Sec. 1, this is the analogue to the speed of light. Note that this speed of sound can be manipulated by modifying the condensate density ρ_c^0 or the interaction strength g_s (e.g., via Feshbach resonances [103]) and thus may depend on space and time $c_s = c_s(t, \mathbf{r})$.

Now we may follow the seminal paper by Unruh [104] and find that the wave equation (2.7) has exactly the same form as that for a mass-less and minimally coupled scalar field in a curved space-time (2.1) provided that we insert the effective sonic or acoustic metric

$$g_{\mu\nu}^{\text{eff}} = \left(\frac{\rho_c^0}{c_s} \right)^{2/(D-1)} \begin{pmatrix} c_s^2 - (\mathbf{v}_c^0)^2 & \mathbf{v}_c^0 \\ \mathbf{v}_c^0 & -1 \end{pmatrix}, \quad (2.8)$$

where D is the number of spatial dimensions to be simulated. In one spatial dimension, the mass-less and minimally coupled scalar field is conformally invariant and thus the identification works – strictly speaking – only if ρ_c^0/c_s is constant. Note that the above metric (2.8) is only defined up to a constant factor.

This analogy (2.8) between sound waves in Bose-Einstein condensates (2.7) on the one hand and mass-less and minimally coupled scalar fields in curved space-times (2.1) on the other hand allows us to simulate many effects such as Hawking radiation (see the next section) in the laboratory. However, as one might already expect from counting the degrees of freedom entering the effective metric (2.8) – three for \mathbf{v}_c^0 , one for c_s and possibly one more for the factor in front of the metric (2.8) – it is not possible to simulate all possible curved space-times. For example, the full Kerr metric of a rotating black hole or the metric describing gravitational waves cannot be modelled with (2.8), see also [105]. Nevertheless, the effective metric (2.8) is flexible enough to simulate many interesting phenomena – which will be the subject of the next sections.

Note that, for predicting quantum effect such as Hawking radiation, the classical equation of motion (2.7) is not sufficient, one should also consider the commutation relations of the field operators, see also [106]. For the original field

operators $\hat{\psi}^\dagger$ and $\hat{\psi}$ of the atoms, they read

$$[\hat{\psi}(t, \mathbf{r}), \hat{\psi}^\dagger(t, \mathbf{r}')] = \delta^3(\mathbf{r} - \mathbf{r}'), \quad [\hat{\psi}(t, \mathbf{r}), \hat{\psi}(t, \mathbf{r}')] = [\hat{\psi}^\dagger(t, \mathbf{r}), \hat{\psi}^\dagger(t, \mathbf{r}')] = 0. \quad (2.9)$$

Now inserting the simplified mean-field split $\hat{\psi}(t, \mathbf{r}) \approx \psi_c + \hat{\chi}(t, \mathbf{r})$, we find the same commutation relations for the Bogoliubov-de Gennes fluctuations $\hat{\chi}^\dagger$ and $\hat{\chi}$. For the more precise ansatz $\hat{\psi}(t, \mathbf{r}) \approx \hat{A}\hat{N}^{-1/2}[\psi_c(t, \mathbf{r}) + \hat{\chi}(t, \mathbf{r})]$, this remains correct for those Bogoliubov-de Gennes fluctuations $\hat{\chi}^\dagger$ and $\hat{\chi}$ which are orthogonal to the spatial mode function $\psi_c(t, \mathbf{r})$ of the condensate itself. Now the linear combinations $\hat{\chi}^\dagger \pm \hat{\chi}$ of the Bogoliubov-de Gennes fluctuations yield the density $\delta\hat{\rho}_c$ and phase $\delta\hat{\phi}_c$ such that they indeed obey the correct commutation relations expected for a scalar quantum field – i.e., the analogy does also hold on the quantum level.

As another important point, sound waves in Bose-Einstein condensates allow us to study deviations from the wave equations (2.8) and thus (2.1) at short length scales, i.e., large wave numbers k . In this regime, the dispersion relation of the sound waves differs from the usual linear dispersion $\omega = c_s k$ which is valid at low k . In order to derive these deviations, one could linearize Eq. (2.6) including the “quantum pressure” term (together with the continuity equation) or insert the mean-field expansion $\hat{\psi}(t, \mathbf{r}) \approx \hat{A}\hat{N}^{-1/2}[\psi_c + \hat{\chi}(t, \mathbf{r})]$ into Eq. (2.2) which yields the Bogoliubov-de Gennes equations for the fluctuations $\hat{\chi}$ and $\hat{\chi}^\dagger$. Both approaches are equivalent and give the modified dispersion relation

$$(\omega - \mathbf{v}_c^0 \cdot \mathbf{k})^2 = c_s^2 \mathbf{k}^2 \left(1 + \frac{\xi^2 \mathbf{k}^2}{4}\right), \quad (2.10)$$

where the healing length $\xi = 1/\sqrt{mg_s \rho_c^0}$ can be used to separate the two regimes. For $\xi^2 \mathbf{k}^2 \ll 1$ we have the usual linear dispersion relation for sound $(\omega - \mathbf{v}_c^0 \cdot \mathbf{k})^2 = c_s^2 \mathbf{k}^2$ while for $\xi^2 \mathbf{k}^2 \gg 1$, the dispersion relation becomes quadratic and approaches the free-particle form $(\omega - \mathbf{v}_c^0 \cdot \mathbf{k})^2 = [\hbar^2 \mathbf{k}^2/(2m)]^2$. As a result, phonons with large k can move faster than c_s , which will be important for the discussions in the next section.

A final remark, the analogy between Eqs. (2.8) and (2.1) applies to the *kinematics* of a scalar field propagating in a given curved space-time, the *dynamics* of the space-time itself, i.e., the Einstein equations, are not reproduced. Instead, the flow background is determined by the Gross-Pitaevskii equation (2.4). Thus, the widely used term “analogue gravity” might actually be a bit misleading – which was the reason for the deviating title of this section. Still, even though the analogy does “only” apply on the kinematical level, it allows us to study several phenomena (see the next sections) and thus it has developed into its own research field by now, which is still growing. Hence, it is impossible to provide a complete list of references here, see, e.g., the overview [107] for a recently updated list.

2.2. Hawking radiation

Let us start with a brief explanation of the mechanism behind Hawking radiation [108, 109]. To this end, we consider the space-time diagram of a star collapsing to a black hole⁶, first on the classical level, see Fig. 2.1. As usual, time t goes up in this diagram, i.e., on the ordinate, while the abscissa represents the radial coordinate r , assuming spherical symmetry. Note that due to $r > 0$ the left and right-hand sides of the space-time diagram should be identified, but we display both of them separately for better visibility. The green curves display the surface of the collapsing star which end

⁶In contrast to some claims in the literature, space-time curvature alone is not sufficient for predicting Hawking radiation. As a counter-example, one may consider a neutron star described by a static metric which is regular everywhere. Then, the ground state (with respect to this static frame) of the quantum field is regular and there is no lasting particle creation such as Hawking radiation. Thus, the existence of the black-hole horizon is essential for Hawking radiation, see also [110].

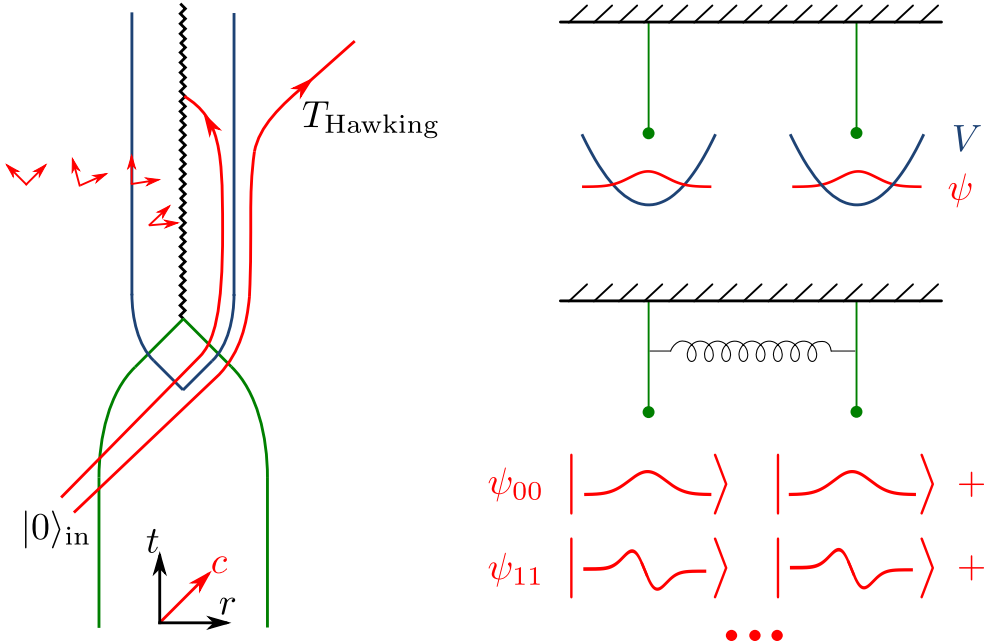


Figure 2.1: Sketch of the space-time diagram of black-hole formation (left) and the intuitive picture for Hawking radiation based on the two harmonic oscillators (right).

up in the central singularity at $r = 0$ (black zigzag line). The red curves and arrows represent light rays, which are tilted due to the strong gravitational field⁷. The event horizon of the black hole is indicated by the blue curve and marks the border between the last light ray which is able to escape to $r \rightarrow \infty$ and the first light ray which is trapped by the strong gravitational field and eventually hits the central singularity at $r = 0$.

Now what Hawking did was to consider quantum fields propagating on this classical background space-time. Strikingly, he found that even when these fields start off in their initial vacuum state $|0\rangle_{\text{in}}$, the final state of those fields which are able to escape to infinity is not the vacuum but instead a thermal state with the famous Hawking temperature

$$T_{\text{Hawking}} = \frac{\hbar c^3}{8\pi G_N k_B M}, \quad (2.11)$$

where M is the mass of the black hole. As a visualization of the order of magnitude, the typical wavelength of photons emitted at such a temperature is comparable to the Schwarzschild radius $R_S = 2G_N M/c^2$ which marks the location of the horizon (blue curve in Fig. 2.1 left). Even though this temperature is extremely small for typical astronomical black holes, it is considered to be very important for our fundamental understanding of nature and has many ramifications such as the concept of black-hole entropy etc.

As an intuitive explanation for Hawking radiation, often the picture based on particle-anti-particle pairs is used. In this picture, the vacuum is visualized as containing many “virtual” particle-anti-particle pairs which are constantly created and annihilated. If one of them (the in-falling partner particle, see also [111]) is then trapped behind the horizon, the other one is free to escape to $r \rightarrow \infty$, i.e., it becomes “real” and constitutes the Hawking radiation. This intuitive picture may be appropriate for visualizing the quantum vacuum fluctuations and their entanglement at finite spatial distances (which are important ingredients for Hawking radiation), but one should be careful and not take it too seriously. For example, taking this picture too seriously, one has to entertain the possibility that a photon and an “anti-photon” annihilate in

⁷For simplicity, we neglect back-scattering effects by the effective potential (angular momentum and curvature).

vacuum without creating any new particles. Furthermore, the concept of classical trajectories for both, the outgoing Hawking radiation and the in-falling partner particle, which are supposed to originate from the same space-time point, does not quite work.

Thus, let us discuss a more refined picture for the origin of Hawking radiation based on two harmonic oscillators, see Fig. 2.1. If these two harmonic oscillators are not coupled, the ground state of the total quantum system is just the product of the two ground states of the two individual oscillators, including the ground-state quantum fluctuations (i.e., Gaussian wave functions). In case of a coupling⁸ between the two oscillators (in Fig. 2.1 depicted by a spring between them) the ground state of the total quantum system is an entangled state where the quantum fluctuations are correlated (it is a two-mode squeezed state). For example, if the position of one oscillator fluctuates a bit to the right, the position of the other oscillator is more likely to fluctuate to the right too. An analogous correlation can be found in the occupation numbers of the two oscillators when considered separately. If the occupation number of one oscillator is zero then the occupation number of the other oscillator vanishes as well. However, in the ground state of the total quantum system (including the coupling by the spring) there is also a finite amplitude for the occupation number of one oscillator being unity – in which case the occupation number of the other oscillator is also unity, and so on.

Now, if we were to switch off the coupling between the two oscillators slowly, i.e., adiabatically, this entangled ground state would evolve into the factorizing ground state of the two individual oscillators discussed above. However, if the coupling is switched off rapidly, i.e., non-adiabatically (say suddenly), the quantum state has not enough time to react and the final state retains some or even all of the initial entanglement, i.e., it deviates from the ground state. In the case of Hawking radiation, this non-adiabatic change arises from the tearing apart of the waves at the horizon, where one part of the wave (represented by one oscillator) falls into the black hole while the other part of the wave (represented by the other oscillator) escapes to infinity. This tearing apart of waves as a non-adiabatic process causes a deviation from the ground state and its rapidity is set by the surface gravity of the black hole, which in turn determined the temperature (2.11). Even though the combined quantum state of the two oscillators is a pure state, the reduced state of the oscillator which escaped to infinity is a thermal, i.e., mixed state. In this picture, the two oscillators initially represent the quantum vacuum fluctuations at two different positions (which are also correlated [112]) which then evolve on trajectories on either side of the horizon, see Fig. 2.1. Due to the tearing apart by the gravitational field of the black hole, one of them escapes to infinity and represents the outgoing Hawking radiation (in a thermal state) while the other one corresponds to the in-falling partner [111]. For real black hole, the correlation between the outgoing Hawking particles and their in-falling partners can obviously not be observed, but for the black-hole analogues discussed below, this is an important point for the experimental observations, see also [113, 114].

Note that for the derivation of Hawking radiation, the regularity at the horizon is a crucial point. While for freely falling observers, the vicinity of the horizon is locally indistinguishable from vacuum (i.e., a regular⁹ state), static observers far away measure thermal radiation. Actually, this argument can even be used to derive Hawking radiation in a rigorous manner, see, e.g., [115]. It has been proposed to abandon the regularity at the horizon (e.g., in “firewall” scenarios [116]) in order to address some open questions such as the black-hole information puzzle. However, by abandoning the regularity at the horizon one also abandons the main reason for the existence of Hawking radiation in the first place. For example, one

⁸Using the analogy sketched in Fig. 1.5, the oscillators could represent the degrees of freedom at two neighboring spatial positions. The coupling between the two (i.e., the spring) then allows the quantum field to propagate from one position to another.

⁹This regularity is usually described by the Hadamard condition.

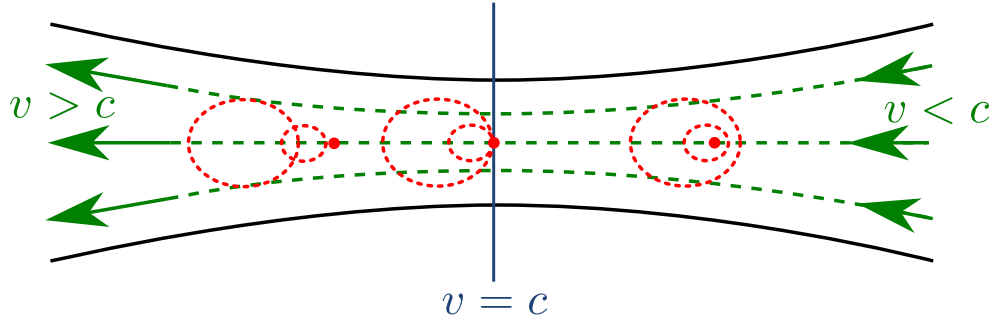


Figure 2.2: De Laval nozzle with streamlines (green) and sound waves (red). The border (blue) between sub-sonic (right) and the super-sonic (left) flow marks the analogue of the horizon. In the super-sonic region (left), sound waves are swept away and form Mach cones.

could consider the quantum field to be in the Boulware state [117] which is the local ground state of all static observers outside the black hole. This state does not contain Hawking radiation and is a well-defined state outside the black hole – the only problem is that it becomes singular at the horizon and thus observers freely falling into the black hole would notice a difference there. However, if that is acceptable, there would be no need nor reason for Hawking radiation.

As a somewhat related issue, it should also be mentioned here that Hawking's derivation [108, 109] is not without any problems. An important point is the so-called trans-Planckian problem [118, 119] which can be illustrated in the following way: If we consider an outgoing particle of the Hawking radiation far away from the black hole and trace it back in time, we have to undo the gravitational red-shift. Thus, its wave packet is squeezed against the horizon (when going back in time) and the wavelengths become shorter and shorter. Since the gravitational red-shift is exponential in time t (where the exponent is determined by the surface gravity of the black hole), these wavelengths become smaller than the Planck length $\ell_{\text{Planck}} = \sqrt{\hbar G_N/c^3} \approx 1.6 \times 10^{-35}$ m after a comparably short time. At this point, one would probably not trust the approach used by Hawking based on the propagation of quantum fields on a given classical background space-time anymore.

2.2.1. Black hole analogues

Actually, the trans-Planckian problem sketched above was one of the main motivations for Unruh [104] to consider laboratory analogues for black holes – or, more precisely, for Hawking radiation. His main idea is already explained in Sec. 2.1 and can be based on the quantitative analogy between Eqs. (2.8) and (2.1). To see how the analogue of a black hole and thus Hawking radiation can arise in such a laboratory set-up, let us consider a de Laval nozzle, see Fig. 2.2. At the entrance of the nozzle, the flow is sub-sonic $v_c < c_s$ and thus sound waves (which represent the analogue of light rays) can propagate in all directions (though dragged by the flow). This region corresponds to the black-hole exterior $r > R_S$. At the exit of the nozzle, the flow is super-sonic $v_c > c_s$ such that sound waves cannot propagate upstream anymore and are swept away. This region corresponds to the black-hole interior $r < R_S$. At the narrowest point of the nozzle, the flow velocity equals the speed of sound $v_c = c_s$ and thus this point is the analogue of the horizon $r = R_S$.

For Bose-Einstein condensates [120], we know what happens at short wavelengths, as explained in Sec. 2.1, and thus we can address the trans-Planckian problem by means of this analogue. In this case, the healing length ξ where the dispersion relation (2.10) changes from linear to quadratic can be used as an analogue for the Planck length. Then the trans-Planckian problem is resolved in the following way: The initial wave packet has large wave number $k \gg 1/\xi$ and is thus faster than c_s such that it can propagate upstream, i.e., it originates in the super-sonic region. While it propagates

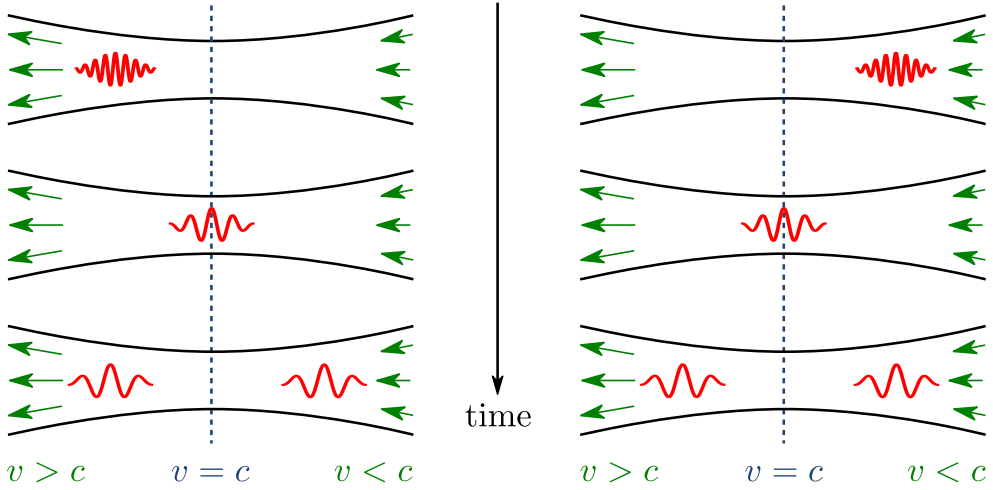


Figure 2.3: Sketch (not to scale) of the evolution (tearing apart) of wave packets giving rise to Hawking radiation (and its in-falling partner particles) for a super-sonic (left) dispersion relation as in Eq. (2.10) and for a sub-sonic dispersion relation (right).

upstream, it is stretched (as the analogue of the gravitational red-shift) because the flow velocity on its right-hand side is smaller than on its left-hand side, see Fig. 2.3. Around the time this wave packet reaches the horizon, its wave number is reduced to $k = \mathcal{O}(1/\xi)$ and thus its group velocity drops down to the sound speed. After that, the part of the wave packet which was already outside the horizon $r > R_S$ can escape while the other part which was inside the horizon $r < R_S$ is swept away. Hence, we find basically the same tearing apart process as discussed above. Actually, detailed calculations (see, e.g., [121, 122, 123] and references therein) show that – if we start with a wave packet in its initial ground state in the locally co-moving fluid frame (which is analogous to the freely falling frame in gravity) – the state of the part of the wave packet which escapes the nozzle on the right-hand side (i.e., its entrance) is indeed a thermal state with the analogue Hawking temperature

$$T_{\text{Hawking}} = \frac{\hbar}{2\pi k_B} \left| \frac{d(v_c - c_s)}{dr} \right|_{r=R_S}, \quad (2.12)$$

provided that the flow profile is smooth enough and that no other excitation mechanisms (such as friction at the walls of the nozzle) are present. As one would expect, this quantity (2.12) matches precisely the surface gravity calculated from the acoustic metric (2.8) for this effectively one-dimensional set-up. Inserting typical values for Bose-Einstein condensates such as length scales in the micrometer regime and velocities of order millimeter per second, we find an effective surface gravity κ of the black-hole analogue in the kilo-Hertz range, which corresponds to a temperature (2.12) of a few nano-Kelvin. Although this is still a rather low temperature, it is much larger than the real Hawking temperature (2.11) for typical astronomical black holes and, even more importantly, it is in the realm of detectability for Bose-Einstein condensates.

Actually, black-hole analogues in Bose-Einstein condensates have already been realized experimentally at the Technion [58, 59, 60, 61, 62] and it was even possible to detect signatures of Hawking radiation in those systems. Instead of a de Laval nozzle as in Fig. 2.2, the effective horizon has been created by a step-like potential (generated by a laser beam) which moved through the condensate and thereby induced a waterfall like flow profile. Now one may transform into the frame co-moving with the potential step (i.e., the “waterfall”) and adjust its sweeping speed such that the flow velocity before the potential step (i.e., upstream) is slower than the sound speed $v_c < c_s$ whereas after the potential step (i.e., downstream) it is faster $v_c > c_s$. Then, the resulting trans-sonic flow generates a sonic horizon in analogy to Fig. 2.2. In

order to detect the created (analogue) Hawking radiation, the Technion experiment [58, 59, 60, 61, 62] used the fact that the outgoing Hawking particles (in this case, phonons) and their in-falling partners are entangled (as explained above) and measured the density-density correlations induced by this entanglement. To this end, the experiment was repeated many times and the density plots measured after each run were used to extract the correlations. Even though such a measurement of the density-density correlations alone does not facilitate a full quantum state tomography and thus does not allow us to demonstrate entanglement, arguments based on some additional assumptions indicate that the state was indeed entangled and hence that the Technion experiment indeed measured a quantum effect. However, at this point it is fair to say that the results and conclusions are not undisputed in the community, see, e.g., [124]. Furthermore, our understanding of the interpretation of the results has been improved since the first run of experiments. Nevertheless, I think that there is a good chance that the Technion experiment did indeed detect Hawking radiation for this black-hole analogue. In any case, I would also say that these experiments mark a decisive breakthrough in the field.

2.2.2. Hawking radiation as tunneling?

To conclude this section, let us discuss another frequently used interpretation of Hawking radiation as a tunneling process, see, e.g., [125]. Clearly, there are similarities: Both are quantum effects which generate a tail at finite spatial distances (the evanescent part of the wave function in tunneling and the correlation of the vacuum fluctuations of quantum fields) which does not exist classically. However, when picturing Hawking radiation as tunneling of a particle from the interior of the black hole to the exterior, one should also be aware of some crucial differences.

Let us start by considering the case of relativistic quantum fields without modifications of the dispersion relation – which is the case discussed in most of the papers devoted to the tunneling picture. First, tunneling in quantum mechanics usually refers to a case where, in classical mechanics, there is no trajectory going from a point in front of the potential barrier to a point behind the barrier if the initial kinetic energy is smaller than the barrier height. Yet, in quantum mechanics, the propagator is non-vanishing (though exponentially suppressed). In contrast, in relativistic quantum field theory, the causal propagator from any space-time point inside the black hole (i.e., behind the horizon) to any space-time point outside vanishes exactly due to causality (without any exponential tails which would correspond to tunneling in quantum mechanics). Second, as a related point, the WKB phase displays a branch-cut singularity at the classical turning points for tunneling – but this singularity is resolved when calculating the full wave function (i.e., beyond the WKB approximation) in quantum mechanics. The situation is different for Hawking radiation in relativistic quantum field theory since there the stationary mode functions at the horizon acquire a different kind of phase singularity which does not go away when considering the full wave equation. Actually, this phase singularity is closely related to the trans-Planckian problem mentioned above. Since the tunneling picture of Hawking radiation makes heavy use of these singularities, see, e.g., [125], this difference is also quite important¹⁰. Third, for tunneling in quantum mechanics, the state which comes out at the rear end of the barrier depends on the state (energy and amplitude etc.) which was incident on the front end (i.e., “trying” to tunnel through). The outgoing Hawking radiation, on the other hand, is independent of the quantum state inside the black hole (at least within relativistic quantum field theory). If there was such a simple

¹⁰Probably one reason for the relative popularity of the tunneling picture for Hawking radiation is that it allows a “short-cut derivation” of the Hawking temperature without a full-fledged quantum-field theory calculation. However, in view of the complexity of the problem, it is important to remember that such a short cut can slur over some of the subtleties of the derivation – which is the main motivation for this subsection.

connection between the quantum state inside the black hole and the outgoing Hawking radiation as in ordinary tunneling in quantum mechanics, it would have profound consequences for our discussions of the black-hole information puzzle. Fourth, for the Sauter-Schwinger effect discussed in Sec. 2.8, the Dirac equation in the presence of a constant electric field, for example, can be cast into a tunneling problem with a spatially oscillating wave function outside the potential barrier and an exponentially decaying wave function in between the classical turning points (i.e., inside the barrier). Thus, in the case of the Sauter-Schwinger effect, the interpretation as tunneling (from the Dirac sea to the positive continuum) can be justified qualitatively as well as quantitatively in this way. For Hawking radiation, on the other hand, I am not aware of such a mapping and it is also not clear what the two classical turning points should be in this case. In view of the points above, such a direct mapping probably does not exist.

Note that, already in the original paper [125], it has been mentioned that an alternative interpretation could be to replace the tunneling of the Hawking particle from inside to outside by the tunneling of its partner particle into the black hole – thereby liberating the Hawking particle to go off to infinity as a real particle. This alternative interpretation evades some of the problems mentioned above and also incorporates the important point of connecting the outgoing Hawking particles with their in-falling partners – which was actually important for the Technion experiment mentioned above.

Taking into account modifications of the dispersion relation such as in Eq. (2.10), some of the above arguments (e.g., the support of the propagator and the WKB approximation, see, e.g., [126]) have to be modified as well. However, since these modifications strongly depend on the actual dispersion relation while the outgoing Hawking radiation does not [122], they do not resolve the problems mentioned above. Furthermore, as can be seen in Fig. 2.3, the semi-classical particle trajectories change (for early times) when modifying the dispersion relation and thus the tunneling picture must be adapted to this case [127].

To view the problem from a different angle, one could imagine simulating the Dirac equation in a black-hole background via fermionic atoms in an optical lattice along the lines sketched in Sec. 1.2.4. Having such a physical realization in mind, one could say that all non-trivial quantum evolution is tunneling (between the lattice sites). However, these tunneling processes leading to Hawking radiation would be more *along* the horizon instead of *across* the horizon – and, if one has hopping across the horizon, it would be mostly from the outside to the inside¹¹.

2.3. Unruh effect

Via the principle of equivalence, the Unruh effect is closely related to Hawking radiation. Actually, Unruh discovered it when trying to understand Hawking radiation better [128]. However, in order to explain this effect, let us first go to flat space-time and consider the usual Minkowski vacuum. Then, imagine placing a photon detector at rest in this vacuum state. Obviously (neglecting possible dark counts) the detector does not click. If we now imagine moving this detector with a constant velocity¹² then it still does not click because the Minkowski vacuum is Lorentz invariant. However, the Unruh effect predicts that the situation changes if we accelerate the detector. In the case of uniform acceleration a , the detector responds as if it was immersed in a thermal bath with the Unruh temperature

$$T_{\text{Unruh}} = \frac{\hbar a}{2\pi k_B c}. \quad (2.13)$$

¹¹A lattice typically induces a sinusoidal dispersion relation where modes with large k are slower than modes with small k . In such a case, Hawking radiation originates from wave packets outside the horizon, see the right panel of Fig. 2.3.

¹²Which is of course smaller than the speed of light, see Sec. 2.6.

One way to demonstrate where the thermal response comes from is to start with the usual two-point (Wightman) function of a mass-less scalar field in the 3+1 dimensional Minkowski vacuum (outside the light cone)

$$\langle \hat{\phi}(t, \mathbf{r}) \hat{\phi}(t', \mathbf{r}') \rangle = -\frac{1}{4\pi^2} \frac{1}{(t-t')^2 - (\mathbf{r}-\mathbf{r}')^2}. \quad (2.14)$$

Now we may evaluate this two-point function along a uniformly accelerated trajectory by inserting $t = \sinh(a\tau)/a$ and $z = \cosh(a\tau)/a$ where τ is the proper time of the detector and we have assumed acceleration in z -direction with $x = y = 0$. Note that this transformation is related to the Rindler coordinates. Insertion into Eq. (2.14) yields

$$\langle \hat{\phi}(\tau) \hat{\phi}(\tau') \rangle = -\frac{a^2}{8\pi^2} \frac{1}{\cosh(a[\tau-\tau']) - 1}. \quad (2.15)$$

This expression is periodic in imaginary proper time with a period of $2\pi/a$. According to the Kubo-Martin-Schwinger (KMS) condition, this periodicity in imaginary time translates to thermal behaviour with the temperature being set by the period $2\pi/a$ which gives Eq. (2.13).

Now let us come back to the relation to Hawking radiation via the principle of equivalence as mentioned above. To this end, let us consider a series of static observers at fixed distances to the black-hole horizon and compare their findings with that of a freely falling observer which starts with small velocity far away from the black hole and then falls in. At large distances, the static and the freely falling observers both see basically the same Hawking radiation emitted by the black hole. However, this agreement changes when the freely falling observer approaches the black hole. On the one hand – as we have already discussed above – the freely falling observer does not notice anything special at the horizon but locally sees a vacuum state. On the other hand, in view of the gravitational red-shift of the photons propagating away from the black hole, static observers closer to the horizon must find a higher temperature than static observers further away for their observations to be consistent (in a stationary quantum state). Thus, the closer they are to the horizon (from which the gravitational red-shift becomes infinitely strong) the higher their observed temperatures must be. This explains the connection to the Unruh effect since these static observers feel a strong gravitational pull and thus must be strongly accelerated (in view of the principle of equivalence) in order to retain their fixed distance to the horizon. In contrast, the freely falling observer corresponds locally to the inertial Minkowski observer. The latter does not detect any photons while the former sees a thermal bath.

2.3.1. Analogue of Unruh effect

Due to the factor \hbar/c in Eq. (2.13), everyday accelerations of order m/s^2 correspond to extremely low temperatures of order 10^{-21} K , i.e., zepto-Kelvin. One way to increase this temperature would be to consider much higher accelerations, e.g., with electrons in ultra-strong laser fields, see, e.g., [129, 130, 131]. For ultra-cold atoms, one usually follows a different route and effectively replaces the speed of light c by the speed of sound c_s which improves the situation by more than eleven orders of magnitude, such that we are approaching the nano-Kelvin regime which is more accessible experimentally. Thus, the idea would be to consider the phonon field in a approximately homogeneous condensate at rest. As explained in Sec. (2.1), this field simulates a mass-less scalar quantum field with the speed of light being replaced by the speed of sound.

Now, another important ingredient for realizing an analogue of the Unruh effect is the detector. Instead of photons, this detector should detect phonons, i.e., density and phase fluctuations of the Bose-Einstein condensate. One promising option could be an atomic quantum dot, i.e., a very tight optical potential (like optical tweezers) which may hold one or a small number of atoms, see, e.g., [132, 30]. The internal states of this detector could then correspond to the internal states

of the trapped atoms or their motional states or even to the number of trapped atoms inside the atomic quantum dot. The atomic quantum dot could be coupled to remaining Bose-Einstein condensate via tunneling or optical transitions, possibly in connection with Rydberg couplings or dipolar couplings.

In order to simulate the accelerated detector, one could imagine moving the atomic quantum dot through the condensate on a non-inertial trajectory, see, e.g., [133]. This would model the coupling of the detector to the field along such a non-inertial trajectory. However, another important ingredient for the Unruh effect is the relativistic time dilatation of the detector (i.e, the difference between the Minkowski time t and the proper time τ of the detector), which is not represented by the atomic quantum dot *a priori*. To take this effect into account, one could externally tune the internal eigen-energies of the atomic quantum dot such that they represent the proper time τ . Alternatively, one could replace the uniformly accelerated trajectory by a circular motion of the detector, e.g., $x(t) = R \cos(\Omega t)$, $y(t) = R \sin(\Omega t)$ and $z = 0$. In this case, the absolute value of the acceleration would be constant but its direction would rotate constantly. The two-point function along the detector trajectory can be obtained by inserting $x(t) = R \cos(\Omega t)$, $y(t) = R \sin(\Omega t)$ and $z = 0$ into Eq. (2.14). The result would be stationary, i.e., only depend on $t - t'$, where this dependence is periodic in real time – but no longer in imaginary time. As a consequence, while the detector on a circular trajectory would also experience particles, their spectrum would not be exactly thermal anymore. On the other hand, one would not have to tune the internal eigen-energies of the atomic quantum since the Lorentz factor determining the relativistic time dilatation of the detector is constant for the circular motion. In principle, this non-thermal excitation spectrum could be measured by moving the atomic quantum dot through the condensate on a circular trajectory, see, e.g., [133].

However, in order to detect the analogue of the Unruh effect as a quantum phenomenon, one should be careful to avoid creating classical excitations by stirring the condensate with the moving atomic quantum dot – which then could also excite it. This is often a problem when trying to observe quantum effects, as competing classical background effects can easily be larger than the usually small quantum phenomena one is interested in. As an idea to avoid these problems, it has been suggested [134] to replace the atomic quantum dots by laser beams which measure the local density of the condensate and move through it on circular orbits, see also [135]. By analysing the density fluctuations measured by those laser beams (in an interferometric set-up), one could then reconstruct the detector response. Using two laser beams, one red and one blue detuned from the resonance frequency of the condensate atoms, one can suppress the classical back-reaction of those laser beams onto the condensate, i.e., avoid unwanted excitations. However, one should still be careful because every measurement perturbs the quantum state of the system – which might in turn react back on the density fluctuations. This back-reaction effect could be minimized by using weak instead of strong measurements of the density fluctuations.

There have also been proposals which focus on other aspects of the Unruh effect instead of the non-inertial trajectories. For example, in [136, 137] an optical lattice simulator for the Rindler geometry (i.e., the Minkowski metric in terms of the Rindler coordinates) has been proposed. In order to observe particle creation, the idea is to start in the ground state of the Minkowski metric and then to suddenly switch (i.e., quench) to the Rindler geometry. This scenario displays some similarities to the (sudden) collapse to a black hole, as depicted in Fig. 2.1, and also to the phenomenon of cosmological particle creation as discussed in the next section. Other proposals focus on the squeezing mechanism because the Minkowski vacuum is a squeezed state in terms of the Rindler creation and annihilation operators (associated to the uniformly accelerated observers). However, since squeezing is important for many phenomena (including Hawking radiation as discussed in the previous section as well as cosmological particle creation as discussed in the next section),

this feature alone is probably not sufficient for claiming to have a simulator for the Unruh effect. As in all of these simulators, it is important to carefully determine which aspects of the phenomenon to be simulated are reproduced and which not – or, equivalently, how many and which steps lie between the original phenomenon and the simulator.

2.4. Cosmological particle creation

Already in the early days of quantum mechanics (long before Hawking and Unruh etc.), Schrödinger [138] understood that the expansion of the Universe can create particles out of the vacuum, see also [139]. In principle, this phenomenon can also be traced back to the tearing apart process as already discussed in Sec. 2.2 but now this tearing apart is caused by the time-dependent expansion of the Universe instead of the stationary gravitational field of the black hole. However, one may also understand the basic mechanism by means of a single harmonic oscillator. To show this, let us consider the spatially flat Friedmann-Lemaître-Robertson-Walker metric¹³

$$ds^2 = a^2(\eta) [d\eta^2 - d\mathbf{r}^2] = d\tau^2 - a^2(\tau) d\mathbf{r}^2, \quad (2.16)$$

where the time-dependent scale factor a corresponds to the cosmic expansion. Here, we used the representation in terms of the conformal time η and the proper time τ which are related by $d\tau = ad\eta$. When simulating such an expanding Universe via an analogue system such as a Bose-Einstein condensate, another important time is the laboratory time t and its relation to η and τ depends on the concrete physical realization, which we shall discuss below.

For later convenience, let us introduce yet another time coordinate defined by $dT = a^{-D} d\tau = a^{1-D} d\eta$ depending on the number D of spatial dimensions, which we shall refer to as internal oscillator time. In terms of this time coordinate, the metric (2.16) reads $ds^2 = a^{2D} dT^2 - a^2 d\mathbf{r}^2$. As a result, we have $\sqrt{-g} = a^{2D}$ and thus the Klein-Fock-Gordon equation (2.1) of a mass-less and minimally coupled scalar field in such a curved space-time simplifies to

$$\left(\frac{d^2}{dT^2} - a^{2(D-1)} \mathbf{k}^2 \right) \phi_{\mathbf{k}} = 0, \quad (2.17)$$

after a spatial Fourier expansion of the scalar field (exploiting the spatial homogeneity). Apart from the special case of one spatial dimension $D = 1$ (where the field is conformally invariant, see also Sec. 2.5) this is the equation of a harmonic oscillator with a time-dependent frequency $\Omega_{\mathbf{k}}^2(T) = a^{2(D-1)}(T) \mathbf{k}^2$, see Fig. 2.4.

Now, in analogy to the line of arguments in Sec. 2.2, if we start in the ground state of this harmonic oscillator and change its frequency $\Omega_{\mathbf{k}}(T)$ slowly enough (i.e., $\dot{\Omega}_{\mathbf{k}} \ll \Omega_{\mathbf{k}}^2$ and $\ddot{\Omega}_{\mathbf{k}} \ll \Omega_{\mathbf{k}}^3$ etc.) the quantum evolution will be adiabatic, i.e., the quantum state will stay close to the instantaneous ground state in view of the adiabatic theorem. However, if the time-dependence of $\Omega_{\mathbf{k}}(T)$ is too fast, there will be deviations, i.e., the final state will differ from the ground state – it will be a squeezed state. As an extreme example, let us consider a sudden change of $\Omega_{\mathbf{k}}(T)$ which is usually referred to as a quench. For such a sudden switch, the wave function has no time to change, i.e., immediately after the quench it will have the same form as before, see Fig. 2.4. For the initial value $\Omega_{\mathbf{k}}^{\text{in}}$ this wave function represents the ground state and thus does not change with time. After the quench to $\Omega_{\mathbf{k}}^{\text{out}} \neq \Omega_{\mathbf{k}}^{\text{in}}$, however, this wave function has the “wrong” width and thus does not represent the ground state for the new value of $\Omega_{\mathbf{k}}^{\text{out}}$. Instead, it is an excited state – in this case, a squeezed state containing pairs of excitation quanta. As a result, it is also no longer a stationary state, but it starts to “breathe” by changing its width in an oscillatory manner, see Fig. 2.4.

¹³In case of spatial curvature, the spatial line element (which reads $d\mathbf{r}^2 = dx^2 + dy^2 + dz^2$ in 3+1 dimensions) would acquire additional position dependent metric coefficients, as discussed below.

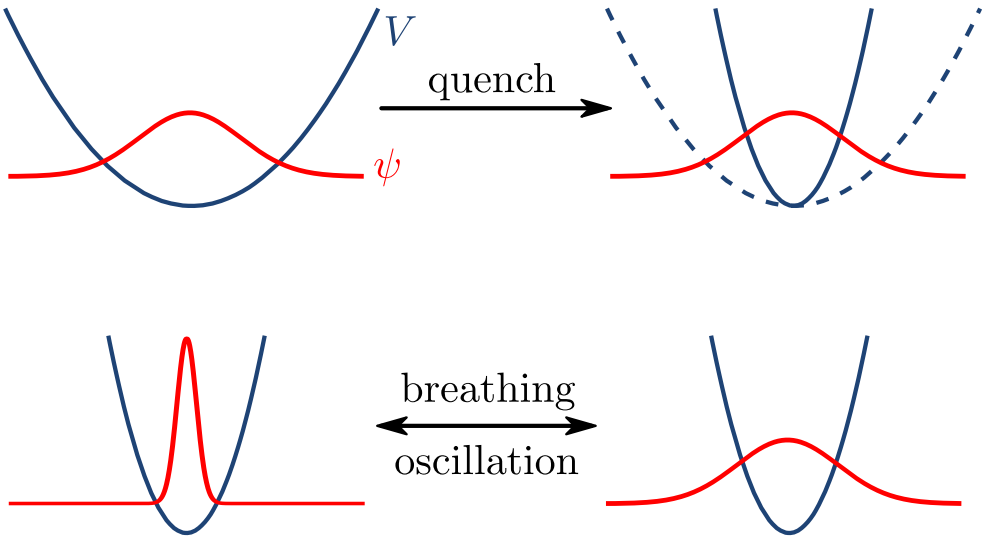


Figure 2.4: Sketch of the main mechanism for cosmological particle creation: When the harmonic oscillator potential V (blue curve) is rapidly (e.g., suddenly) switched to a new value (top right), the wave function ψ (red curve) has no time to adapt and thus becomes a squeezed state. After that, the wave function ψ undergoes an oscillatory breathing motion (bottom).

Going back from this mode picture to the particle picture, one finds that the expanding Universe creates pairs of particles moving in opposite directions (i.e., with opposite momenta \mathbf{k} and $-\mathbf{k}$), as already expected from momentum conservation. Thus, we may also visualize this effect as the tearing apart of the initial quantum vacuum fluctuations by the cosmic expansion – in analogy to the picture based on the coupled harmonic oscillators in Fig. 2.1. As a result, these particles do also generate a specific imprint in the space-time dependent correlation functions (see also [140]), quite in analogy to the black-hole case, which the Hawking particles and their in-falling partners move away from the horizon in opposite directions.

2.4.1. Analogue Universe in condensate at rest

In order to simulate an expanding Universe, let us first consider an effectively two-dimensional homogeneous condensate at rest with $\mathbf{v}_c^0 = 0$ and $\rho_c^0 = \text{const}$. In this case ($D = 2$), the effective line element (2.8) reads

$$ds_{\text{eff}}^2 = \left(\frac{\rho_c^0}{c_s(t)} \right)^{2/(D-1)} [c_s^2(t)dt^2 - d\mathbf{r}^2] = \rho_c^0 \left[dt^2 - \frac{d\mathbf{r}^2}{c_s^2(t)} \right]. \quad (2.18)$$

We see that (up to the irrelevant constant pre-factor ρ_c^0) the laboratory time t equals the proper time τ in this case. Furthermore, changing the coupling strength g_s and thereby the speed of sound c_s in a time-dependent manner (e.g., via Feshbach resonances [103]) models a dynamical scale factor $a(t)$ in Eq. (2.16). More specifically, decreasing the speed of sound c_s increases the sound distance (i.e., acoustic run-time $\Delta t = |\mathbf{r}_1 - \mathbf{r}_2|/c_s$) between two positions \mathbf{r}_1 and \mathbf{r}_2 and thus corresponds to the expansion of the Universe¹⁴.

Such an expanding Universe has been successfully simulated in the Heidelberg experiment [64], see also [142, 143]. As in the Technion experiment [58, 59, 60, 61, 62] aiming at Hawking radiation, the phenomenon of cosmological particle creation has been detected by measuring the density-density correlations. In this way, it was also possible to observe

¹⁴More involved schemes open up additional possibilities. For example, a two-component condensate supports two species of quasi-particles: In addition to the mode associated with fluctuations of the total density, one has the mode corresponding to the density differences, which is typically much softer and thus easier to manipulate and to excite, see, e.g., [141].

how the phonons move away from each other (into opposite directions) with the speed of sound after their creation. Translating from the particle picture in real space to the mode picture in momentum space facilitated the observation of Sakharov oscillations (in analogy to those observed in the cosmic microwave background), which are associated to the oscillatory breathing motion sketched in Fig. 2.4 (bottom), see also [144].

Besides the spatially flat metric (2.16) corresponding to an approximately constant condensate density, it was also possible to simulate Universes with spatial curvature in the Heidelberg experiment [64]. For example, in a parabolic confinement potential, the condensate density decreases when going from the centre to the edge of the condensate. This implies that the speed of sound shrinks such that the acoustic distance grows – which corresponds to a spatially hyperbolic geometry. In a nut-shell, the spatial dependence of the sound speed represents the spatial curvature of the Universe while the time dependence of the sound speed models the cosmic expansion.

Instead of a monotonically expanding Universe, an oscillating scale factor has been simulated in the Chicago experiment [145] by modulating the external magnetic field near a Feshbach resonance [103]. By measuring the number of excited atoms *in situ*, it was possible to observe the thermal character of the radiation emitted into a certain direction. In terms of the coupled harmonic oscillator picture sketched in Fig. 2.1, the reduced density matrix of one oscillator is thermal, i.e., a mixed state, even though the total quantum state of both oscillators is a pure (entangled) state. Indeed, the coherence associated to this two-mode squeezed state could also be tested in the Chicago experiment [145]. Note that the title of the publication [145] refers to Unruh radiation, which can probably be explained by the fact that squeezing underlies both phenomena, cosmological particle creation and the Unruh effect (as well as many others), but the analogy to cosmological particle creation as considered in this section is apparently closer and more quantitative.

The creation of pairs of particles with opposite momenta has also been observed in the Palaiseau experiment [56]. Instead of varying the interaction strength g_s as in the Heidelberg experiment [64] or the Chicago experiment [145], here the trap stiffness was modulated – which changes the condensate density in time and thereby the speed of sound, see also the next section. Besides a ramp of the trap stiffness, it was also modulated in an oscillatory manner in the Palaiseau experiment [56], which would correspond to a Universe with an oscillating scale factor (as in the Chicago experiment [145]). Via parametric resonance, such a modulation predominantly creates specific phononic modes whose energy is half that of the trap modulation frequency. The phonon pairs created in this way were detected via time-of-flight measurements (i.e., in momentum space, see Sec. 1.2.2) and the correlations between the two phonons in a pair have also been observed in the Palaiseau experiment [56]. Although the title of the publication [56] refers to the dynamical Casimir effect, it can also be viewed as an analogue to cosmological particle creation, see also Sec. 2.9.

In this context, one should also mention the Boulder experiment [146, 147] where a “Bose nova” was created by switching the coupling g_s from a positive value (corresponding to repulsion between the condensate atoms) to a negative value (corresponding to attraction). In terms of the speed of sound, this would translate to replacing c_s^2 by $-c_s^2$. As a result, modes with sufficiently long wavelengths (above the healing length ξ), such that the term $c_s^2 \mathbf{k}^2$ in the dispersion relation (2.10) dominates in comparison to the term $\mathbf{k}^4/(2m)$, become unstable and start to grow exponentially. In terms of the effective metric (2.8) for $D = 2$, for example, this would correspond to changing the signature form $(+,-,-)$ to $(+,+,+)$, i.e., going from a hyperbolic to an elliptic case. Fortunately, this probably does not happen in our Universe.

2.4.2. Expanding condensates

Apart from a homogeneous condensate at rest with a time-dependent speed of sound, there are also other options for simulating an expanding Universe. As one might already intuitively expect (see also the Palaiseau experiment [56]), letting the condensate expand has an analogous effect. To see this, let us go back to the metric (2.16) and transform it to co-moving coordinates $\mathbf{R} = a(\tau)\mathbf{r}$ such that $d\mathbf{R} = a(\tau)d\mathbf{r} + \dot{a}(\tau)\mathbf{r}d\tau$. Then, insertion into the metric (2.16) yields

$$ds^2 = d\tau^2 - \left(d\mathbf{R} - \mathbf{R} \frac{\dot{a}}{a} d\tau \right)^2 = \left(1 - \mathbf{R}^2 \frac{\dot{a}^2}{a^2} \right) d\tau^2 + 2 \frac{\dot{a}}{a} \mathbf{R} \cdot d\mathbf{R} d\tau - d\mathbf{R}^2. \quad (2.19)$$

For these co-moving coordinates \mathbf{R} , the scale factor in front of the spatial line element $d\mathbf{R}^2$ disappears at the expense of additional terms in the temporal and mixed components containing the Hubble velocity $\mathbf{R}\dot{a}/a$. Thus, apart from the pre-factor, we find a form quite reminiscent of the acoustic metric (2.8) where the condensate velocity \mathbf{v}_c represents the Hubble velocity $\mathbf{R}\dot{a}/a$. Note, however, that the pre-factor must be considered as well because the expansion of the condensate naturally leads to a decreasing density – which, in turn, reduces the speed of sound (unless this is counterbalanced by a corresponding growth of the coupling g_s). On the other hand, as explained above, a shrinking speed of sound does also model the expansion of the Universe such that one can consider both effects together, see also [148, 149].

In summary, different laboratory scenarios – condensates at rest with time-dependent speed of sound or expanding condensates – can represent the same expanding Universe. One of the main differences between the two scenarios is the role of the laboratory time t and how it compares to the conformal time η , the proper time τ or the oscillator time T . As another important difference, the frequency or wave number scale where the dispersion relation (2.10) changes from linear to quadratic (i.e., the analogue of the Planck scale) behaves differently in the two scenarios. In view of those differences, one scenario might be better suited for observing a specific phenomenon of an expanding Universe than the other one – while it could be the other way around for another specific phenomenon.

An expanding ring-shaped Bose-Einstein condensate has been realized in the Maryland experiment [150]. Since the wave-length of the phonons expands with the condensate, such a set-up is well suited for observing the red-shift of the field modes within an expanding Universe. In the Maryland experiment [150], this has been achieved by imprinting a sound wave (i.e., a classical excitation) in the initial state of the condensate. As a related but more subtle phenomenon, the Maryland experiment [150] did also find evidence for Hubble friction. To explain this phenomenon, let us consider the equation of motion (2.1) for a mass-less scalar field in the Friedmann-Lemaitre-Robertson-Walker metric (2.16) in 3+1 dimensions in terms of the proper time τ

$$\left(\frac{d^2}{d\tau^2} + \frac{3\dot{a}}{a} \frac{d}{d\tau} + \frac{\mathbf{k}^2}{a^2} \right) \phi_{\mathbf{k}} = 0, \quad (2.20)$$

again after a spatial Fourier transformation. If we now insert the scale factor $a(\tau)$ of the de Sitter metric $a(\tau) = \exp\{H\tau\}$ with the Hubble constant H , we see that the above equation looks like that of a harmonic oscillator with a constant damping term $\propto H$ and a potential term (i.e., spring strength) which is exponentially decaying in time $\propto \exp\{-2H\tau\}$. This exponential decay is a consequence of the red-shift of the modes due to the cosmic expansion. As a result of Eq. (2.20), all modes go through the same sequence (though at different times): Initially $\mathbf{k}^2/a^2 \gg H^2$, they are in the under-damped regime and oscillate. Once a has grown sufficiently, however, they reach the over-damped regime and freeze in to an asymptotically constant (and typically non-zero) value. This transition from oscillation to freezing is an important mechanism for amplifying the initial quantum vacuum fluctuations of the inflaton field during cosmic inflation, which are supposed to be the responsible for the seeds of structure formation in our Universe.

After the initial period of linear evolution, the Maryland experiment [150] was also able to observe the subsequent non-linear dynamics, which are qualitatively analogous to the pre-heating and re-heating periods in the early Universe after the end of inflation.

2.5. Gibbons-Hawking effect

The Gibbons-Hawking effect [151] is sometimes mixed up with the phenomenon of cosmological particle creation, but it is actually a different mechanism. Even though both can occur in an expanding Universe, cosmological particle creation refers to the generation of particle pairs as lasting excitations – whereas the Gibbons-Hawking effect is associated to the response of a detector in such a curved space-time (analogous to the Unruh effect in Sec. 2.3). In order to clearly separate the two concepts, let us study a scenario in which there is no cosmological particle creation.

For simplicity – and because it will be relevant for the experimental proposal discussed below – we consider the massless and minimally coupled scalar field (2.1) within a spatially flat Friedmann-Lemaitre-Robertson-Walker metric (2.16) in 1+1 dimensions. In this case, the internal oscillator time T coincides with the conformal time η and thus the evolution equation (2.17) becomes independent of scale factor – which reflects the conformal invariance of the field in this case. As a result, the solutions of the wave equation (2.1) have exactly the same form $\exp\{-i\omega\eta + ikx\}$ as in flat space-time when expressed in terms of η . Thus, the same applies to the two-point function in the conformal vacuum state which reads

$$\langle \hat{\phi}(\eta, x) \hat{\phi}(\eta', x') \rangle = -\frac{1}{4\pi} \ln [(\eta - \eta')^2 - (x - x')^2], \quad (2.21)$$

up to an undetermined additive term which is spatially constant and related to the infra-red divergence of the mass-less and minimally coupled scalar field in 1+1 dimensions. Because the time-dependent scale factor $a(\eta)$ does neither show up in this expression nor in the evolution equation (2.17), there is no cosmological particle creation in this case, which becomes also evident by a direct comparison to Sec. 2.4.

However, that fact that the two-point function (2.21) has the same form as in the usual Minkowski vacuum does *not* mean that a particle detector would not click. The two-point function (2.21) is expressed in conformal time η whereas the internal dynamics of a detector at rest would be determined by the proper time τ , and they are different in an expanding Universe. To simplify the analysis, let us consider the de Sitter space-time with $a(\tau) = \exp\{H\tau\}$ where H is the Hubble constant¹⁵. In this case, the conformal time is given by $\eta = -\exp\{-H\tau\}/H$ and runs from $-\infty$ to zero. Inserting this transformation in the two-point function (2.21) we find that it acquires a more involved dependence on τ and does no longer coincide with the vacuum behaviour which would go as $\ln[(\tau - \tau')^2 - (x - x')^2]$. Instead, we again find periodicity along the imaginary time axis, which is related to thermal behaviour via the Kubo-Martin-Schwinger (KMS) condition already discussed in Sec. 2.3 and allows us to read off the Gibbons-Hawking temperature

$$T_{\text{GH}} = \frac{\hbar H}{2\pi k_{\text{B}}}. \quad (2.22)$$

In analogy to the Unruh effect, the detector experiences the conformal vacuum state (2.21) as a thermal state with the Gibbons-Hawking temperature (2.22). Note that all three temperatures, the Hawking temperature (2.11), the Unruh temperature (2.13), as well as the Gibbons-Hawking temperature (2.22), have exactly the same form – one just has to replace the surface gravity κ of the black hole by the acceleration a or the Hubble constant H , respectively.

¹⁵In contrast to the general Hubble parameter $H(\tau) = \dot{a}/a$ it is really a constant here.

Note that, strictly speaking, concluding thermal behaviour would also require showing that the detector response is stationary. Due to the aforementioned infra-red divergence, this is a bit more involved in this case. On the other hand, in view of the time-dependent scale factor $a(\tau)$, one could wonder whether such an expanding space-time can actually lead to a stationary response at all. This objection can be resolved by transforming to the co-moving coordinates (2.19) after which the metric becomes stationary for the de Sitter Universe. By yet another coordinate transformation of the time variable, one can get rid of the mixed components and cast this stationary metric into a static form

$$ds^2 = (1 - H^2 r^2) dt^2 - \frac{dr^2}{1 - H^2 r^2}, \quad (2.23)$$

at the expense of introducing coordinate singularities at the de Sitter horizon $r = 1/H$. In 3+1 dimensions, we would find the same form with an additional $r^2 d\Omega^2$ for the angular part.

2.5.1. Analogue of Gibbons-Hawking effect in expanding condensate

In view of the coordinate singularities at the de Sitter horizon $r = 1/H$, the static form (2.23) is not very suitable for the experimental realization as an analogue model, so let us go back to the original form (2.19) corresponding to an expanding condensate. Indeed, it has been proposed to observe the analogue of the Gibbons-Hawking effect in an expanding cigar-shaped (i.e., effectively 1+1 dimensional) Bose-Einstein condensate [152]. Similar to Sec. 2.3.1, the idea is to realize the detector by an atomic quantum dot at the centre of the condensate. Assuming that we have two species of atoms (e.g., different hyper-fine levels), the condensate is supposed to be formed by one species a while the tightly confining atomic quantum dot potential traps atoms of the other species b . Then, laser-driven transitions between the two states a and b with adjustable Rabi frequency and detuning can ensure that the internal time of the detector indeed corresponds to the proper time τ and that it is coupled to the phonon field of the expanding condensate [152].

2.6. Ginzburg effect

In Sec. 2.3, we stated that a detector moving through the Minkowski vacuum with a constant velocity does not click because it can be Lorentz transformed to a detector at rest. Strictly speaking, this is only true for sub-luminal detector velocities. Trajectories with super-luminal velocities always stay super-luminal, i.e., space-like, under (proper) Lorentz transformations. Indeed, if a detector would move through the Minkowski vacuum with a constant velocity that is larger than the speed of light, it would experience the quantum vacuum fluctuations as real excitations and thus it would click. In contrast to the Unruh effect, the spectrum would not be thermal – but still the detector response would be non-zero.

This phenomenon is referred to as the Ginzburg effect [153, 154] or Ginzburg radiation or the anomalous Doppler effect, even though the latter is also used to describing frequency inversion on the purely classical level. Note that – in contrast to Cherenkov radiation for a charge moving with super-luminal velocity – the Ginzburg effect is a purely quantum phenomenon which is also related to quantum friction. Obviously, the laws of special relativity prohibit observing this effect with real detectors in the real Minkowski vacuum, but one could try to realize an analogue with ultra-fast atoms moving through a dielectric medium with a reduced speed of light, for example, see, e.g., [155].

On the other hand, considering the phonon field in Bose-Einstein condensates, the comparably slow speed of sound (of order mm/s) allows us to realize an analogue of the Ginzburg effect at much smaller detector velocities, as proposed in [156]. In analogy to our discussion of the Unruh effect in Sec. 2.3.1 and the Gibbons-Hawking effect in the previous section, the detector could be realized by an atomic quantum dot, but now moving through the condensate with a constant

velocity above the sound speed. In the proposal [156], the idea is to have one “impurity” atom inside the atomic quantum dot which has two internal levels which couple differently to the density of the surrounding condensate. In contrast to the simulator for the Gibbons-Hawking effect in the previous section, there is no tunnel coupling between the atom in the condensate and the “impurity” atom inside the atomic quantum dot, but only a collisional coupling. The coupling of this “impurity” atom to the phonon modes of the condensate is then analogous to the usual dipole coupling of an atom to the electromagnetic field – which allows us to simulate phenomena such as the Casimir effect (see also Sec. 2.9) or the Ginzburg effect [156].

Nevertheless, one should also keep in mind that basically the same problems arise as in the Unruh effect since one should also take into account the disturbance caused by the “impurity” atom on the classical level. Actually, these problems might even become more pronounced here, since its super-sonic velocity opens up more classical excitation channels (think of the Landau criterion etc.).

2.7. Super-radiance and Penrose process

In order to avoid confusion, this section should start with a disclaimer: The term “super-radiance” is used in different contexts in physics and thus has no unique meaning. One important example is Dicke super-radiance [157] which refers to the amplification of spontaneous emission from an ensemble of atoms due to the constructive interference of their emission amplitudes, see also [54, 55]. That is not the subject of this section. To explain what is meant by “super-radiance” here, let us write down the effective Lagrangian \mathcal{L}_{eff} for the phonon field $\delta\phi_c$ in a given background flow determined by \mathbf{v}_c^0 and ρ_c^0 such that the Euler-Lagrange equation yields the wave equation (2.7)

$$\mathcal{L}_{\text{eff}} = \frac{1}{2} \left[\frac{m}{g_s} (\partial_t \delta\phi_c + \mathbf{v}_c^0 \cdot \nabla \delta\phi_c)^2 - \rho_c^0 (\nabla \delta\phi_c)^2 \right]. \quad (2.24)$$

This allows us to derive the canonical field momentum density $\Pi = \partial \mathcal{L}_{\text{eff}} / \partial \dot{\delta\phi}_c$ and the effective Hamiltonian density¹⁶

$$\mathcal{H}_{\text{eff}} = \Pi \dot{\delta\phi}_c - \mathcal{L}_{\text{eff}} = \frac{1}{2} \left[\frac{m}{g_s} (\partial_t \delta\phi_c)^2 + \rho_c^0 (\nabla \delta\phi_c)^2 - \frac{m}{g_s} (\mathbf{v}_c^0 \cdot \nabla \delta\phi_c)^2 \right]. \quad (2.25)$$

For stationary background flows $\mathbf{v}_c^0 = \mathbf{v}_c^0(\mathbf{r})$ and $\rho_c^0 = \rho_c^0(\mathbf{r})$, the associated effective energy $E_{\text{eff}} = \int d^3r \mathcal{H}_{\text{eff}}$ is conserved for all solutions $\delta\phi_c(t, \mathbf{r})$ of the wave equation (2.7). Now the major point here is the following: Comparison of the last two terms in the square brackets in Eq. (2.25) shows that the effective energy density could become negative for supersonic flow $|\mathbf{v}_c^0| > c_s = \sqrt{\rho_c^0 g_s / m}$. Actually, this is related to the energy balance in Hawking radiation because the in-falling partner particles carry negative effective energy E_{eff} (from the point of view of an outside observer).

For one-dimensional $\mathbf{v}_c^0 = v_c^0(x) \mathbf{e}_x$ or radial flow profiles $\mathbf{v}_c^0 = v_c^0(r) \mathbf{e}_r$, the point where the flow becomes supersonic is the horizon of the black-hole analogue. For more complex flow profiles, however, this coincidence is no longer granted. As a simple example, let us consider the draining vortex or draining “bathtub” flow (see, e.g., [158]) in 2+1 dimensions

$$\mathbf{v}_c^0 = -\frac{C}{r} \mathbf{e}_r + \frac{L}{r} \mathbf{e}_\varphi, \quad (2.26)$$

where C and L are constant. Apart from the singularity at $r = 0$, this flow is locally irrotational $\nabla \times \mathbf{v}_c^0 = 0$. The effective horizon (i.e., point of no return) is then the radius at which the radial flow velocity $|\mathbf{v}_c^0 \cdot \mathbf{e}_r| = C/r$ equals the speed of sound. However, the radius at which the total flow velocity $|\mathbf{v}_c^0|$ equals the speed of sound, i.e., where the effective energy

¹⁶Note that, for deriving the Hamilton equations, one should write down the Hamiltonian density as a function of $\nabla \delta\phi_c$ and Π instead of $\partial_t \delta\phi_c$. However, for our purposes, the form (2.25) is sufficient.

can become negative, is larger. In analogy to rotating black holes, this radius marks the beginning of the ergo-region. In this region, sound waves cannot propagate into all directions anymore, but they could still escape (unless they are already beyond the horizon).

Now one could imagine the following situation: A wave packet $\delta\phi_c(t, \mathbf{r})$ approaches the draining vortex flow (2.26) from the outside and enters the ergo-region. There, it is torn apart by the strong inhomogeneous flow profile (2.26) such that part of it falls into the horizon and the other part escapes to the outside again. Then, for certain parameters (azimuthal number and frequency) of the initial wave packet $\delta\phi_c(t, \mathbf{r})$, it is possible that the part falling into the horizon has a negative effective energy E_{eff} . Since the effective energy E_{eff} of the total solution $\delta\phi_c(t, \mathbf{r})$ is conserved, this means that the effective energy E_{eff} of the outgoing wave packet is higher than that of the initial wave packet. This amplification process is also called super-radiance – and that is the denomination we use here.

So far, the phenomenon of super-radiance discussed above refers to purely classical wave dynamics. Actually, it even has an analogue in terms of classical particles, which is the Penrose process [159] and allows us to extract energy from a rotating black hole. Furthermore, the phenomenon of super-radiance can be generalized to other scenarios such as a rotating body [160]. Generally speaking, super-radiance requires an effective energy which can become negative, some sort of scattering or tearing apart process and some mechanism to absorb the parts with negative energy. For surface waves [158], this phenomenon has actually been observed for such a vortex flow (2.26) in the Nottingham experiment [161]. Replacing the water as used in the Nottingham experiment [161] by a “photon super-fluid”, an analogous effect has been observed in the Glasgow experiment [162], see also [163] and [164].

On the other hand, as one should already expect from our discussion of Hawking radiation, this classical wave phenomenon has also a quantum counterpart. When the draining vortex flow (2.26) takes an initial (classical) wave packet and returns it with a higher energy, i.e., amplitude, it acts as an amplifier. Since the underlying evolution equation (2.7) is linear, we can transfer the results to the quantum regime, where this amplification process translates into a squeezing operation. Thus, such a quantum amplifier takes the initial quantum vacuum state and returns a squeezed, i.e., excited state, where the emitted particles are again entangled with their in-falling partners, see also [165].

2.7.1. Quantum vortices in Bose-Einstein condensates

Actually, flow profiles as in Eq. (2.26), but with $C = 0$, are naturally realized in Bose-Einstein condensates (and other super-fluids) in the form of vortices. In this case, the Bose-Einstein condensate or super-fluid “drills a hole in itself” and changes its phase by an integer multiple (which is called the winding number) of 2π when going around this hole (the vortex core) because it must end up with the same wave function. As a result, the circulation is quantized

$$\oint d\mathbf{r} \cdot \mathbf{v}_c \in \frac{2\pi\hbar}{m} \mathbb{Z}, \quad (2.27)$$

such that we have $L \in \mathbb{N}\hbar/m$ in Eq. (2.26). In this case, we do not have a horizon (because $C = 0$), but we find an ergo-region – where one would expect potentially negative effective energies. However, if we consider a singly quantized vortex with $L = \pm\hbar/m$ and calculate the radius of the ergo-region (i.e., the value of r where $|\mathbf{v}_c^0| = c_s = \sqrt{\rho_c^0 g_s/m}$) we find that it coincides with the healing length ξ as discussed in Sec. 2.1 after Eq. (2.10), i.e., the length scale below which the effective description (2.24) breaks down. This is perhaps no too surprising since we know that singly quantized vortices are stable to linear perturbations.

If we consider higher winding numbers, on the other hand, the ergo-region becomes larger and thus eventually overlaps with the region where the effective description (2.24) provides a good approximation. Hence, one may ask the question of

whether super-radiance phenomena could be found in such systems, see also [166]. This is a valid question since we know that multiply quantized vortices are unstable in the absence of additional stabilization mechanisms (such as a repulsive potential at the vortex core), see also [167, 168, 169]. As an important difference to the case studied above, there is no horizon here and thus one should wonder what happens to the negative-energy parts moving inwards. When approaching the vortex core, the condensate density ρ_c^0 drops and at some point, the linearization $\phi_c = \phi_c^0 + \delta\phi_c$ and $\rho_c = \rho_c^0 + \delta\rho_c$ breaks down. Thus, these parts may trigger non-linear processes such as the splitting of the multiply quantized vortex into several single quantized vortices – which is how the multiply quantized vortex decays. This process is somewhat analogous to the absorption of the in-falling negative-energy parts by the horizon or their absorption by some sort of dissipation. In this sense, one could relate the decay of a multiply quantized vortex to super-radiance [170, 171, 172].

Of course, it would be nice to study such super-radiance phenomena in the quantum regime – in analogy to the Technion experiment (see Sec. 2.2) devoted to Hawking radiation, for example. Unfortunately, such an experiment seems to be even harder than the Technion experiment. On the one hand, the background flow containing a multiply quantized vortex is intrinsically unstable – which complicates the experiment. On the other hand, the in-falling partners are scrambled by the non-linearity at the vortex core such that the detection method based on the correlations does also require special care. In view of these obstacles, it might be advantageous to add a radial flow component $C \neq 0$ as in Eq. (2.26) which could stabilize the flow and might help us to extract the in-falling partners. However, this would require a non-trivial (e.g., funnel like) geometry or removing condensate atoms from the core by some mechanism.

Apart from the single-component Bose-Einstein condensate considered above, one can also study super-radiance phenomena in more complex scenarios (which typically offer more options for manipulation and control) such as two-component Bose-Einstein condensates (see, e.g., [173]) or additional synthetic gauge fields (see, e.g., [174, 175]). The latter scenario displays interesting connections to the Sauter-Schwinger effect discussed in Sec. 2.8.1.

As a further outlook, the evolution (motion, re-connection etc.) of vortices in Bose-Einstein condensates is also closely related to the subject of quantum turbulence, see, e.g., [176, 177, 178, 179, 180, 181]. However, a more detailed discussion of this topic is outside the scope of the present article.

2.7.2. Quasi-normal modes

To conclude this section, let us briefly discuss a somewhat related topic, the quasi-normal modes of black holes (and their analogues). In the discussion above, we explained super-radiance via the scattering picture where an incoming wave packet is scattered at the inhomogeneous flow profile (2.26) and thus splits (or is torn apart) into an in-falling and an outgoing part. Of course, using such a scattering picture, one is led to the question of whether there are bound states – which would then affect the dynamics. Even though there are typically no real bound states in such black-hole space times, there can be quasi-bound states or quasi-normal modes.

In order to sketch the main idea by means of a simple picture, let us consider the one-dimensional Schrödinger equation in the presence of a rectangular (i.e., box) potential barrier such as $V(x) = V_0\Theta(L^2 - x^2)$. In classical mechanics, a particle with an energy $E > V_0$ starting at $x = 0$ with $\dot{x} > 0$ would just fall off the potential edge at $x = L$ and continue its propagation. In quantum mechanics, however, we have the phenomenon of quantum reflection and the particle can actually be reflected at the potential edge. Thus, we may approximate the two potential edges at $x = \pm L$ by (imperfectly) reflecting boundary conditions – where we find approximate bound state at quasi-discrete energy levels. However, since there is also a non-vanishing transmission probability at the edges, these are not exact bound state because the wave

function would slowly leak out. They are quasi-bound states or quasi-normal modes or resonances, characterized by a discrete set of frequencies with real and imaginary part. These frequencies allow us to infer properties of the potential. Roughly speaking, the spacing between the real parts tells us the potential length L while the lowest real part and the imaginary parts are related to the potential height V_0 .

Very analogous phenomena occur in other wave equations, such as that for a mass-less and minimally coupled scalar field (2.1) in the Schwarzschild metric, for example. In terms of the Regge-Wheeler tortoise coordinate r_* and after the usual separation ansatz $\phi(t, r_*, \vartheta, \varphi) = e^{-i\omega t} \phi_{\omega, \ell}(r_*) Y_{\ell, m}(\vartheta, \varphi)$, the remaining equation for $\phi_{\omega, \ell}(r_*)$ can be cast into a Schrödinger-like form with an effective potential $V_{\text{eff}}(r_*)$. In the case of gravitational waves $h_{\mu\nu}$, the underlying wave equation is a bit more complicated, but it also supports quasi-normal modes. Actually, they are related to the ring-down signal at late times which has been observed at LIGO for the black-hole merging event [182].

Even though quasi-normal modes can already be discussed on the level of purely classical wave equations, it has been speculated that they might be related to black-hole quantization, see, e.g., [183]. For this specific relation, black-hole analogues can probably not be used as a fully quantitative analogue, because they do not reproduce the Einstein equations (which are presumably important for black-hole quantization). Nevertheless, black-hole analogues can serve as a qualitative analogue for quasi-normal modes themselves, see, e.g., [184, 185, 186, 187, 188].

As a related phenomenon, one can also study modes which propagate *along* the vortex. For free vortices in super-fluids such as Bose-Einstein condensates, one important example are Kelvin waves which correspond to oscillating displacements of the vortex core. If the vortex is pinned (e.g., by a laser potential in a Bose-Einstein condensate or a wire in super-fluid Helium), one can have other phenomena such as an analogue of whispering-gallery modes which are trapped in the vicinity of the vortex and thus can only propagate along it, see, e.g., [189].

2.8. Electromagnetic fields: Sauter-Schwinger and Breit-Wheeler effect

2.8.1. Sauter-Schwinger effect

While in Hawking radiation and cosmological particle creation, the quantum vacuum fluctuations are torn apart by the strong gravitational field of the black hole or the cosmic expansion, respectively, this tearing apart is caused by a strong electric field in the Sauter-Schwinger effect [190, 191]. In the latter, the picture based on the particles and anti-particles (here electrons and positrons) works a bit better than in the former two – but the tunneling picture provides a much more adequate description (in contrast to the case of Hawking radiation). To understand why, let us first consider a massive charged (i.e., complex) scalar field ψ minimally coupled to the electrostatic potential ϕ via

$$[(\partial_t + iq\phi)^2 - \nabla^2 + m^2] \psi = 0. \quad (2.28)$$

For simplicity, let us assume that the electrostatic potential depends on x only $\phi = \phi(x)$, for example $\phi(x) = -qEx$ for a constant electric field E . This allows us to insert the ansatz $\psi(t, x, y, z) = e^{-i\omega t + ik_y y + ik_z z} \psi_\omega(x)$ into Eq. (2.28) which then simplifies to $[-(\omega - q\phi)^2 - \partial_x^2 + \mathbf{k}_\perp^2 + m^2] \psi_\omega = 0$ where the transversal wave number $\mathbf{k}_\perp^2 = k_y^2 + k_z^2$ can be absorbed into an effective mass $m_{\text{eff}}^2 = \mathbf{k}_\perp^2 + m^2$. We see that this differential equation is formally equivalent to a stationary Schrödinger equation in ordinary (non-relativistic) quantum mechanics where $-(\omega - q\phi)^2$ plays the role of the potential. E.g., for a constant electric field $\phi(x) = -qEx$, it would just be an inverted parabola. Up to a minus sign, the effective mass $m_{\text{eff}}^2 = \mathbf{k}_\perp^2 + m^2$ determines the effective energy, which is negative and thus lies below the top of the potential barrier. As a result, we have the analogue of a Schrödinger tunneling scenario where we can apply the same tools and methods as in

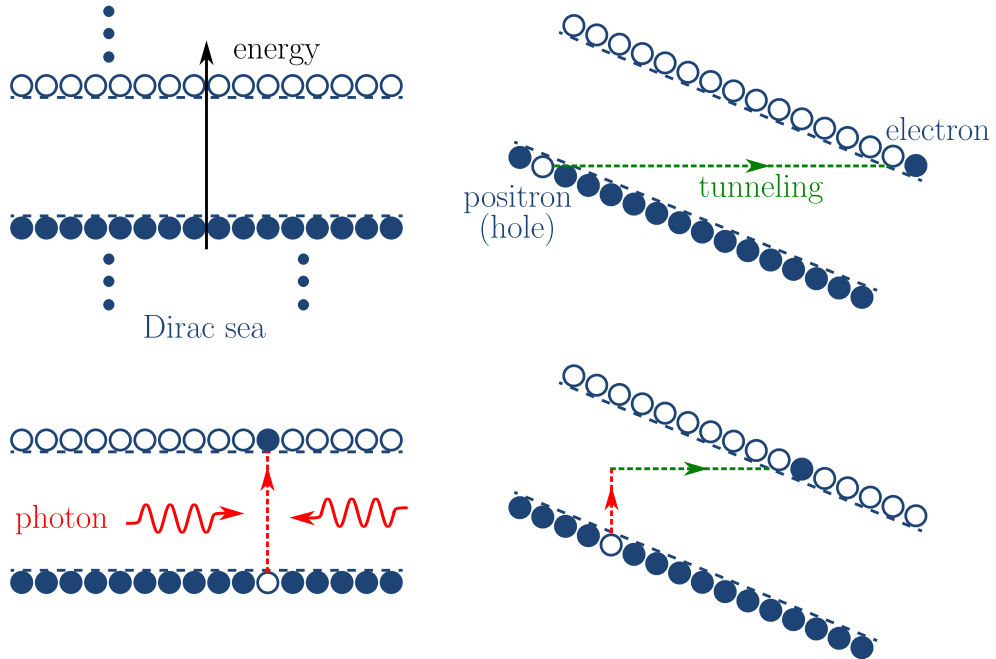


Figure 2.5: Sketch of the Dirac sea (top left) where the filled blue dots depict occupied electron states while the empty blue dots denote unoccupied states. The Sauter-Schwinger effect (top right) can then be visualized by tunneling through the classically forbidden region. In the Breit-Wheeler effect (bottom left), on the other hand, an electron is directly lifted up from the Dirac sea to the positive continuum, where the required energy is provided by photons. Finally, the dynamically assisted Sauter-Schwinger effect (or the tunnel-assisted Breit-Wheeler effect) can be understood as a combination of the two effects (bottom right).

ordinary (non-relativistic) quantum mechanics.

However, building a quantum simulator based on ultra-cold atoms for the dynamics in Eq. (2.28) may be non-trivial due to the second derivative terms. Thus, let us instead focus on the Dirac equation in 1+1 dimensions from Eq. (1.11) as already discussed in Sec. 1.2.4

$$i\partial_t \Psi = (-i\alpha\partial_x + m\beta + q\phi) \Psi = (i\sigma_y\partial_x + m\sigma_z + q\phi) \Psi, \quad (2.29)$$

again minimally coupled to the electrostatic potential $\phi(x)$. In analogy to the discussion above, this stationary problem facilitates the ansatz $\Psi(t, x) = e^{-i\omega t} \Psi_\omega(x)$ after which Eq. (2.29) simplifies to

$$\partial_x \Psi_\omega = \begin{pmatrix} 0 & q\phi - \omega - m \\ \omega - q\phi - m & 0 \end{pmatrix} \cdot \Psi_\omega = \mathbf{M}_\omega \cdot \Psi_\omega. \quad (2.30)$$

The eigen-values of the matrix \mathbf{M}_ω read $\lambda_\omega = \pm\sqrt{m^2 - (\omega - q\phi)^2}$. In complete analogy to the effective Schrödinger tunneling problem derived above from Eq. (2.28), they vanish at the classical turning points where $\omega - q\phi = \pm m$. In between these turning points (i.e., inside the potential barrier), these eigen-values are real, which corresponds to the exponential decaying (or growing) wave function in the classically forbidden region. Outside these turning points, the eigen-values are imaginary, which represents the spatially oscillating wave function in the classically allowed region.

However, as a major distinction to ordinary tunneling in non-relativistic quantum mechanics, here the tunneling occurs between the negative continuum $\omega - q\phi < -m$ (i.e., the Dirac sea) and the positive continuum $\omega - q\phi > +m$, as in Klein tunneling. Thus, we arrive at the following picture: Even in the vacuum state, the Dirac sea is filled with electrons and due to the electric field E , it can happen that one of these electrons tunnels through the classically forbidden region (i.e., the mass gap between $-m$ and $+m$) into the positive continuum, where it emerges as a real particle. Since the total

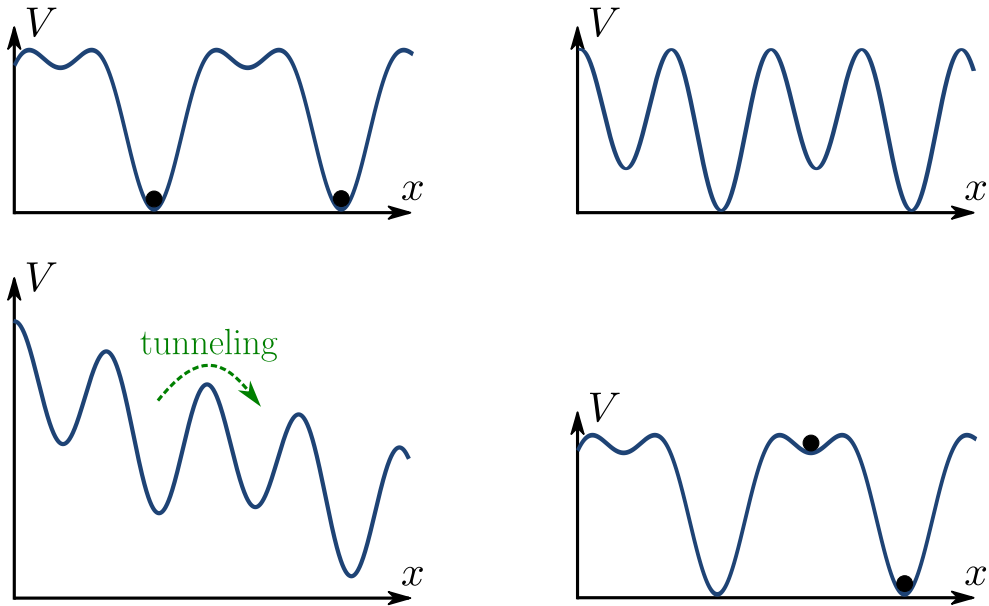


Figure 2.6: Possible sequence for an analogue of the Sauter-Schwinger effect in optical lattices, see also Fig. 1.4. Starting with a strongly bi-chromatic optical lattice (top left), one could place atoms in the energetically low even lattice sites. Then, by slowly (i.e., adiabatically) lowering the energy gap to the desired value (to right), which determines the effective mass m_{eff} in the Dirac equation (2.29), one can ensure that the upper (conduction) band in Fig. 1.4 remains empty while the lower (valence) band stays filled (and represents the Dirac sea). Then, one can apply the lattice deformation or tilt (bottom left) which simulates the external electric field E and allows the atoms to tunnel from the lower to the upper band. Finally, after reversing this sequence, atoms on the high-lying (odd) lattice sites would be the hallmark of the Sauter-Schwinger effect (bottom right).

number of fermions is conserved, it leaves behind a hole in the Dirac sea – which is then a positron. Thus, the electric field E should be able to spontaneously create electron-positron pairs out of the vacuum, as depicted in Fig. 2.5.

In order to estimate the probability for such a process, we may employ the WKB approximation and integrate λ_{ω} over x from one turning point to the other which then yields the tunneling exponent. For a constant electric field E , we find the tunneling and thus electron-positron pair creation probability

$$P_{e^+e^-} \sim \exp \left\{ -\pi \frac{m^2}{qE} \right\} = \exp \left\{ -\pi \frac{E_{\text{crit}}}{E} \right\}, \quad (2.31)$$

where $E_{\text{crit}} = m^2 c^3 / (q\hbar) \approx 1.3 \times 10^{18} \text{ V/m}$ is usually referred to as the Schwinger limit or the Schwinger critical field. Reaching such a strong field in large enough space-time volumes (such that it can be considered as approximately constant) is extremely hard¹⁷ which explains why a conclusive experimental verification of this prediction is still lacking. On the other hand, for a quantum simulator, the effective speed of light c_{eff} as well as the effective mass gap $m_{\text{eff}} c_{\text{eff}}^2$ are typically many orders of magnitude smaller – which helps us to realize a suitable analogue of this effect, see Fig. 2.6.

Note that the applicability of the WKB approximation requires that the eigen-values do not change too fast, which translates to $qE \ll m^2$, i.e., $E \ll E_{\text{crit}}$. Furthermore, the WKB approximation breaks down at the classical turning points (as usual in such tunneling scenarios). In addition, if the electric field is not constant but changes with space and/or time, the associated rate of change must be taken into account as well. Especially a time-dependence of the electric field

¹⁷Such extremely high field strengths are reached very close to highly charged nuclei, but the spatial extent of these high field strengths is too small to induce the Sauter-Schwinger effect. Otherwise, these nuclei would not be stable. Note that this phenomenon is related to the behaviour of the Dirac equation for point-like nuclei, were the energy eigen-values become complex for atomic numbers Z larger than $1/\alpha_{\text{QED}} \approx 137$.

may also lead to electron-positron pair creation – in addition to the tunneling phenomenon explained above. This brings us to the Breit-Wheeler effect [192].

2.8.2. Breit-Wheeler effect

To explain this phenomenon, let us consider a spatially homogeneous but time-dependent electric field $\mathbf{E}(t)$. In this case, it is advantageous to perform a gauge transformation¹⁸ such that the electric field $\mathbf{E}(t)$ is represented by the vector potential $\mathbf{A}(t)$. For simplicity, we again start with the complex scalar field

$$\left[\partial_t^2 - (\nabla - iq\mathbf{A})^2 + m^2 \right] \psi = 0. \quad (2.32)$$

In analogy to Eq. (2.17) in Sec. 2.4, exploiting the spatial homogeneity by an expansion into spatial plane waves $\exp\{i\mathbf{k}\cdot\mathbf{r}\}$, this equation becomes equivalent to that of a harmonic oscillator with a frequency $\Omega_{\mathbf{k}}^2(t) = [\mathbf{k} - q\mathbf{A}(t)]^2 + m^2$. Using again the analogy to the Schrödinger equation in ordinary (non-relativistic) quantum mechanics, this now corresponds to a negative effective potential – such that we have scattering above the potential (e.g., quantum reflection) instead of tunneling through the potential. The reflection and transmission coefficients then determine the Bogoliubov coefficients for this problem, which in turn yield the pair-creation probability $P_{e^+e^-}$.

However, before going into more details, let us switch back to the Dirac equation in 1+1 dimensions

$$i\partial_t \Psi = (-i\alpha\partial_x - \alpha qA + m\beta) \Psi = (i\sigma_y\partial_x + \sigma_y qA + m\sigma_z) \Psi, \quad (2.33)$$

which is more suitable for a quantum simulator. After an expansion into spatial plane waves e^{ikx} , it can be written as $i\partial_t \Psi_k = \mathbf{M}_k \cdot \Psi_k$ where the eigen-values of the matrix \mathbf{M}_k are the eigen-frequencies $\pm\Omega_k(t) = \pm\sqrt{[k - qA(t)]^2 + m^2}$. The corresponding eigen-vectors $u_k(t)$ and $v_k(t)$ represent the particle and anti-particle components and thus an expansion of the wave function into those eigen-vectors $\Psi_k = \alpha_k u_k + \beta_k v_k$ can be used to define the Bogoliubov coefficients α_k and β_k . Inserting this expansion into Eq. (2.33) and considering the ratio $R_k = \beta_k/\alpha_k$ we arrive at the Riccati equation¹⁹

$$\dot{R}_k(t) = \frac{mqE(t)}{\Omega_k^2(t)} \left(e^{2iS_k(t)} + R_k^2(t)e^{-2iS_k(t)} \right), \quad (2.34)$$

with the phase (eikonal) function $\dot{S}_k(t) = \Omega_k(t)$. For slowly varying fields $E(t)$, the solution to this equation reproduces the Sauter-Schwinger result (2.31). Rapidly varying fields, on the other hand, can open up additional channels for electron-positron pair creation. For example, if the electric field is oscillating $E(t) \propto \cos(\omega_E t)$ with a frequency ω_E in resonance with the $e^{2iS_k(t)}$ term, which requires $\omega_E \geq 2m$, we would obtain a resonant growth of $R_k(t)$ and thus β_k . In this case, we have a quadratic scaling of the pair-creation probability $P_{e^+e^-} \sim E^2$ instead of the exponential scaling (2.31).

As an intuitive picture, the frequency ω_E of the electric field can directly transfer enough energy $\hbar\omega_E$ to an electron in the Dirac sea to lift it up to the positive continuum – depicted as a vertical line in Fig. 2.5 (bottom left). In contrast, the tunneling in the Sauter-Schwinger effect for a constant electric field occurs at *constant* energy and is thus depicted as a horizontal line in Fig. 2.5 (top right). One can also have a mixture of these two effects, which is usually referred to as the dynamically assisted Sauter-Schwinger effect, see, e.g., [193]. Again using the above intuitive picture, a frequency $\omega_E < 2m$ can lift up an electron from the Dirac sea a little bit into the classical forbidden region (but not all the way up

¹⁸For lattice systems, such a gauge transformation is usually referred to as Peierls transformation or Peierls substitution. The basic idea is the same as already discussed in Secs. 1.2.4 and 1.2.6.

¹⁹Here we have used the convention that the phases $e^{\pm 2iS_k(t)}$ are absorbed into the eigen-vectors $u_k(t)$ and $v_k(t)$.

to the positive continuum) such that the remaining way to tunnel is shorter and thus the tunneling exponent (2.31) is reduced, see Fig. 2.5 (bottom right).

One might object that the case of a purely time-dependent electric field considered above is un-physical (e.g., because it is not a vacuum solution of the Maxwell equations). While this is a valid point, it does not spoil the analysis of the Sauter-Schwinger or Breit-Wheeler effect, which are a consequence of the Dirac (2.33) or Klein-Fock-Gordon (2.32) equations and *per se* independent of the Maxwell equations. E.g., if \mathbf{A} would instead be a Proca field, the solutions of the Dirac (2.33) or Klein-Fock-Gordon (2.32) equations (for the same \mathbf{A}) would not change. This situation is a bit similar to the case of Hawking radiation discussed in Sec. 2.2, which can be derived from the Klein-Fock-Gordon equation (2.1) in a given background metric, but does not require this metric to be a vacuum solution of the Einstein equations.

Coming back to the Sauter-Schwinger and Breit-Wheeler effect, another way to resolve the objection above is to consider the collision of two plane-wave laser pulses (which are vacuum solutions of the Maxwell equations). Then it can be shown [194] that electron-positron pair creation is dominated by the field at the collision point and that the local pair-creation probability (density) can be well approximated by the scenario of a purely time-dependent field.

2.8.3. Quantum simulator for Sauter-Schwinger and Breit-Wheeler effect

As already explained in Sec. 1.2.4, the 1+1 Dirac Hamiltonian (1.11) can modeled by fermionic atoms in a bi-chromatic optical lattice, see Fig. 1.4. Quite intuitively, an electric field can then be simulated by applying a force to the atoms in the lattice – such that we arrive at a quantum simulator as sketched in Fig. 2.6, see also [75, 76]. The bosonic²⁰ analogue of such a simulator has been realized in another experiment [195] at Maryland (not to be confused with the expanding Universe simulator [150]). Since the bosonic (Rubidium) atoms used in this experiment [195] do not obey the Pauli principle, one does not have the precise analogue of the Dirac sea as sketched above. Therefore, the experiment [195] instead created an initial state where all the states in the lower band (which would correspond to the Dirac sea) were occupied by some bosons (with a certain probability) while the upper band was still empty. To ensure that the upper band was not excited in this initialization process, they started with a large gap, as in Fig. 2.6 (top left), and later adiabatically reduced it to the desired value, as in Fig. 2.6 (top right), thereby enabling tunneling transitions from the lower band to the upper band, i.e., the analogue of the Sauter-Schwinger effect²¹.

So far, in the considerations in this section, the gauge field has been treated as an external field, i.e., the back-reaction of the created electron-positron pairs onto the electric field was not included, see also the discussion in Sec. 1.2.6. A very first step into this direction could be the combined quantum simulator sketched in Fig. 1.6 which corresponds to the coupled field theory in Eq. (1.16). More elaborated schemes have been discussed as well, see, e.g., [197, 198, 199, 200] as well as the references mentioned in Sec. 1.2.6. However, they are already beyond the realm of linear fields as discussed in this chapter, but belong to the class of non-linear fields considered in the next chapter 3. In this context, it might also be worth mentioning here that the mass gap m_{eff} can also be generated (instead of using a bi-chromatic lattice) by the interaction U between the atoms in Eqs. (1.7) and (1.8), see also [201, 202] and references therein.

²⁰Due to the Pauli principle, bosonic atoms can be cooled down much better than fermionic atoms.

²¹As one might expect, tunneling from the valence band to the conduction band as an analogue of the Sauter-Schwinger effect is not restricted to ultra-cold atoms, similar effects can also occur in other systems, such as semi-conductors, see, e.g., [196] and references therein.

2.9. Dynamical Casimir effect

To conclude this chapter, let us briefly discuss the dynamical Casimir effect, see, e.g., [203] for a review of recent developments. While the original Casimir effect [204] refers to the attraction of two parallel mirrors in vacuum and related phenomena, i.e., static situations, the dynamical Casimir effect typically denotes generalizations to the time-dependent case, see, e.g., [205]. Even though there are also alternative derivations, the static (i.e., original) Casimir effect can be explained by the modification of the quantum vacuum fluctuations by the presence of the two mirrors (or analogous external conditions, such as dielectric media). This modification changes (reduces) the vacuum energy which then results in an attraction between the mirrors.

In order to visualize this attractive force, it is sometimes argued that there are less modes allowed in between the mirrors than outside – and that, therefore, the vacuum energy must be smaller. While it is correct that there are less allowed modes in between the mirrors (perpendicular to the mirrors, we have a discrete spectrum inside but a continuous spectrum outside), this picture is oversimplified: Even though there are less modes, they have a higher weight and thus the calculation of the vacuum energy requires a subtle subtraction procedure (where the infinite vacuum energy cancels). The failure of the above oversimplified arguments can be illustrated by comparing different boundary conditions at the mirrors. While two mirrors with the same boundary conditions (e.g., both Dirichlet or both Neumann) indeed attract each other, two different mirrors, one with Dirichlet and one with Neumann boundary conditions, repel each other. Similarly, two dielectric or two paramagnetic media typically attract each other while a dielectric and a paramagnetic medium tend to have a repulsive Casimir force.

After this detour to the static Casimir effect, let us turn to the dynamical Casimir effect. Using the example of the two parallel mirrors, one could now imagine moving one or both of them. In this way, one should be able to create pairs of particles (in this case, photons) out of the initial vacuum state. There are two main contributions to this phenomenon. First, the squeezing effect stemming from the change of the distance between the mirrors (or, more precisely, the variation of the eigen-frequencies), which results in single-mode squeezing – analogous to the parametrically driven harmonic oscillator as in Eq. (2.17). Second, the acceleration effect is induced by the motion of the mirrors and results in multi-mode squeezing, see, e.g., [206]. Even if we consider a single moving mirror, we could still have the second effect (but not the first one) such that we could also emit pairs of particles.

If we consider a cavity with a finite volume instead, we may enhance the effect by harmonically oscillating one (or more) of the mirrors where the driving frequency matches twice one of the discrete eigen-frequencies of the cavity such that we achieve parametric resonance in this mode according to Eq. (2.17). In this way, it may be possible to resonantly select one mode in which the pairs are predominantly created via the squeezing effect while the other modes and the acceleration effect can be neglected since they are off-resonant.

As a generalization, one could also imagine a cavity filled with some dielectric medium whose index of refraction is modulated. Even if there is no real motion of the mirrors encapsulating the cavity, the effective distance “felt” by the electromagnetic field (i.e., the light travel time) changes and thus it should not be surprising that one can also create pairs of particles in this case. Actually, even without any mirrors, a temporal $n(t)$ or spatio-temporal $n(t, \mathbf{r})$ change of the refractive index can create pairs of particles. In order to accommodate all these scenarios, one could associate the dynamical Casimir effect to the creation of pairs of photons (or other particles) out of the vacuum (or ground state) induced by time-dependent external conditions, which could be mirrors or media with an index of refraction. However, it is fair to say that probably not everybody in the community would fully agree to this definition.

As a result, although the static Casimir effect has been verified experimentally (see, e.g., [207]), the situation for the dynamical Casimir effect is more complicated. The analogue of the dynamical Casimir effect has been observed in the Gothenburg [208] and Helsinki [209] experiments in time-dependent electromagnetic wave guides²², but a conclusive verification of photon pair creation due to the real motion of a mirror in vacuum remains yet to be observed. As another point, one could argue that the well-known phenomenon of parametric down conversion in non-linear optical media can be interpreted as the creation of photon pairs by a spatio-temporal change of the refractive index $n(t, \mathbf{r})$.

Depending on which aspects are deemed to be more important and which less, the dynamical Casimir effect can be related to many of the phenomena discussed above. Thus, it is not so easy to draw a clear and unique separation line between the dynamical Casimir effect (or its analogues) and the signatures of the Unruh effect, Hawking radiation or cosmological particle creation (and their analogues). For example, a purely time-dependent refractive index $n(t)$ is very analogous to cosmological particle creation discussed in Sec. 2.4. In this case, photons are also created in pairs with opposite momenta and the underlying evolution equation for a single mode is formally equivalent to Eq. (2.17). In view of this formal equivalence, it is perhaps not surprising that the paper reporting on the Palaiseau experiment [56] was referring to the dynamical Casimir effect instead of cosmological particle creation.

As a more involved scenario, one could also consider a space-time dependent refractive index $n(t, \mathbf{r}) = n(\mathbf{r} - \mathbf{v}t)$ moving with a constant velocity \mathbf{v} . If this velocity \mathbf{v} is smaller than the speed of light inside the entire medium, no photons would be created. If it is faster (e.g., generated by a flying laser focus in a non-linear Kerr medium), one could create signatures of the Ginzburg effect discussed in Sec. 2.6. If this velocity \mathbf{v} lies in between the medium speed of light of the regions with large n and small n , one could obtain an optical or dielectric black-hole analogue and create the analogue of Hawking radiation discussed in Sec. 2.2, see, e.g., [210, 211, 212, 213, 214, 215]. A refractive index $n(t, \mathbf{r}) = n(\mathbf{r} - \mathbf{r}_D[t])$ moving along an accelerated trajectory $\mathbf{r}_D[t]$, on the other hand, could create (in addition to the effects mentioned above) signatures of the Unruh effect discussed in Sec. 2.3.

In summary, we see that quantum electrodynamics in media with space-time dependent refractive indices $n(t, \mathbf{r})$, moving dielectric bodies or flowing dielectric fluids is a very rich field and offers many fascinating phenomena – where it is not always easy to draw a clear line between the different effects, see also [216]. As in Bose-Einstein condensates (2.10), it is also important to take into account the dispersion relation, see, e.g., [218] and references therein. Furthermore, remembering the Kramers-Kronig relations, one should also investigate the impact of dissipation on those phenomena, see also [217]. Note that such dissipative effects are also present in Bose-Einstein condensates, e.g., in the form of three-body losses (see, e.g., [39, 40]) and should there be investigated as well.

²²Electromagnetic wave guides with suitable properties could also be used to generate the analogue of Hawking radiation, see also [210].

3. Non-linear fields

After having discussed several effects of linear fields (propagating on non-trivial backgrounds), let us turn our attention to fields which obey inherently non-linear evolution equations. Of course, for all the phenomena discussed in the previous chapter, one can ask the question of how they change for non-linear fields, i.e., in the presence of interactions. For example, the Coulomb attraction between electrons and positrons should affect their creation via the Sauter-Schwinger or Breit-Wheeler effect, see Sec. 2.8. As another example, one would expect that small black holes with a Hawking temperature far above the QCD scale $\Lambda_{\text{QCD}} = \mathcal{O}(100 \text{ MeV})$ emit quasi-free quarks and gluons, which only later (outside the black hole) combine to hadrons. For larger black holes with a Hawking temperature below the QCD scale $\Lambda_{\text{QCD}} = \mathcal{O}(100 \text{ MeV})$, on the other hand, this behaviour should change drastically due to confinement. Confirming this expectation by solid calculations, however, is a highly non-trivial task.

Even though these are very interesting and important questions – which could, at least qualitatively, be addressed with quantum simulators, see also chapter 4 – the next sections instead focus on new phenomena caused by non-linearities of the field equations.

3.1. Sine-Gordon model

An important example for a non-linear field theory is the sine-Gordon model as described by the Lagrangian density

$$\mathcal{L} = \frac{1}{2g_\phi^2} [(\partial_t\phi)^2 - (\partial_x\phi)^2 + 2\cos\phi] . \quad (3.1)$$

Although the pre-factor g_ϕ is not relevant for the classical equation of motion $\square\phi + \sin\phi = 0$, it does play a role for the associated quantum field theory or thermal field theory since it is then combined with the Planck constant \hbar or the temperature, respectively. Note that g_ϕ can be identified with a coupling strength. To see that, let us consider a field re-definition $\phi \rightarrow g_\phi\phi$ after which the pre-factor disappears and the potential terms is modified to $\cos(g_\phi\phi)$. Taylor expanding this term for small g_ϕ , we see that the theory approaches a free field in the limit $g_\phi \rightarrow 0$.

Let us first discuss the classical field theory. The sine-Gordon model (3.1) combines at least three important features. First, it is relativistic, i.e., invariant under Lorentz transformations. Second, it is integrable (in 1+1 dimensions). Third, it is invariant under the symmetry $\phi \rightarrow \phi + 2\pi$ and displays topological properties. This combination entails several interesting consequences. For example, the sine-Gordon model (3.1) supports soliton solutions in the form of kinks and anti-kinks. These are topological defects which connect the asymptotic field values $\phi(x \rightarrow -\infty) = 0$ and $\phi(x \rightarrow +\infty) = 2\pi$ for kinks or $\phi(x \rightarrow -\infty) = 0$ and $\phi(x \rightarrow +\infty) = -2\pi$ for anti-kinks – both modulo global shifts $\phi \rightarrow \phi + 2\pi$ due to the aforementioned symmetry. Note that the difference between these asymptotic values $\phi(x \rightarrow -\infty)$ and $\phi(x \rightarrow +\infty)$ corresponds to the topological charge or winding number multiplied by 2π . Due to the Lorentz invariance of the sine-Gordon model (3.1), these kinks and anti-kinks obey the relativistic energy-momentum relation $E^2 = m^2 + p^2$ and thus can be viewed as toy models for relativistic particles. Moreover, the sine-Gordon model (3.1) facilitates simple analytic expressions (in terms of the inverse tangent and exponential functions) for single or even multiple solitons. These could be scattering solutions where the solitons just go through each other and even bound-state solutions (breathers).

Upon quantization, the sine-Gordon model (3.1) becomes more complicated. Apart from the non-trivial structure of the vacuum state, the spectrum contains single-particle states as described by the same relativistic energy-momentum relation $E^2 = m^2 + p^2$ as in the classical case (with suitably renormalized values). The states with two or more particles are more involved due to their interaction – which is the usual case in interacting quantum field theories. Instead of the

eigen-states of the Hamiltonian, let us consider the n -point functions $\langle \hat{\phi}(t_1, x_1) \dots \hat{\phi}(t_n, x_n) \rangle$ in the vacuum state. They allow us to calculate the S -matrix or the generating functional, for example. For the case of a free (linear) field, the vacuum state is a Gaussian state and hence the Wick theorem allows us to express all n -point functions as a sum of products of two-point functions. For interacting quantum field theories, on the other hand, this is no longer true and the deviations from a Gaussian state depend on the parameters of the model, such as g_ϕ . Turning this argument around, these deviations from Gaussianity, i.e., the “error” in the Wick expansion, can be used to infer those parameters.

To conclude this brief introduction into the sine-Gordon model, it should be mentioned here that it is equivalent (in a certain region of parameter space, see [219]) to the massive Thirring model [220] describing fermions in 1+1 dimensions with a four-fermion interaction term

$$\mathcal{L} = \bar{\Psi} (i\gamma^\mu \partial_\mu - m) \Psi - \frac{g_\Psi}{2} (\bar{\Psi} \gamma^\mu \Psi) (\bar{\Psi} \gamma_\mu \Psi) . \quad (3.2)$$

Generalizing this ansatz to more than one fermion species Ψ_a and replacing the interaction term by $(\bar{\Psi}_a \Psi^a)(\bar{\Psi}_b \Psi^b)$, one obtains the Gross-Neveu model [221]. As usual in such bosonization approaches (think of the Jordan-Wigner transformation of the quantum Ising model, for example), the mapping between the fermionic degrees of freedom in the Thirring model (3.2) and the bosonic degrees of freedom in the sine-Gordon model (3.1) is non-local in space and works in this way in one spatial dimension only.

3.1.1. Analogues for the sine-Gordon model

In view of the equivalence between the sine-Gordon model (3.1) and the Thirring model (3.2), let us start with ultracold atom simulators for the latter. As already explained in Sec. 1.2.4, the bi-linear part of the Dirac Hamiltonian in Eq. (3.2), i.e., the free-field contribution, can be modeled with fermionic atoms in bi-chromatic optical lattices. In this representation, the remaining interaction terms $(\bar{\Psi} \gamma^\mu \Psi)(\bar{\Psi} \gamma_\mu \Psi)$ in the Thirring model or that of the Gross-Neveu model $(\bar{\Psi}_a \Psi^a)(\bar{\Psi}_b \Psi^b)$ can be modeled by suitable on-site interaction terms between the different species such as the U term in the Fermi-Hubbard model (1.8), see also [74]. As another possibility, a Boson-Fermion interaction as sketched in Fig. 1.6 could generate, after integrating out the bosonic degrees of freedom, to an effective four-Fermion interaction, as explained after Eq. (1.16). By arranging the lattice representation in a suitable way, one could then generate the desired structure of the interaction term.

However, since bosonic atoms can be cooled down much easier than fermionic atoms (due to the Pauli principle), let us now turn to the original sine-Gordon model (3.1). One way of simulating this model could be a lattice of Rydberg atoms as sketched in Fig. 1.5 with a harmonic on-site potential V which can be obtained by a standing wave laser field in z direction (i.e., along the q_I). Another option has been realized in the Vienna experiment [222, 223, 224, 225] where two effectively one-dimensional Bose-Einstein condensates were generated parallel to each other at a small distance such that the atoms could still tunnel from one condensate to the other. Then, the dynamics of the phase difference between the two condensates can be approximately described by the sine-Gordon model (3.1). As an intuitive picture, the atoms can most efficiently reduce their energy by tunneling between the two condensates if they have the same phase (modulo 2π) which explains the $\cos(\phi)$ potential in Eq. (3.1). In order to measure the relative phase (as a function of x , i.e., the coordinate along the effectively one-dimensional Bose-Einstein condensates), one can release the condensates (in analogue to the time-of-flight technique sketched in Sec. 1.2.2) and let them interfere. Then, taking a picture of the resulting pattern, the measured interference fringes allow us to reconstruct the relative phase, cf. [222, 223, 224, 225].

Having realized such a simulator for the sine-Gordon model (3.1), one could first study its classical solutions such as kinks and anti-kinks and how they go through each other (as in Newton’s cradle, see also [226]). Going to the quantum regime, one can also study n -point functions $\langle \hat{\phi}(t_1, x_1) \dots \hat{\phi}(t_n, x_n) \rangle$, how they deviate from a Gaussian state (i.e., the “error” in the Wick expansion), and how this deviation is related to the effective Lagrangian (3.1), cf. [222, 223, 224]. In addition to the correlation between different space-time points $(t_1, x_1) \dots (t_n, x_n)$, one can also study the correlation between two (or more) regions A and B by considering the von Neumann entropy of the reduced density matrix of these regions S_A , S_B and $S_{A \cup B}$, see also [225].

Note that the schemes for experimental realization mentioned above are not the only ones. As another possibility, the Innsbruck experiment [227] realized the sine-Gordon model (3.1) in a suitable limiting case of an optical lattice realizing the Bose-Hubbard Hamiltonian (1.7) in one spatial dimension.

3.2. Kibble-Zurek mechanism

The Kibble-Zurek mechanism [228, 229, 230, 231] refers to the creation of topological defects in symmetry-breaking phase transitions. Before turning to their creation mechanism, let us briefly discuss the concept of topological defects, where we focus on classical fields for the moment. Examples for topological defects are the kinks and anti-kinks discussed in the previous section, as well as vortices in Bose-Einstein condensates discussed in Sec. 2.7.1. Generally speaking, topological defects can occur in a phase of broken symmetry where the ground state is not unique but we have a set or manifold of ground states. In such a case, the vacuum would be a state with the same position in the ground-state manifold everywhere – often called the order parameter. A topological defect is then an inhomogeneous deviation from this homogeneous vacuum state where different spatial points assume distinct order parameters such that smooth deformations of the order parameter cannot transform the defect away (i.e., it is topologically protected).

As a rule of thumb²³, topological defects can be characterized by the dimension D_{gs} of the ground-state manifold in the broken-symmetry phase and the space-time dimension D_{st} , which then determine the dimensionality D_{td} of possible topological defects via $D_{\text{td}} = D_{\text{st}} - D_{\text{gs}} - 2$. Kinks and anti-kinks in the sine-Gordon model (3.1) correspond to a breaking of the discrete \mathbb{Z} symmetry $\phi \rightarrow \phi + 2\pi\mathbb{Z}$ such that ground-state manifold is discrete, i.e., zero-dimensional $D_{\text{gs}} = 0$. Thus, in 1+1 dimensions $D_{\text{st}} = 2$, they are point-like defects (i.e., also zero-dimensional) $D_{\text{td}} = 0$. In 2+1 dimensions $D_{\text{st}} = 3$, they would be line-like defects (i.e., one-dimensional) $D_{\text{td}} = 1$, and so on. As our second example, vortices in Bose-Einstein condensates correspond to a breaking of the $U(1)$ symmetry of the original Hamilton (1.4) by the phase of the condensate wave function ψ_c . Thus, the ground-state manifold is one-dimensional, i.e., a circle, $D_{\text{gs}} = 1$. As already discussed in Sec. 2.7.1, a vortex is a point-like defect $D_{\text{td}} = 0$ in 2+1 dimensions $D_{\text{st}} = 3$ and a line-like defect $D_{\text{td}} = 1$ in 3+1 dimensions $D_{\text{st}} = 4$. As an intuitive picture, if we encircle a (singly quantized) vortex in real space, the phase (i.e., order parameter) describes a circle in order-parameter space. For multiply quantized vortices, the phase would wind around the circle in internal space several times, where the number of revolutions corresponds to the winding number, i.e., the topological charge.

When investigating possible symmetry-breaking phase transitions in the early Universe, Kibble [228, 229] found that they could entail the creation of such topological defects – which might (due to their topological protection) still be present today, for example in the form of cosmic strings. In spite of extensive search for such objects, their existence has not been

²³A more rigorous approach can be based on homotopy groups or homotopy classes.

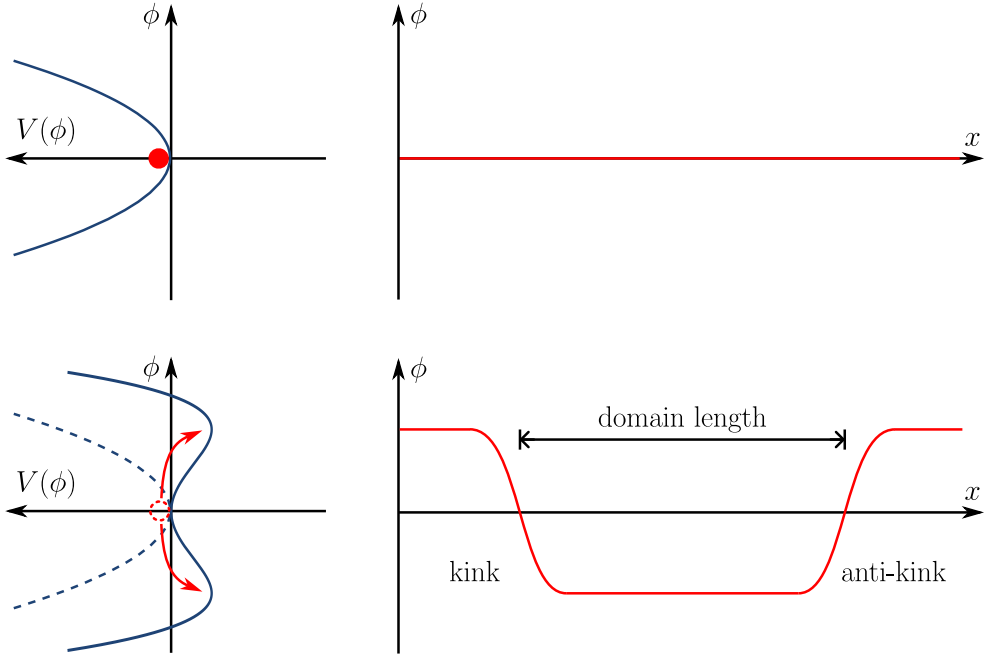


Figure 3.1: Schematic of the Kibble-Zurek mechanism for the example of a 1+1 dimensional real scalar field (3.3).

conclusively confirmed (yet). Later on Zurek [230, 231] realized that an analogous mechanism should also be possible in symmetry-breaking phase transitions in condensed matter, e.g., in Helium. As an important point, the response time of the system diverges when approaching the critical point, which facilitates the observation of non-equilibrium phenomena such as the creation of topological defects. Note that the condensed-matter systems do typically not obey precisely the same equations of motion as the fields in the early Universe, such that we do not have an exact quantitative analogy – instead the qualitative features such as symmetry-breaking phase transitions with diverging response times (where the scaling depends on the universality class) are reproduced.

In order to explain the main idea of the Kibble-Zurek mechanism, let us consider the simple example of a real scalar field ϕ in 1+1 dimensions with a double-well potential, see also Fig. 3.1

$$\mathcal{L} = \frac{1}{2} [(\partial_t \phi)^2 - (\partial_x \phi)^2 + c_2 \phi^2 - c_4 \phi^4]. \quad (3.3)$$

Symmetry-breaking phase transitions are often realized via decreasing the temperature. However, according to the theme “quantum simulators”, let us consider zero-temperature phase transitions or quantum phase transitions instead, where an external parameter is varied rather than the temperature²⁴. In this case (3.3), changing c_2 with time brings us from the symmetric phase $c_2 < 0$ with one potential minimum at $\phi = 0$ to the broken-symmetry phase $c_2 > 0$ with two potential minima at $\phi = \pm\sqrt{2c_4/c_2}$ (assuming $c_4 > 0$). Now, if we start in the symmetric phase $c_2 < 0$ with $\phi = 0$ and imagine increasing c_2 infinitely slowly, the system would stay in the ground state and thus has to “choose” one of the two minima (either left $\phi = -\sqrt{2c_4/c_2}$ or right $\phi = +\sqrt{2c_4/c_2}$) when passing the critical point at $c_2 = 0$. However, when traversing the critical point with a finite velocity, the system has not enough time to “communicate” its choice to all other spatial positions and thus it could be that it chooses the left minimum at one point but the right minimum at some other point. As a result, there must be at least one topological defect in the form of a kink in between these two points. If there

²⁴In this way, we also avoid problems due to the Mermin-Wagner theorem [232].

happens to be an anti-kink close to a kink, the two can annihilate each other in the subsequent course of time²⁵ but topological defects well separated from others would be long lived.

Since the Kibble-Zurek mechanism itself already refers to laboratory analogues of cosmological phenomena, it is probably redundant to speak of an analogue. There have been various experimental realizations, especially in the classical regime (e.g., in thermal phase transitions). Besides Helium (see, e.g., [233, 234]) as the system originally envisaged by Zurek [230], defect creation has been observed in several scenarios, including liquid crystals, non-linear optical systems, and superconductors etc., see also [235]. Consistently with our topic and in order to avoid spreading out too much, let us focus on ultra-cold atoms. As in the previous Section, one option would be to use a lattice simulator as sketched in Fig. 1.5, which directly models the Lagrangian (3.3) and would allow us to study the formation of kinks and anti-kinks, see Eq. (1.14) in Sec. 1.2.5. On the other hand, vortices in Bose-Einstein condensates are also topological defects (as discussed above) and vortex formation in Bose-Einstein condensates consistent with the Kibble-Zurek mechanism has already been observed [236, 237] in different geometries, e.g., harmonic (i.e., simply connected) and toroidal (i.e., ring). Going from the case of higher dimensions to very elongated, i.e., effectively one-dimensional, condensates, one would have kinks instead of vortices and their creation has also been observed [238]. If we have more than one species of atoms, e.g., spinor or multi-component condensates, the effective spin can play the role of the order parameter (instead of the $U(1)$ breaking phase of the wave function) and the formation of the associated topological defects in such systems has also been observed [239, 240]. As a completely different scenario, one could replace the bosonic atoms by fermionic ones. Of course, they cannot directly form a Bose-Einstein condensate, but two Fermions can combine to a Cooper pair, which can then condense to the analogue of a super-conducting state. This super-conducting state can also support vortices – which facilitate the Kibble-Zurek mechanism [241, 242].

A completely different kind of phase transition has been realized [48] with Rydberg atoms where two effects compete with each other. On the one hand, an external optical laser induces (detuned) Rabi oscillations between the ground state level and the highly excited Rydberg level of these atoms. In terms of the quantum Ising model, this would correspond to an on-site σ_I^x term. On the other hand, two atoms I and J in the highly excited Rydberg state experience the van-der-Waals interaction, which translates to a $\sigma_I^z \sigma_J^z$ contribution in terms of the quantum Ising model. (The remaining on-site σ_I^z terms can be canceled by suitably choosing the detuning.) The competition between these two contributions, similar to a local magnetic field in x direction σ_I^x versus the (anti) ferromagnetic interaction $\sigma_I^z \sigma_J^z$ induces a symmetry-breaking quantum phase transition.

Having realized such a (quantum) simulator for the Kibble-Zurek scenario, one can study several interesting questions. As one example, one can investigate the number density of the created topological defects (e.g., the inverse domain length in Fig. 3.1) depending on the transition velocity, such as \dot{c}_2 in the case discussed above. For sufficiently slow transitions (which are still non-adiabatic because the response time diverges at the critical point), one would usually expect the Kibble-Zurek scaling $\propto \dot{c}_2^{\nu/(1+z\nu)}$ which is based on the idea to employ the equilibrium critical exponents (i.e., the critical exponent ν for the correlation length and the dynamical exponent z for the response time) to infer non-equilibrium properties such as the created defect density. For faster transitions, however, there could be deviations from this behaviour (see, e.g., [243] and references therein). Apart from their pure number (density), the correlations between the created

²⁵Note that this is not possible for the sine-Gordon model (3.1) since this model is integrable and thus kinks and anti-kinks would just go through each other or form stable bound states. This shows that topological defects and solitons are not always the same – even though these terms are sometimes mixed up.

defects is also an interesting question. For the simple \mathbb{Z}_2 breaking case of the double-well potential in Eq. (3.3) and Fig. 3.1, it is obvious that one can only have a kink and an anti-kink beside each other. For other systems, however, such as the \mathbb{Z} breaking case of the $\cos\phi$ potential in the sine-Gordon model (3.1), one can have two kinks or two anti-kinks beside each other – and thus the question of their correlations becomes more interesting. Going to higher dimensions, one can ask an analogous question regarding the correlation between (anti) vortices in Bose-Einstein condensates (created by the Kibble-Zurek mechanism), which correspond to a breaking of the $U(1)$ symmetry. As one possible measure, these correlations would determine how the expectation value of the total winding number squared²⁶, after going around a circle (which may encompass several vortices and anti-vortices), scales with the radius of this circle. These questions can be generalized to other broken symmetries and higher dimensions, where it is also interesting to investigate the difference in scaling between topological defects and other quasi-particles (e.g., phonons in Bose-Einstein condensates) created by traversing the critical point, see, e.g., [244, 245, 246] and references therein.

3.3. False-vacuum decay

Another interesting phenomenon where we can apply many of the concepts discussed above is false-vacuum decay [247, 248]. Again, let us explain the main idea by means of a very simple model, the real scalar field in 1+1 dimensions

$$\mathcal{L} = \frac{1}{2} [(\partial_t \phi)^2 - (\partial_x \phi)^2] - V(\phi), \quad (3.4)$$

but now with a slightly different potential $V(\phi)$. As in the double-well potential (3.3), let us assume that $V(\phi)$ possesses two local minima – which are, however, no longer degenerate but slightly differ in depth by ΔV . One possibility would be to add a small linear term $c_1 \phi$ to the double-well potential (3.3). The global (i.e., lower) minimum is then referred to as the true vacuum while the other (local) minimum is called the false vacuum, see Fig. 3.2.

Now let us imagine that we initialize the system in the false vacuum at all positions x . Similar to the Kibble-Zurek mechanism discussed in the previous section, this could happen via a change of the potential landscape $V(\phi)$ in the early Universe (then in 3+1 dimensions, of course) after which one could end up in a local minimum instead the global one, i.e., the true vacuum. However, in contrast to the scenario of the Kibble-Zurek mechanism which is analogous to a second-order (symmetry-breaking) phase transition, this change of the potential landscape $V(\phi)$ would correspond to a first-order phase transition²⁷. Even though the false vacuum is not the lowest-energy state, it can be a metastable state – in analogy to supercooled or undercooled water which can stay liquid after cooling it down carefully below the freezing temperature. Taking the analogy even further, the transition or decay to the real ground state (such as the freezing of the water) does typically not occur homogeneously, but in the form of expanding domains which require a nucleation seed. For the model (3.4), this seed would be a kink and an anti-kink at a sufficient distance L such that energy gain $L\Delta V$ in the region given by this distance is large enough to compensate the energy cost of creating the kink and anti-kink. In the absence of external perturbations (such as sticking a spoon into the supercooled water) this kink–anti-kink pair could be created by tunneling through the potential barrier or by quantum vacuum (or thermal) fluctuations which happen to conspire such that the field can climb over the potential barrier on a sufficiently large length L . Comparing this kink–anti-kink pair creation to the Sauter-Schwinger effect discussed in Sec. 2.8.1 we find several similarities. After the kink–anti-kink pair has been created, it can mediate or catalyze the transition to the true vacuum by expanding, i.e.,

²⁶The expectation value of the total winding number itself must vanish due to symmetry.

²⁷Note that this important distinction bears similarities to the case of adiabatic quantum algorithms discussed in Sec. 1.1.2.

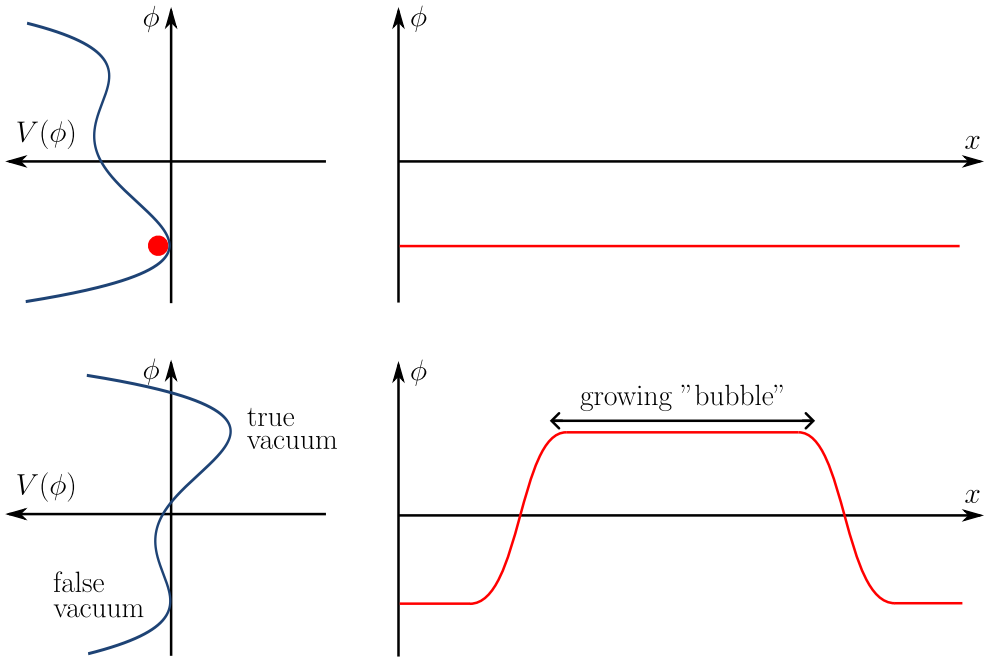


Figure 3.2: Sketch of false-vacuum decay for a 1+1 dimensional scalar field (3.4). Initially (top), the field ϕ sits in the true ground state, i.e., the global minimum of the potential $V(\phi)$. After this potential has been deformed (bottom), however, this field value is no longer the global minimum, but only a local minimum – i.e., the false vacuum. In order to go to the true minimum, the field forms a “bubble” which must be large enough such that the energy gained inside the bubble compensates the energy cost of the kink and the anti-kink at its boundary.

increasing the distance (similar to the electron-positron pairs in the Sauter-Schwinger effect which move way from each other after their creation).

In 2+1 (or 3+1) dimensions, this nucleation seed would be an expanding bubble of the true vacuum state surrounded by a domain of the false vacuum. In this case, the energy gain given by ΔV times the bubble area (or the bubble volume) should be large enough to compensate the energy cost of the domain boundary which scales with the bubble radius (or the bubble surface area), see Fig. 3.2.

As we have seen in the undercooled water example discussed above, there are everyday analogues to false-vacuum decay – at least in the classical regime. Therefore, let us focus on ultra-cold atoms. Similar to the previous sections, the correspondence between Eq. (3.4) above and Eq. (1.14) in Sec. 1.2.5 shows that one way to model false-vacuum decay could be the lattice simulator sketched in Fig. 1.5. Going from the lattice to the continuum case, there have been several proposals for quantum simulators based on multi-component or spinor Bose-Einstein condensates under the influence of an external drive (e.g., microwave radiation), see, e.g., [249, 250, 251, 252, 253, 254, 255, 256, 257, 258]. Such an external drive can generate new minima of effective potential and thereby generate a potential landscape as in Fig. 3.2. The emergence of a new potential minimum in driven systems can be visualized by an example from classical mechanics, the Kapitza pendulum. If its pivot point oscillates vertically sufficiently fast and with large enough amplitude, then the stable configuration would be that the pendulum points up instead of down (this phenomenon is also referred to as “dynamical stabilization”). In systems with more degrees of freedom such as Bose-Einstein condensates, one has to make sure that the external drive does not generate additional instabilities, e.g., acts as a seed for the decay of the false vacuum (similar to sticking a spoon into undercooled water). On the other hand, it has also been suggested to introduce such a seed in a controlled way, e.g., in the form of a vortex in the Bose-Einstein condensate [259]. Similar to the Kibble-Zurek mechanism discussed in the previous section, a different realization could be based on Rydberg atoms, see, e.g., [260].

An important step into the direction of simulating false-vacuum decay in the laboratory is the Trento experiment [261] where an elongated (cigar shaped) spinor Bose-Einstein condensate has been realized. In analogy to the Vienna experiment [222, 223, 224, 225], one may split up the degrees of freedom into the total density $\rho_+ = \rho_\uparrow + \rho_\downarrow$ (and phase) components plus density (and phase) differences $\rho_- = \rho_\uparrow - \rho_\downarrow$, which represent the pure spin degrees of freedom. For the latter, we get an effective double-well like potential as in Fig. 3.2 where the energy of the two minima can be changed by varying the detuning of the external microwave radiation which induces Rabi oscillations between the spin states \uparrow and \downarrow , similar to the Kibble-Zurek experiment [48] using Rydberg atoms discussed in the previous section. Due to the strong elongation of the Bose-Einstein condensate, the system is effectively 1+1 dimensional, as in Eq. (3.4). Indeed, bubble formation in analogy to false-vacuum decay has been observed in the Trento experiment [261], but one should be aware of two major deviations from original idea. First, in contrast to the homogeneous case as in Eq. (3.4), the Bose-Einstein condensate is inhomogeneous even in x direction and hence bubbles are formed predominantly at or near the centre of cloud. This is in contrast to spontaneous bubble creation mechanism which can occur anywhere with equal probability²⁸. Second, the experimental results and parameters indicate that the false-vacuum decay in the Trento experiment [261] is not caused by quantum fluctuations. Probably it is also not induced by purely thermal (equilibrium) fluctuations, but instead by classical noise generated by the preparation steps. As a result, it is not fully clear (yet) to which extent the quantitative analogy to false-vacuum decay – such as caused by relativistic tunneling in the system (3.4) – can be applied. Nevertheless, the experimental results, such as the observed exponential dependence of the bubble formation probability on experimental parameters over more than one order of magnitude, are a real impressive achievement.

As an alternative realization, one should also mention the Cambridge experiment [262]. In contrast to the scenarios above which are based on weakly interacting condensates, the Cambridge experiment [262] employs strongly interacting (i.e., correlated) bosonic atoms in an optical lattice²⁹. They can be described by an extended Bose-Hubbard Hamiltonian as in Eq. (1.7), but generalized to two atomic species in the presence of an external drive. By resonantly shaking the optical lattice, one can destabilize the Mott insulator state such that it is analogous to the meta-stable false vacuum state, while the true vacuum state (of the driven system) would be a super-fluid state with a staggered order parameter³⁰. The meta-stability of the Mott insulator state and its decay to the true ground state have been observed in the Cambridge experiment [262] as a function of the experimental parameters such as the shaking amplitude. Similarly to the Trento experiment [261], the Cambridge experiment [262] is clearly a qualitative analogy to false-vacuum decay (and thus a very important step), but the extent of the quantitative analogy requires further studies.

Having realized a quantum simulator for false-vacuum decay would allow us to address several interesting questions. As a non-perturbative phenomenon of an interacting quantum field theory, false-vacuum decay is a highly non-trivial problem and it is probably fair to say that our understanding is far from complete, see also [264, 265] and references therein. As already indicated above, open questions exist regarding the microscopic mechanism, including the role of quantum and thermal fluctuations, their space-time conspiracy versus a simple one-dimensional tunneling picture etc. Similar to the Kibble-Zurek mechanism discussed in the previous section, the correlations between different bubbles is

²⁸In this regard, the centre of cloud acts a bit like the nucleation seeds (e.g., spoon) for under-cooled water discussed above.

²⁹Thus, the Cambridge experiment [262] simulating false-vacuum decay displays some similarities to the Sauter-Schwinger or Breit-Wheeler effect in Sec. 2.8 which can also be modeled with strongly interacting fermionic or bosonic atoms in optical lattices, see, e.g., [201, 202] and references therein.

³⁰Such a spatially modulated super-fluid order parameter is often also referred to as super-solid and the associated instability can be visualized via the dispersion relation, where an effective “roton” dip touches the k axis, see, e.g., [263] and references therein.

also an interacting (and related) question. The same applies to the symmetry of bubbles: usually, one starts with an ansatz of a highly symmetric (e.g., spherical) bubble, but the probabilities for symmetric and asymmetric bubbles should be determined and compared. As another point, it would also be very interesting to generalize the static Lagrangian (3.4) to an explicitly time-dependent background (such as an expanding Universe). The additional time dependence could dynamically assist (or even suppress) false-vacuum decay via tunneling, see also [266, 267] and references therein. As a final remark, such a quantum simulator would also allow us to investigate the impact of the (omnipresent) environment. For example, it could stabilize the false vacuum via the quantum Zeno effect [268].

3.4. Back-reaction and cosmological constant

A less obvious but very important point where the non-linearity plays a role is the back-reaction of the quantum effects discussed in chapter 2 onto the (approximately classical) background. As an example, let us take the case of Hawking radiation where the in-falling partner particles carry negative energy (from the point of view of a static observer far away). They should decrease the mass of the black hole in order to compensate for the energy emitted via Hawking radiation. However, how this should work in detail is still a matter of debate³¹.

In this respect, one can hope to learn something from the black-hole analogues, e.g., in Bose-Einstein condensates, because there the microscopic physics is better understood. However, one should also be aware of some important differences between the two cases. First, the fluid analogue such as the de Laval nozzle in Fig. 2.2 is not a closed system – there is a constant in- and out-flux of matter and energy which changes the concept of energy balance in comparison to the real black-hole case. Second, as already discussed above, the black-hole analogues in Bose-Einstein condensates do not reproduce the Einstein equations, which are crucial for the back reaction in real black holes.

Taking into account the above differences, there have been several theoretical investigations regarding the back-reaction for black-hole analogues in Bose-Einstein condensates, see, e.g., [272, 273, 274, 275, 276, 277, 278]. It should also be mentioned here that there were experimental studies [279] of the back-reaction in black-hole analogues – but instead of phonons in Bose-Einstein condensates, surface waves in flowing liquids [158] where used to realize a black-hole analogue (which then typically recovers classical aspects instead of quantum phenomena, at least for the experiments so far).

3.4.1. Cosmological constant problem

In order to circumvent some of the difficulties of the black-hole analogues mentioned above, let us consider the much simpler case of a homogeneous condensate at rest. Still, the quantum fluctuations of the phonon field (in its ground state) should have some impact – which might be interpreted as a zero-point pressure contribution. This zero-point pressure can be considered as a toy model for studying the cosmological constant problem, see also [280, 281].

When trying to measure how the expansion of our present Universe slows down, it has been found that it does not, but is actually accelerating. This striking finding has been awarded with the Nobel prize in physics 2011. To understand why this came as a surprise to many, let us consider the Friedmann equation (with vanishing spatial curvature)

$$\frac{\ddot{a}}{a} = -\frac{4\pi G_N}{3} (\rho + 3p) , \quad (3.5)$$

³¹This debate is also related to the black-hole information puzzle. One can try to gain some insight using simplified toy models (see, e.g., [269, 270, 271]), but there are many open questions.

which governs the time-dependence of the scale factor a representing the expansion of our Universe. Since all matter we know of has positive energy or mass density $\rho > 0$ and positive (or negligible) pressure $p \geq 0$, one would expect $\ddot{a} < 0$, i.e., a deceleration of the expansion. Intuitively speaking, gravity is attractive for all kinds of ordinary matter – which should slow down the expansion. Thus, the observed acceleration of the expansion indicates some sort of repulsive effect of gravity. These observations suggest adding a cosmological constant Λ to the Einstein equations or, equivalently, a term $\propto \Lambda g_{\mu\nu}$ to the energy-momentum tensor $T_{\mu\nu}$. Such a cosmological constant Λ yields an effective pressure $p_\Lambda = -\rho_\Lambda$ which equals the *negative* density ρ_Λ . In analogy to dark matter, such a contribution is often referred to as “dark energy”. However, this is a bit misleading since the energy density $\rho_\Lambda = \Lambda > 0$ is not the dominant term in the Friedmann equation (3.5), i.e., it does not change the sign of the right-hand side – it is the negative pressure $p_\Lambda = -\rho_\Lambda$ which is important here. Thus, “dark energy” should actually better be called “dark pressure”.

A prominent idea to explain this contribution $\propto \Lambda g_{\mu\nu}$ to the energy-momentum tensor $T_{\mu\nu}$ is the energy and pressure of the vacuum itself. However, this requires calculating that quantity. A naive approach would be to consider the zero-point energy $\hbar\omega_{\mathbf{k}}/2$ of each mode \mathbf{k} and then to sum up all these contributions. Of course, this yields an ultra-violet divergence scaling with \mathbf{k}^4 in 3+1 dimensions. Now, one could argue that this d^3k -integration should be cut off at the Planck scale $k_{\text{Planck}} \sim 1/\ell_{\text{Planck}} = \sqrt{c^3/\hbar G_N}$ already discussed in Sec. 2.2 because the quantum field theory we are using is probably only valid for ω and k scales below k_{Planck} . Using k_{Planck} as a sharp cut-off would give us $\Lambda = \mathcal{O}(k_{\text{Planck}}^4)$ which is a huge energy or mass density.

Comparing the value $\Lambda = \mathcal{O}(k_{\text{Planck}}^4)$ estimated in this way with the value for Λ obtained from the observed acceleration of our Universe $\Lambda = \mathcal{O}(10^{-26} \text{ kg/m}^3)$, one finds that they differ by 120 orders of magnitude. This is sometimes called the “biggest discrepancy” or the “worst prediction” in physics. However, calling the above estimate giving $\Lambda = \mathcal{O}(k_{\text{Planck}}^4)$ a prediction is an exaggeration. There are at least two major problems. First, the dominant contribution to the value $\Lambda = \mathcal{O}(k_{\text{Planck}}^4)$ stems from fluctuations at the Planck scale – where we do not know what happens. For the above estimate, one implicitly assumes that the low-energy behaviour we know is correct up to the Planck scale $k < k_{\text{Planck}}$ and that afterwards $k > k_{\text{Planck}}$ no further contributions arise. This is a very strong assumption which is not really justified. For example, it could well be that modifications at the Planck scale lead to a completely different behaviour, possibly even with negative contributions – which might cancel the low-energy part, see also [282]. Second, a proper calculation should start with the full underlying interacting theory in terms of the fundamental degrees of freedom and their correct operator ordering (which unfortunately we do not have). Then, one should split this up (if it is possible at all) into an approximately classical background space-time plus quantum fluctuations in top of it. For example, there might be some sort of symmetry principle which enforces the effective cosmological constant Λ derived in this way to vanish in flat space-times³².

3.4.2. Back-reaction in fluids and Bose-Einstein condensates

When faced with a difficult problem such as the one described above, it can be useful to consider a much simpler scenario where an analogous problem occurs. Thus, let us study a perfect fluid described by the Bernoulli equation $\dot{\phi} + V/m + g_s \rho/m + (\nabla \phi)^2/2 = 0$ as derived in Sec. 2.1. Now we take this classical equation and assume that it is valid for operator-valued fields $\hat{\phi}$ and $\hat{\rho}$ (see also the next subsection). Then we split these quantum fields up into their classical

³²Such a symmetry principle could perhaps also explain why the QCD trace anomaly – which would also lead to an effective cosmological constant which is far too large – does not contribute, at least not in flat space-times, see also [283].

background values $\phi_{\text{class}} = \langle \hat{\phi} \rangle$ and $\rho_{\text{class}} = \langle \hat{\rho} \rangle$ plus quantum fluctuations $\hat{\phi} = \phi_{\text{class}} + \delta\hat{\phi}$ and $\hat{\rho} = \rho_{\text{class}} + \delta\hat{\rho}$. Inserting this split into the (quantum) Bernoulli equation and taking the expectation value yields

$$\dot{\phi}_{\text{class}} + \frac{V}{m} + \frac{g_s \rho_{\text{class}}}{m} + \frac{1}{2} (\nabla \phi_{\text{class}})^2 = -\frac{1}{2} \left\langle \left(\nabla \delta\hat{\phi} \right)^2 \right\rangle, \quad (3.6)$$

where the quantum correction on the right-hand side describes the back-reaction of the quantum fluctuations of the phonon field onto the classical background. Qualitatively, this would be the analogue to the cosmological constant discussed above. Even quantitatively, we find the same dependence k_{cut}^4 on the cut-off scale since the phonon field $\delta\hat{\phi}$ behaves as a mass-less scalar field at small k , see Sec. 2.1.

For Bose-Einstein condensates, the first natural cut-off scale would be the healing length ξ where the dispersion relations changes, as discussed in Sec. 2.1. At these length scales, we also have to include the “quantum pressure” term in Eq. (2.6). Taking the “quantum pressure” term into account, we may now apply the same procedure as for Eq. (3.6). Assuming that the quantum fluctuations $\delta\hat{\rho}$ are much smaller than the classical background ρ_{class} we may Taylor expand in terms of $\delta\hat{\rho}$ and arrive at an additional back-reaction term [277]

$$\dot{\phi}_{\text{class}} + \frac{V}{m} + \frac{g_s \rho_{\text{class}}}{m} + \frac{1}{2} (\nabla \phi_{\text{class}})^2 = -\frac{1}{2} \left\langle \left(\nabla \delta\hat{\phi} \right)^2 \right\rangle - \frac{\hbar^2}{8m^2 \rho_{\text{class}}^2} \langle \delta\hat{\rho} \nabla^2 \delta\hat{\rho} \rangle + \mathcal{O}(\delta\hat{\rho}^4). \quad (3.7)$$

After an integration by parts, we see that the additional term containing the density fluctuations $\delta\hat{\rho}$ and the previous term (3.6) from the phase fluctuations $\delta\hat{\phi}$ have the opposite sign and thus partly cancel each other. Moreover, if we take the naive analogy to the scalar field and forget about the modified dispersion relation, this additional term would have an even stronger ultra-violet divergence k_{cut}^6 because $\delta\hat{\rho}$ represents the field momentum density $\propto \partial_t \delta\hat{\phi}$.

When taking into account the full dispersion relation, however, the leading divergences cancel each other – including the k_{cut}^4 divergence which would be the analogue to the estimate in Sec. 3.4.1. What remains is a k_{cut}^3 divergence, but now the cut-off is no longer determined by the healing length since the associated change of the dispersion relation is already included [277]. Instead, this cut-off stems from the approximation of a contact interaction $W(\mathbf{r} - \mathbf{r}') \approx g_s \delta^3(\mathbf{r} - \mathbf{r}')$. For a smooth and regular function $W(\mathbf{r} - \mathbf{r}')$ such as a Gaussian, this divergence would disappear. Still, it would be premature to associate this result k_{cut}^3 to the back-reaction of the quantum fluctuations. As we shall see below, this k_{cut}^3 contribution is just an artifact of operator ordering.

For Bose-Einstein condensates, we actually know what the correct result should be (up to the level of accuracy under consideration). Instead of the effective Bernoulli equation, one should start from the evolution equation (2.2) in terms of the original many-body field operators $\hat{\psi}$ and insert the split $\hat{\psi} = \psi_c + \hat{\chi}$ (or its particle-number conserving version). Then we find the modified Gross-Pitaevskii equation including the back-reaction corrections

$$i\hbar \frac{\partial \psi_c}{\partial t} = \left(-\frac{\hbar^2}{2m} \nabla^2 + V + g_s |\psi_c|^2 + 2g_s \langle \hat{\chi}^\dagger \hat{\chi} \rangle \right) \psi_c + g_s \langle \hat{\chi}^2 \rangle \psi_c^*. \quad (3.8)$$

The term $\langle \hat{\chi}^\dagger \hat{\chi} \rangle$ is referred to as the quantum depletion and corresponds to the (small) density of atoms which are pushed out of the condensate state ψ_c by the finite interaction g_s . Even using the contact interaction $W(\mathbf{r} - \mathbf{r}') \approx g_s \delta^3(\mathbf{r} - \mathbf{r}')$, this term $\langle \hat{\chi}^\dagger \hat{\chi} \rangle$ is finite. The so-called anomalous term $\langle \hat{\chi}^2 \rangle$ displays weak ultra-violet divergence $\sim k_{\text{cut}}$ which disappears when more realistic interaction potentials $W(\mathbf{r} - \mathbf{r}')$ are considered, see, e.g., [102].

Even though many important details are left out here, this analogy shows that the naive estimate k_{cut}^4 sketched in the previous Sec. 3.4.1 should not be trusted too much. Of course, apart from these theoretical investigations, one could ask for experimental verification, e.g., how to actually measure the quantum depletion $\langle \hat{\chi}^\dagger \hat{\chi} \rangle$. One way of doing so are time-of-flight measurements as discussed in Sec. 1.2.2 where one can also increase the signal by imposing an optical lattice

potential which effectively enhances the interaction strength, see, e.g., [284]. Note that a non-adiabatic evolution is crucial for such a measurement of $\langle \hat{\chi}^\dagger \hat{\chi} \rangle$. To see that, let us imagine the following scenario: We start with the many-body ground state of N atoms in a finite volume and with a finite interaction strength g_s , which implies a finite $\langle \hat{\chi}^\dagger \hat{\chi} \rangle > 0$. If we then increase the volume or decrease the interaction strength g_s (or both) very slowly, i.e., adiabatically, we stay in the many-body ground state. Thus, we would end up in a final ground state of negligible density or interaction strength g_s (or both) which then also has a vanishing quantum depletion $\langle \hat{\chi}^\dagger \hat{\chi} \rangle = 0$. In contrast, if we suddenly (or rapidly) switch off the interaction strength g_s or let the condensate expand quickly, i.e., non-adiabatically, not all the atoms can “find their way back” to the ground state and thus we are left with a finite number of atoms in excited states – which are a smoking gun for the initial quantum depletion $\langle \hat{\chi}^\dagger \hat{\chi} \rangle$. Thus, by changing the interaction strength g_s or by letting the condensate expand – both depending on how fast those variations occur – we may influence the quantum depletion $\langle \hat{\chi}^\dagger \hat{\chi} \rangle$, which can also be measured *in situ* by momentum-selective two-photon Bragg scattering, see, e.g., [285]. As a result, we find close analogies to the analogue of cosmological particle creation, as discussed in Sec. 2.4.

3.4.3. Quantum fluid dynamics

To conclude this section, let us sketch the operator-ordering problems mentioned above. We start from the full microscopic description in terms of the many-body field operators $\hat{\psi}$ and $\hat{\psi}^\dagger$ and their Hamiltonian (in normal ordering)

$$\hat{H} = \int d^3r \left(\frac{(\nabla \hat{\psi}^\dagger) \cdot (\nabla \hat{\psi})}{2m} + V \hat{\psi}^\dagger \hat{\psi} + \frac{g_s}{2} (\hat{\psi}^\dagger)^2 \hat{\psi}^2 \right). \quad (3.9)$$

The next step would be to generalize the Madelung split (2.5) to the quantum case where the many-body field operators are represented by self-adjoint density and phase operators (more precisely, operator-valued distributions)

$$\hat{\psi} = \exp \{i\hat{S}\} \sqrt{\hat{\rho}}. \quad (3.10)$$

Note that the commutation relation $[\hat{\psi}^\dagger(\mathbf{r}), \hat{\psi}(\mathbf{r}')] = \delta^3(\mathbf{r} - \mathbf{r}')$ implies that \hat{S} and $\hat{\rho}$ do not commute. As a result, operator ordering is important here and other forms such as $\hat{\psi} = \sqrt{\hat{\rho}} \exp\{i\hat{S}\}$ are inconsistent with $\hat{\rho} = \hat{\psi}^\dagger \hat{\psi}$. Apart from the difficulties stemming from the character of \hat{S} and $\hat{\rho}$ as operator-valued distributions, the phase operator \hat{S} should be treated with special care³³.

At this point, we can already identify the operator-ordering problem mentioned in the previous Sec. 3.4.2. If we translate the interaction term $(\hat{\psi}^\dagger)^2 \hat{\psi}^2$ in the Hamiltonian (3.9) into density operators, we find $(\hat{\psi}^\dagger)^2 \hat{\psi}^2 = \hat{\rho}^2 - \hat{\rho} \delta^3(0)$ in view of the commutation relation $[\hat{\psi}^\dagger(\mathbf{r}), \hat{\psi}(\mathbf{r}')] = \delta^3(\mathbf{r} - \mathbf{r}')$. Then, if we try to derive the quantum version of the Bernoulli equation and calculate $\partial_t \hat{S}$ via the commutator $[\hat{S}, \hat{H}]$, we see that it acquires a singular contribution $\propto \delta^3(0)$ which explains the ultra-violet singularity k_{cut}^3 found above.

In order to avoid such problems, let us start from the evolution equation $\partial_t \hat{\psi}$ of the original field operator and insert the quantum Madelung representation (3.10). As expected, we find a quantum version of the equation of continuity

$$\partial_t \hat{\rho} + \nabla \cdot \hat{\mathbf{j}} = 0 \quad \text{with} \quad \hat{\mathbf{j}} = \frac{\hat{\psi}^\dagger \nabla \hat{\psi} - \text{h.c.}}{2mi} = \frac{\sqrt{\hat{\rho}} (\nabla \hat{S}) \sqrt{\hat{\rho}}}{m}, \quad (3.11)$$

which is exact. Note that the symmetric form $\sqrt{\hat{\rho}} (\nabla \hat{S}) \sqrt{\hat{\rho}}$ ensures that $\hat{\mathbf{j}}$ is self-adjoint. In order to define a velocity operator $\hat{\mathbf{v}}$ one should multiply $\hat{\mathbf{j}}$ with $\hat{\rho}^{-1/2}$ from left and right – which becomes problematic if the density can become zero (such as at a vortex core).

³³Some of the problems can already arise for the simpler case of a harmonic oscillator if we set $\hat{a}^\dagger = \sqrt{\hat{n}} \exp\{-i\hat{S}\}$ and $\hat{a} = \exp\{i\hat{S}\} \sqrt{\hat{n}}$.

Since the quantum version of the equation of continuity (3.11) has exactly the same form as in the classical case, one could say that it does not acquire any quantum back-reaction corrections³⁴. However, the situation is more complicated for the quantum version of the Euler or Bernoulli equation

$$i\partial_t \hat{\psi} = i\partial_t \left(e^{i\hat{S}} \sqrt{\hat{\rho}} \right) = \left(-\frac{i\nabla^2 \hat{S} - (\nabla \hat{S})^2}{2m} + V + g_s \hat{\rho} \right) e^{i\hat{S}} \sqrt{\hat{\rho}}. \quad (3.12)$$

Here operator ordering is a much more severe issue. Note that, even though $\hat{\rho}$ and \hat{S} at different spatial positions (but the same time) commute and thus $\nabla \hat{\rho}$ commutes with $\hat{\rho}$ (again at the same time), this is no longer true for the time derivatives, i.e., $\hat{\rho}$ and $\partial_t \hat{\rho}$ do not commute (same for \hat{S} and $\partial_t \hat{S}$).

³⁴Note that such a statement depends on the definition of the classical background. For example, if takes the condensate wave function ψ_c as the classical background, the associated density ρ_c would acquire a quantum correction $\langle \hat{\rho} \rangle = \rho_c + \langle \hat{\chi}^\dagger \hat{\chi} \rangle$ due to the quantum depletion discussed after Eq. (3.8).

4. Summary and outlook

Ultra-cold atoms possess many features which make them very good candidates for realizing quantum simulators. They can be isolated very well from the environment and cooled down (as the nomenclature already suggests) to extremely low temperatures. Furthermore, their characteristic energy scales are very low and thus the associated internal frequency scales very slow such that it is possible to externally manipulate them quite fast in comparison, i.e., non-adiabatically (sometimes also called diabatically). The means for external manipulation are also quite advanced, one can tune the one-particle potential felt by the atoms to a large degree (e.g., by optical lasers) and even change their two-particle interaction strength (e.g., by a magnetic field via Feshbach resonances). In addition, one can exploit the various internal atomic states and induce resonant or near-resonant transitions, e.g., via optical lasers or microwaves. Finally, the state of the quantum simulator – usually the atom number or density – can be read out with high accuracy down to the single-atom level. In contrast to all these advantages, one should also keep in mind an important drawback of ultra-cold atoms – the problem of three-body losses – which places ultimate limits on their performance.

Apart from these experimental aspects, our theoretical understanding of ultra-cold atoms is also quite advanced, e.g., regarding Bose-Einstein condensates in the dilute-gas limit. This combination of experimental and theoretical progress allowed us to propose and even realize several quantum simulators based on ultra-cold atoms – in the spirit of the famous quote from Feynman: “The same equations have the same solutions.” Especially for relativistic phenomena, a selection of proposals, theoretical investigations and experimental realizations have been discussed in the previous sections. In chapter 2, we discussed examples for linear fields – though under the influence of non-trivial external conditions. A recurring theme was the tearing apart of quantum vacuum fluctuations, by gravitational or electric fields, the cosmic expansion or other external influences. Another common feature is quantum squeezing³⁵, which can be visualized by means of the coupled oscillator picture sketched in Fig. 2.1. In chapter 3, we considered some cases of non-linear fields. Here the competition between (local) minima in the potential landscape leads to interesting phenomena beyond standard perturbation theory.

4.1. Lessons (to be) learned

Of course, when discussing such quantum simulators, one should also think about the question of what we can actually learn from this endeavour. Clearly, one of the ultimate goals of quantum simulators is to simulate a quantum system of interest which is so complex that we cannot do these calculations on a classical computer anymore. Even though we are (depending on who is asked that question) not quite there yet³⁶, it is very likely that we can realize such a quantum simulator long before we have a sufficiently large quantum computer that is able to solve classical problems (e.g., factoring large numbers) better than any classical computer. On the other hand, even before reaching the “holy grail” of a quantum simulation impossible on a classical computer, the study of quantum simulators can and does create useful insights – as in the well-known saying attributed to Confucius: “The journey is the reward.” In the following, a personal and probably incomplete list is given:

³⁵However, claiming the experimental verification of Hawking radiation or the Unruh effect just because the appearance of squeezing in an experiment is not really justified.

³⁶Note that it is a non-trivial task to define that question properly. For example, one could argue that a system of strongly interacting electrons in a solid (whose complex quantum dynamics cannot be simulated on available classical computers) is a quantum simulator for itself. Thus, one should impose certain demands (e.g., regarding state preparation and read-out) on a quantum simulator.

Benchmarking If we want to use a quantum simulator in order to perform a simulation which is intractable on any available classical computer, we have to make sure that this quantum simulator is behaving in precisely the same way we think it is, see also [12]. Unless we have an analytic solution to compare with (e.g., in integrable systems such as the sine-Gordon model discussed in Sec. 3.1), the intractability on any available classical computer prevents us from checking the obtained results. Thus, in order to reach the “holy grail” mentioned above, it is crucial to benchmark the quantum simulator – e.g., by applying it to cases where we already know what the result should be. This allows us to estimate the performance and accuracy of the quantum simulator (see also the next point).

Robustness Turning the argument around, one can use the imperfections present in a given quantum simulator in order to investigate the robustness of the phenomenon under consideration. Since basically all of our descriptions are based on idealizations and/or approximations, it is important to study how the resulting predictions “survive” in reality. Taking Hawking radiation discussed in Sec. 2.2 as an example, the theoretical calculations of this effect in the presence of the modified dispersion relation (2.10) of a Bose-Einstein condensate show that the particles emitted at long wavelengths do basically not depend on these modifications at short length scales (even though its original derivation might suggest that, cf. the trans-Planckian problem), see also Fig. 2.3 and [286]. On the experimental side, the observation of Hawking emission at the Technion [58, 59, 60, 61, 62] indicate that the main mechanism of Hawking radiation is not destroyed by the imperfections which are undoubtedly present in the experimental apparatus.

Connecting theory and experiment As Goethe said, “Gray, dear friend, is all theory.” Physics is one of the natural sciences and its goal is to describe the world around us. Thus, theoretical physicists should leave their “ivory tower” from time to time and have their theories tested in experiments (or at least compared to observations). Real progress is only possible via an interplay of theory and experiment (or observations). In cases where direct experimental tests are out of reach, such as Hawking radiation or cosmological particle creation, quantum simulators are an interesting alternative to test some of the underlying principles and mechanisms via the analogy.

Essential and inessential features As another important point, studying the analogies between the quantum simulators and the phenomena to be simulated helps us to distinguish their essential and inessential features, cf. [287]. Again taking Hawking radiation discussed in Sec. 2.2 as an example, we find that it requires an effective black-hole horizon (as in Fig. 2.2) but it does not hinge on the Einstein equations. Similarly, the Sauter-Schwinger effect discussed in Sec. 2.8.1 can be deduced from the Dirac equation or the Klein-Fock-Gordon equation describing charged spinor or scalar particles in the presence of an external electromagnetic field, but it does not really depend on the origin of that electromagnetic field, e.g., whether it is a solution of the Maxwell equations³⁷ or the Proca equation.

Physics intuition In order to explain this point, it might be useful to make a small detour into the field of artificial intelligence (AI). Nowadays artificial neural networks can perform tasks such as speech recognition, reading handwriting, or even playing chess with astonishing performances – provided that they are trained well. As a rule of thumb, the performance increases with the amount of data available for training and the diversity of the data (e.g., different samples of handwriting). Now, since such artificial neural networks are motivated by our brain, it is probably not too much a stretch to conclude that our physics intuition can also be trained by studying different analogies, especially those between seemingly unrelated areas (see also the next point).

At the same time, this intuition should be substantiated by hard facts and actual calculations in order to avoid

³⁷Actually, for a given vector potential A_μ , the Maxwell equations just tell us which sources j_μ would be required to generate this field configuration. A similar argument can be made for the Einstein equations in terms of the metric $g_{\mu\nu}$ and the source term $T_{\mu\nu}$.

misconceptions and confusion – as Einstein said: “Make things as simple as possible, but no simpler.” In the AI context, training with bad data can lead to wrong recognitions and false classifications. Thus, for each quantum simulator, one must clarify to which extent the analogy applies and where the limits of the analogy are³⁸.

Crossing borders In the history of physics and other sciences, transferring ideas from one sub-discipline to another has often led to great breakthroughs. As one example, the Nobel price in physics 2024 was awarded for the application of methods from statistical physics to artificial neural networks. Another example is the Anderson-Higgs mechanism bridging solid state and particle physics. It is very likely that some of today’s open problems in physics (e.g., in quantum gravity) can also be solved by such a transfer of methods and ideas – thereby connecting different communities. Actually, as became (hopefully) evident from the discussions in this article, the study of quantum simulators is precisely doing that, i.e., transferring methods and ideas across the borders of sub-disciplines and connecting different communities. Thus, studying quantum simulators can help us to break through the walls which (unfortunately) separate the sub-disciplines and to apply ideas which are well known and understood in one community to another community where they are less known. This is especially important for the training of young researchers and might help them to “look beyond their own nose” and to see the bigger picture. Last but not least, venturing into new regimes often yields totally unexpected new discoveries and ideas, which prove very important in hindsight.

4.2. Outlook

Obviously, there are many remaining open questions, to say it with Newton: “What we know is a drop, what we don’t know is an ocean.” For example, comparison between Figs. 1.2 and 1.3 on the one hand and Figs. 3.1 and 3.2 on the other hand suggests an intriguing triangle of analogy including quantum information (e.g., adiabatic quantum algorithms), relativistic quantum field theory, and condensed matter/solid state physics (e.g., Landau-Zener tunneling, quantum phase transitions of first and second order) which promises to yield further fascinating insights.

As another point, many of the proposals discussed above have yet to be realized experimentally and it would be very interesting and exciting to see how far one can push the analogy and how accurate it can be made. Furthermore, some of the experimental realizations “only” apply on the classical level – i.e., they are not really *quantum* simulators yet – and it would be great to push them into or towards the quantum regime. Examples include super-radiance in Sec. 2.7 and Hubble friction as discussed in Sec. 2.4.2. For the latter example, it would be nice to observe the amplification of quantum fluctuations in analogy to cosmic inflation via the transition from oscillation to freezing and the resulting squeezing, see also [288].

On the theory side, the impact of a modified dispersion relation such as in Eq. (2.10) on phenomena like Hawking radiation and cosmological particle creation (including the case of Hubble friction mentioned above) have been studied in various works. In contrast, the role of dissipation is far less understood, see, e.g., [217] and references therein. On the experimental side, quantum simulators could also facilitate an investigation of the effects of dissipation and decoherence caused by the coupling of the system to some reservoir. For example, in the Sauter-Schwinger effect or in false-vacuum decay, quantum tunneling plays an important role. The quantum Zeno effect [268] shows that such tunneling processes

³⁸For example, just finding indications of thermal behaviour and thus concluding (without further arguments) that one found signatures of the Unruh effect or Hawking radiation is probably an exaggeration. As another example, a system where the effective propagation speed vanishes at some position is not necessarily a good analogue for a black hole (where everything can fall in but nothing can escape). As a counter-example, consider the shore line of the ocean where the speed of the water waves goes to zero.

can be influenced by the coupling to the environment (which effectively monitors the state of the system permanently). Usually, the quantum Zeno effect is discussed in the context of tunneling between discrete levels. In order to apply it to the Sauter-Schwinger effect for a constant electric field, for example, one should generalize it to a continuum of states, see also [289].

In addition to the interaction with an environment, non-linear fields as discussed in chapter 3 can also interact with themselves and the impact of this self-interaction on phenomena like Hawking radiation and cosmological particle creation is far from being completely understood. For linear fields, the main mechanism for Hawking radiation, focusing on the vicinity of the horizon, is very similar (in suitable coordinates) to cosmological particle creation and can also be mapped to harmonic oscillators with time-dependent potentials. It is not clear how far this similarity extends for the case of non-linear fields – here quantum simulators could help us understanding this point. One could speculate that these investigations could also shed light on other open issues, such as the the black-hole information puzzle, the origin of the black-hole entropy and its relation to the entanglement entropy associated to the emitted Hawking radiation – but this must be illuminated by future studies.

Of course, apart from black holes, there are many more scenarios where it would be nice to deepen our understanding of interaction effects via suitable quantum simulators. An obvious example is QCD as the theory of the strong interaction featuring phenomena such as confinement (see, e.g., [90]) and string breaking (see, e.g., [49]) etc. As already explained in Sec. 1.2.6, external (artificial or synthetic) gauge fields as well as dynamical gauge fields (as in full-fledged QCD) have been discussed in several works, but actually realizing such a quantum simulator for a large enough lattice is a formidable challenge. As another example, neutron stars can also give rise to complex dynamics including vortices (similar to those in Sec. 2.7.1) and it has been proposed [290] to simulate some of their properties via the analogy to super-solids in dipolar atom systems (see also [263]).

Of course, for each phenomenon, one should look for the best way of realizing a suitable quantum simulator – or, if possible, different quantum simulators in order to benchmark and compare their results. Hence, one should not restrict this search *a priori* to ultra-cold atoms (in spite of their advantages explained above) but also consider trapped ions [1], for example. However, this is then another story and beyond the scope of the present article.

Acknowledgements

This review is partly based on invited lectures at the first international school on “Quantum Sensors for Fundamental Physics” (6th to 10th January 2020 in Durham) and the summer school “Concepts and Novel Applications of Quantum Information” (29th August to 2nd September 2022 in Vienna) and on other occasions. Some of the questions addressed here came up in discussions with the audiences – so thank you for the feedback. Fruitful discussions at many workshops, conferences, schools and research stays are also gratefully acknowledged, such as in Bad Honnef, Benasque and at Perimeter Institute (e.g., “Quantum Simulators of Fundamental Physics” June 5-9, 2023). Research at Perimeter Institute is supported in part by the Government of Canada through the Department of Innovation, Science and Economic Development Canada and by the Province of Ontario through the Ministry of Colleges and Universities. Funded by the Deutsche Forschungsgemeinschaft (DFG, German Research Foundation) through the Collaborative Research Center SFB 1242 “Nonequilibrium dynamics of condensed matter in the time domain” (Project-ID 278162697). Financial support from and collaborations with the initiative Quantum Simulators for Fundamental Physics (QSimFP) are also gratefully acknowledged.

I thank A. Weitzel for test reading and help with the figures. Then I would also like to take the opportunity and thank my fellow scientists for many inspiring discussions, where I learned a lot. Even though we often do not agree on everything, an open and constructive scientific debate across all borders (national and other) is extremely valuable. First and foremost, I would like to thank G. Plunien and W. G. Unruh as well as my former and present colleagues from TU Dresden, HZDR, the University of Duisburg-Essen, the University of British Columbia and from the SFB-TR12, SFB1242 and COSLAB. Furthermore, I would like to thank³⁹ A. Achucarro, I. Affleck, Y. Aharonov, E. Akkermans, A. Andreev, J. Anglin, M. Arndt, M. Aspelmeyer, R. Balbinot, C. Barcelo, I. Bialynicki-Birula, R. Blatt, M. Blencowe, M. Bordag, J. Braden, R. Brandenberger, A. Calogeracos, I. Carusotto, L. Chomaz, M. Choptuik, I. Cirac, E. Cornell, P. Davies, L. Davidovich, B. Dittrich, V. Dodonov, G. Dunne, R. Durrer, F. Dyson, A. Eckardt, J. Edwards, D. Faccio, U. Fischer, S. Floerchinger, L. Ford, K. Fredenhagen, V. Frolov, S. Fulling, L. Garay, B. Geyer, H. Gies, D. Habs, F. Hebenstreit, T. Heinzl, M. Hotta, B.-L. Hu, T. Jacobson, M. Jacquet, M. Johnson, I. Khriplovich, T. Kibble, B. King, A. Kitaev, H. Kleinert, F. Koenig, M. Krusius, T. Kugo, A. Leggett, L. Lehner, U. Leonhardt, S.-P. Kim, S. Liberati, J. Louko, R. Mann, D. Marolf, E. Martín-Martínez, G. Morigi, I. Moss, G. Mourou, V. Mostepanenko, N. Narozhny, M. Oberthaler, D. Page, G. Paraoanu, R. Penrose, T. Pfau, G. Pickett, L. Pitaevskii, S. Popescu, J. Rafelski, M. Raizen, D. Rätzel, J.-M. Rost, A. Roura, M. Sakellariadou, R. Sauerbrey, C. Savage, T. Schaetz, J. Schmiedmayer, C. Schubert, M. Scully, G. Semenoff, S. Shankaranarayanan, L. Skrbek, P. Stamp, J. Steinhauer, G. t’ Hooft, K. Thorne, C. Timm, R. Verch, G. Vidal, M. Visser, G. Vitiello, M. Vojta, G. Volovik, R. Wald, S. Weinfurtner, A. Wipf, R. Woodard, J. Yngvason, A. Zhitnitsky, W. Zurek.

Finally, I would like to dedicate this work to the memory of R. Parentani and G. Soff.

³⁹Most probably, I forgot several important names, for which I apologize – this is no bad intention, but just my poor memory for names.

References

- [1] R. Blatt and C. F. Roos, "Quantum simulations with trapped ions," *Nature Phys.* **8**, 277-284 (2012)
- [2] P. M. Alsing, J. P. Dowling and G. J. Milburn, "Ion Trap Simulations of Quantum Fields in an Expanding Universe," *Phys. Rev. Lett.* **94**, no.22, 220401 (2005)
- [3] L. Lamata, J. Leon, T. Schaetz and E. Solano, "Dirac equation and quantum relativistic effects in a single trapped ion," *Phys. Rev. Lett.* **98**, 253005 (2007)
- [4] R. Schützhold, M. Uhlmann, L. Petersen, H. Schmitz, A. Friedenauer and T. Schaetz, "Analogue of cosmological particle creation in an ion trap," *Phys. Rev. Lett.* **99**, 201301 (2007)
- [5] B. Horstmann, B. Reznik, S. Fagnocchi and J. I. Cirac, "Hawking Radiation from an Acoustic Black Hole on an Ion Ring," *Phys. Rev. Lett.* **104**, 250403 (2010)
- [6] N. C. Menicucci, S. J. Olson and G. J. Milburn, "Simulating quantum effects of cosmological expansion using a static ion trap," *New J. Phys.* **12**, 095019 (2010)
- [7] B. Horstmann, R. Schützhold, B. Reznik, S. Fagnocchi and J. I. Cirac, "Hawking Radiation on an Ion Ring in the Quantum Regime," *New J. Phys.* **13**, 045008 (2011) [erratum: *New J. Phys.* **13**, 069601 (2011)]
- [8] M. Wittemer, F. Hakelberg, P. Kiefer, J. P. Schröder, C. Fey, R. Schützhold, U. Warring and T. Schaetz, "Phonon Pair Creation by Inflating Quantum Fluctuations in an Ion Trap," *Phys. Rev. Lett.* **123**, no.18, 180502 (2019)
- [9] M. K. Joshi, C. Kokail, R. van Bijnen, F. Kranzl, T. V. Zache, R. Blatt, C. F. Roos and P. Zoller, "Exploring large-scale entanglement in quantum simulation," *Nature* **624**, no.7992, 539-544 (2023)
- [10] E. Altman, K. R. Brown, G. Carleo, L. D. Carr, E. Demler, C. Chin, B. DeMarco, S. E. Economou, M. A. Eriksson and K. M. C. Fu, et al, "Quantum Simulators: Architectures and Opportunities," *PRX Quantum* **2**, no.1, 017003 (2021)
- [11] I. Buluta and F. Nori, "Quantum Simulators," *Science* **326**, no.5949, 108-111 (2009)
- [12] P. Hauke, F. M. Cucchietti, L. Tagliacozzo, I. Deutsch, and M. Lewenstein, "Can one trust quantum simulators?," *Rept. Prog. Phys.* **75**, no.8, 082401 (2012)
- [13] I. M. Georgescu, S. Ashhab and F. Nori, "Quantum Simulation," *Rev. Mod. Phys.* **86**, 153 (2014)
- [14] M. A. Nielsen and I. L. Chuang, "Quantum Computation and Quantum Information," Cambridge University Press, 2012, ISBN 978-0-521-63503-5
- [15] L. K. Grover, "Quantum mechanics helps in searching for a needle in a haystack," *Phys. Rev. Lett.* **79**, 325-328 (1997)
- [16] P. W. Shor, "Polynomial-Time Algorithms for Prime Factorization and Discrete Logarithms on a Quantum Computer," *SIAM Rev.* **41**, no.2, 303-332 (2006)
- [17] A. Das and B. K. Chakrabarti, "Colloquium: Quantum annealing and analog quantum computation," *Rev. Mod. Phys.* **80**, 1061-1081 (2008)

[18] E. Farhi, J. Goldstone, S. Gutmann and M. Sipser, “Quantum Computation by Adiabatic Evolution,” arXiv:quant-ph/0001106

[19] E. Farhi, J. Goldstone, S. Gutmann, J. Lapan, A. Lundgren and D. Preda, “A Quantum Adiabatic Evolution Algorithm Applied to Random Instances of an NP-Complete Problem,” *Science* **292**, no.5516, 1057726 (2001)

[20] J. Roland and N. J. Cerf, “Quantum search by local adiabatic evolution,” *Phys. Rev. A* **65**, no.4, 042308 (2002)

[21] G. Schaller, S. Mostame, and R. Schützhold, “General error estimate for adiabatic quantum computing,” *Phys. Rev. A* **73**, 062307 (2006)

[22] G. Schaller and R. Schützhold, “Adiabatic quantum algorithms as quantum phase transitions: First versus second order,” *Phys. Rev. A* **74**, 060304(R) (2006)

[23] G. Schaller and R. Schützhold, “The role of symmetries in adiabatic quantum algorithms,” *Quant. Inf. Comput.* **10**, no.1-2, 0109-0140 (2010)

[24] A. M. Childs, E. Farhi and J. Preskill, “Robustness of adiabatic quantum computation,” *Phys. Rev. A* **65**, 012322 (2002)

[25] M. Tiersch and R. Schützhold, “Non-Markovian decoherence in the adiabatic quantum search algorithm,” *Phys. Rev. A* **75**, 062313 (2007)

[26] S. Mostame, G. Schaller, and R. Schützhold, “Decoherence in a dynamical quantum phase transition,” *Phys. Rev. A* **81**, 032305 (2010)

[27] R. P. Feynman, “Simulating physics with computers,” *Int. J. Theor. Phys.* **21**, 467-488 (1982)

[28] R. P. Feynman, “Quantum Mechanical Computers,” *Optics News* **11**, no.2, 11-20 (1985)

[29] B. Fauseweh, “Quantum many-body simulations on digital quantum computers: State-of-the-art and future challenges,” *Nature Commun.* **15**, no.1, 2123 (2024)

[30] D. Jaksch, P. Zoller, “The cold atom Hubbard toolbox,” *Annals of Physics* **315**, 52-79 (2005)

[31] I. Bloch, “Ultracold quantum gases in optical lattices,” *Nature Phys.* **1**, no.1, 23-30 (2005)

[32] I. Bloch, J. Dalibard and S. Nascimbène, “Quantum simulations with ultracold quantum gases,” *Nature Phys.* **8**, 267-276 (2012)

[33] D. S. Weiss and M. Saffman, “Quantum computing with neutral atoms,” *Phys. Today* **70**, no.7, 44-50 (2017)

[34] C. Gross and I. Bloch, “Quantum simulations with ultracold atoms in optical lattices,” *Science* **357**, no.6355, aal3837 (2017)

[35] F. Schäfer, T. Fukuhara, S. Sugawa, Y. Takasu & Y. Takahashi, “Tools for quantum simulation with ultracold atoms in optical lattices,” *Nature Rev. Phys.* **2**, 411-425 (2020)

[36] B. Yang, H. Sun, C. J. Huang, H. Y. Wang, Y. Deng, H. N. Dai, Z. S. Yuan and J. W. Pan, “Cooling and entangling ultracold atoms in optical lattices,” *Science* **369**, no.6503, aaz6801 (2020)

[37] A. M. Kaufman and K. K. Ni, “Quantum science with optical tweezer arrays of ultracold atoms and molecules,” *Nature Phys.* **17**, no.12, 1324-1333 (2021)

[38] L. Pause, L. Sturm, M. Mittenbühler, S. Amann, D. Schäffner, M. Schlosser and G. Birkl, “Supercharged two-dimensional tweezer array with more than 1000 atomic qubits,” *Optica* **11**, no.2, 222-226 (2024)

[39] M. W. Jack, “Decoherence due to Three-Body Loss and its Effect on the State of a Bose-Einstein Condensate,” *Phys. Rev. Lett.* **89**, 140402 (2002)

[40] D. Rätzel and R. Schützhold, “Decay of quantum sensitivity due to three-body loss in Bose-Einstein condensates,” *Phys. Rev. A* **103**, no.6, 063321 (2021)

[41] F. Mivehvar, F. Piazza, T. Donner and H. Ritsch, “Cavity QED with Quantum Gases: New Paradigms in Many-Body Physics,” *Adv. Phys.* **70**, 1 (2021)

[42] T. Lahaye, C. Menotti, L. Santos, M. Lewenstein and T. Pfau, “The physics of dipolar bosonic quantum gases,” *Rept. Prog. Phys.* **72**, no.12, 126401 (2009)

[43] L. Chomaz, I. Ferrier-Barbut, F. Ferlaino, B. Laburthe-Tolra, B. L. Lev and T. Pfau, “Dipolar physics: a review of experiments with magnetic quantum gases,” *Rept. Prog. Phys.* **86**, no.2, 026401 (2023)

[44] H. Weimer, M. Müller, I. Lesanovsky, P. Zoller and H. P. Büchler, “A Rydberg quantum simulator,” *Nature Phys.* **6**, no.5, 382-388 (2010)

[45] M. Saffman, T. G. Walker and K. Mølmer, “Quantum information with Rydberg atoms,” *Rev. Mod. Phys.* **82**, no.3, 2313-2363 (2010)

[46] H. Bernien, S. Schwartz, A. Keesling, H. Levine, A. Omran, H. Pichler, S. Choi, A. S. Zibrov, M. Endres and M. Greiner, et al, “Probing many-body dynamics on a 51-atom quantum simulator,” *Nature* **551**, 579-584 (2017)

[47] T. L. Nguyen, J. M. Raimond, C. Sayrin, R. Cortiñas, T. Cantat-Moltrecht, F. Assemat, I. Dotsenko, S. Gleyzes, S. Haroche, G. Roux, Th. Jolicoeur, and M. Brune, “Towards Quantum Simulation with Circular Rydberg Atoms,” *Phys. Rev. X* **8**, 011032 (2018)

[48] A. Keesling, A. Omran, H. Levine, H. Bernien, H. Pichler, S. Choi, R. Samajdar, S. Schwartz, P. Silvi and S. Sachdev, et al, “Quantum Kibble–Zurek mechanism and critical dynamics on a programmable Rydberg simulator,” *Nature* **568**, no.7751, 207-211 (2019)

[49] F. M. Surace, P. P. Mazza, G. Giudici, A. Leroose, A. Gambassi and M. Dalmonte, “Lattice gauge theories and string dynamics in Rydberg atom quantum simulators,” *Phys. Rev. X* **10**, no.2, 021041 (2020)

[50] A. Browaeys and T. Lahaye, “Many-body physics with individually controlled Rydberg atoms,” *Nature Phys.* **16**, no.2, 132-142 (2020)

[51] S. Ebadi, T. T. Wang, H. Levine, A. Keesling, G. Semeghini, A. Omran, D. Bluvstein, R. Samajdar, H. Pichler and W. W. Ho, et al, “Quantum phases of matter on a 256-atom programmable quantum simulator,” *Nature* **595**, no.7866, 227-232 (2021)

[52] S. R. Cohen and J. D. Thompson, “Quantum Computing with Circular Rydberg Atoms,” PRX Quantum **2**, no.3, 030322 (2021)

[53] D. Malz and J. I. Cirac, “Few-Body Analog Quantum Simulation with Rydberg-Dressed Atoms in Optical Lattices,” PRX Quantum **4**, no.2, 020301 (2023)

[54] N. ten Brinke, R. Schützhold, “Dicke superradiance as a nondestructive probe for quantum quenches in optical lattices,” Phys. Rev. A **92**, 013617 (2015)

[55] N. ten Brinke, R. Schützhold, “Dicke superradiance as nondestructive probe for the state of atoms in optical lattices,” Eur. Phys. J. D **70**, 102 (2016)

[56] J. C. Jaskula, G. B. Partridge, M. Bonneau, R. Lopes, J. Ruaudel, D. Boiron and C. I. Westbrook, “An acoustic analog to the dynamical Casimir effect in a Bose-Einstein condensate,” Phys. Rev. Lett. **109**, 220401 (2012)

[57] L. Tarruell and L. Sanchez-Palencia, “Quantum simulation of the Hubbard model with ultracold fermions in optical lattices,” Comptes Rendus Physique **19**, 365-393 (2018)

[58] O. Lahav, A. Itah, A. Blumkin, C. Gordon and J. Steinhauer, “Realization of a sonic black hole analogue in a Bose-Einstein condensate,” Phys. Rev. Lett. **105**, 240401 (2010)

[59] J. Steinhauer, “Measuring the entanglement of analogue Hawking radiation by the density-density correlation function,” Phys. Rev. D **92**, no.2, 024043 (2015)

[60] J. Steinhauer, “Observation of quantum Hawking radiation and its entanglement in an analogue black hole,” Nature Phys. **12**, 959 (2016)

[61] J. R. Muñoz de Nova, K. Golubkov, V. I. Kolobov and J. Steinhauer, “Observation of thermal Hawking radiation and its temperature in an analogue black hole,” Nature **569**, no.7758, 688-691 (2019)

[62] V. I. Kolobov, K. Golubkov, J. R. Muñoz de Nova and J. Steinhauer, “Observation of stationary spontaneous Hawking radiation and the time evolution of an analogue black hole,” Nature Phys. **17**, no.3, 362-367 (2021)

[63] R. Schützhold, “Detection Scheme for Acoustic Quantum Radiation in Bose-Einstein Condensates,” Phys. Rev. Lett. **97**, 190405 (2006)

[64] C. Viermann, M. Sparn, N. Liebster, M. Hans, E. Kath, Á. Parra-López, M. Tolosa-Simeón, N. Sánchez-Kuntz, T. Haas and H. Strobel, et al, “Quantum field simulator for dynamics in curved spacetime,” Nature **611**, no.7935, 260-264 (2022)

[65] D. Jaksch, C. Bruder, J. I. Cirac, C. W. Gardiner and P. Zoller, “Cold Bosonic Atoms in Optical Lattices,” Phys. Rev. Lett. **81**, 3108-3111 (1998)

[66] M. Greiner, O. Mandel, T. Esslinger, T. W. Hänsch and I. Bloch, “Quantum phase transition from a superfluid to a Mott insulator in a gas of ultracold atoms,” Nature **415**, 39-44 (2002)

[67] R. Jördens, N. Strohmaier, K. Günter, H. Moritz and T. Esslinger, “A Mott insulator of fermionic atoms in an optical lattice,” Nature **455**, no.7210, 204-207 (2008)

[68] W. S. Bakr, J. I. Gillen, A. Peng, S. Fölling and M. Greiner, “A quantum gas microscope for detecting single atoms in a Hubbard-regime optical lattice,” *Nature* **462**, no.7269, 74-77 (2009)

[69] A. Masurenko, C. S. Chiu, G. Ji, M. F. Parsons, M. Kanász-Nagy, R. Schmidt, F. Grusdt, E. Demler, D. Greif and M. Greiner, “A cold-atom Fermi–Hubbard antiferromagnet,” *Nature* **545**, no.7655, 462-466 (2017)

[70] B. Yang, H. Sun, R. Ott, H. Y. Wang, T. V. Zache, J. C. Halimeh, Z. S. Yuan, P. Hauke and J. W. Pan, “Observation of gauge invariance in a 71-site Bose–Hubbard quantum simulator,” *Nature* **587**, no.7834, 392-396 (2020)

[71] L. Su, A. Douglas, M. Szurek, R. Groth, S. F. Ozturk, A. Krahn, A. H. Hébert, G. A. Phelps, S. Ebadi and S. Dickerson, et al, “Dipolar quantum solids emerging in a Hubbard quantum simulator,” *Nature* **622**, no.7984, 724-729 (2023)

[72] F. Queisser, G. Schaller, R. Schützhold, “Attraction Versus Repulsion Between Doubly-Charged Particles in Mott-Hubbard Systems,” *Int. J. Theor. Phys.* **62**, 239 (2023)

[73] L. Mazza, A. Bermudez, N. Goldman, M. Rizzi, M. A. Martin-Delgado and M. Lewenstein, “An Optical-Lattice-Based Quantum Simulator For Relativistic Field Theories and Topological Insulators,” *New J. Phys.* **14**, 015007 (2012)

[74] J. Ignacio Cirac, P. Maraner and J. K. Pachos, “Cold atom simulation of interacting relativistic quantum field theories,” *Phys. Rev. Lett.* **105**, 190403 (2010)

[75] N. Szpak and R. Schützhold, “Quantum simulator for the Schwinger effect with atoms in bichromatic optical lattices,” *Phys. Rev. A* **84**, 050101(R) (2011)

[76] N. Szpak and R. Schützhold, “Optical lattice quantum simulator for QED in strong external fields: Spontaneous pair creation and the Sauter-Schwinger effect,” *New J. Phys.* **14**, 035001 (2012)

[77] A. H. Castro Neto, F. Guinea, N. M. R. Peres, K. S. Novoselov and A. K. Geim, “The electronic properties of graphene,” *Rev. Mod. Phys.* **81**, 109-162 (2009)

[78] U. J. Wiese, “Ultracold Quantum Gases and Lattice Systems: Quantum Simulation of Lattice Gauge Theories,” *Annalen Phys.* **525**, 777-796 (2013)

[79] D. Jaksch and P. Zoller, “Creation of effective magnetic fields in optical lattices: the Hofstadter butterfly for cold neutral atoms,” *New J. Phys.* **5**, no.1, 56 (2003)

[80] J. Ruseckas, G. Juzeliūnas, P. Oehberg and M. Fleischhauer, “Non-Abelian gauge potentials for ultra-cold atoms with degenerate dark states,” *Phys. Rev. Lett.* **95**, 010404 (2005)

[81] F. Gerbier and J. Dalibard, “Gauge fields for ultracold atoms in optical superlattices,” *New J. Phys.* **12**, 033007 (2010)

[82] D. W. Zhang, Z. D. Wang and S. L. Zhu, “Relativistic quantum effects of Dirac particles simulated by ultracold atoms,” *Front. Phys. (Beijing)* **7**, 31-53 (2012)

[83] N. Goldman, G. Juzeliūnas, P. Öhberg and I. B. Spielman, “Light-induced gauge fields for ultracold atoms,” *Rept. Prog. Phys.* **77**, no.12, 126401 (2014)

[84] A. Celi, P. Massignan, J. Ruseckas, N. Goldman, I. B. Spielman, G. Juzeliūnas and M. Lewenstein, “Synthetic gauge fields in synthetic dimensions,” *Phys. Rev. Lett.* **112**, no.4, 043001 (2014)

[85] M. Aidelsburger, S. Nascimbene and N. Goldman, “Artificial gauge fields in materials and engineered systems,” *Comptes Rendus Physique* **19**, 394-432 (2018)

[86] D. Hey and E. Li, “Advances in Synthetic Gauge Fields for Light Through Dynamic Modulation,” *R. Soc. open sci.* **5**, 172447 (2018)

[87] F. Görg, K. Sandholzer, J. Minguzzi, R. Desbuquois, M. Messer and T. Esslinger, “Realization of density-dependent Peierls phases to engineer quantized gauge fields coupled to ultracold matter,” *Nature Phys.* **15**, no.11, 1161-1167 (2019)

[88] V. Galitski, G. Juzeliūnas and I. B. Spielman, “Artificial gauge fields with ultracold atoms,” *Phys. Today* **72**, 28 (2019)

[89] E. Zohar and B. Reznik, “Confinement and lattice QED electric flux-tubes simulated with ultracold atoms,” *Phys. Rev. Lett.* **107**, 275301 (2011)

[90] E. Zohar, J. I. Cirac and B. Reznik, “Simulating Compact Quantum Electrodynamics with ultracold atoms: Probing confinement and nonperturbative effects,” *Phys. Rev. Lett.* **109**, 125302 (2012)

[91] E. Zohar, J. I. Cirac and B. Reznik, “Cold-Atom Quantum Simulator for SU(2) Yang-Mills Lattice Gauge Theory,” *Phys. Rev. Lett.* **110**, no.12, 125304 (2013)

[92] E. Zohar, J. I. Cirac and B. Reznik, “Quantum simulations of gauge theories with ultracold atoms: local gauge invariance from angular momentum conservation,” *Phys. Rev. A* **88**, 023617 (2013)

[93] E. Zohar, J. I. Cirac and B. Reznik, “Quantum Simulations of Lattice Gauge Theories using Ultracold Atoms in Optical Lattices,” *Rept. Prog. Phys.* **79**, no.1, 014401 (2016)

[94] D. González-Cuadra, E. Zohar and J. I. Cirac, “Quantum Simulation of the Abelian-Higgs Lattice Gauge Theory with Ultracold Atoms,” *New J. Phys.* **19**, no.6, 063038 (2017)

[95] L. Barbiero, C. Schweizer, M. Aidelsburger, E. Demler, N. Goldman and F. Grusdt, “Coupling ultracold matter to dynamical gauge fields in optical lattices: From flux attachment to \mathbb{Z}_2 lattice gauge theories,” *Sci. Adv.* **5**, no.10, eaav7444 (2019)

[96] C. Schweizer, F. Grusdt, M. Berngruber, L. Barbiero, E. Demler, N. Goldman, I. Bloch and M. Aidelsburger, “Floquet approach to \mathbb{Z}_2 lattice gauge theories with ultracold atoms in optical lattices,” *Nature Phys.* **15**, no.11, 1168-1173 (2019)

[97] N. D. Birrell and P. C. W. Davies, “Quantum Fields in Curved Space,” Cambridge University Press, 1982

[98] F. Dalfovo, S. Giorgini, L. P. Pitaevskii and S. Stringari, “Theory of Bose-Einstein condensation in trapped gases,” *Rev. Mod. Phys.* **71**, 463-512 (1999)

[99] C. W. Gardiner, “A Particle number conserving Bogolyubov method which demonstrates the validity of the time dependent Gross-Pitaevskii equation for a highly condensed Bose gas,” *Phys. Rev. A* **56**, no.2, 1414-1423 (1997)

[100] M. D. Girardeau, “Comment on *Particle-number-conserving Bogoliubov method which demonstrates the validity of the time-dependent Gross-Pitaevskii equation for a highly condensed Bose gas*,” Phys. Rev. A **58**, 775 (1998)

[101] M. Girardeau and R. Arnowitt, “Theory of Many-Boson Systems: Pair Theory,” Phys. Rev. **113**, 755-761 (1959)

[102] R. Schützhold, M. Uhlmann, Y. Xu, U. R. Fischer, “Mean-field expansion in Bose-Einstein condensates with finite-range interactions,” Int. J. Mod. Phys. B **20**, 3555 (2006)

[103] C. Chin, R. Grimm, P. Julienne and E. Tiesinga, “Feshbach resonances in ultracold gases,” Rev. Mod. Phys. **82**, no.2, 1225-1286 (2010)

[104] W. G. Unruh, “Experimental black hole evaporation,” Phys. Rev. Lett. **46**, 1351-1353 (1981)

[105] S. S. Baak, S. Datta and U. R. Fischer, “Petrov classification of analogue spacetimes,” Class. Quant. Grav. **40**, no.21, 215001 (2023)

[106] W. G. Unruh and R. Schützhold, “On slow light as a black hole analog,” Phys. Rev. D **68**, 024008 (2003)

[107] C. Barcelo, S. Liberati and M. Visser, “Analogue gravity,” Living Rev. Rel. **8**, 12 (2005)

[108] S. W. Hawking, “Black hole explosions,” Nature **248**, 30-31 (1974)

[109] S. W. Hawking, “Particle Creation by Black Holes,” Commun. Math. Phys. **43**, 199-220 (1975) [erratum: Commun. Math. Phys. **46**, 206 (1976)]

[110] R. Schützhold and W. G. Unruh, “Space-time toy model for Hawking radiation,” arXiv:2412.10202

[111] M. Hotta, R. Schützhold and W. G. Unruh, “Partner particles for moving mirror radiation and black hole evaporation,” Phys. Rev. D **91**, no.12, 124060 (2015)

[112] R. Schützhold and W. G. Unruh, “On Quantum Correlations across the Black Hole Horizon,” Phys. Rev. D **81**, 124033 (2010)

[113] R. Balbinot, A. Fabbri, S. Fagnocchi, A. Recati and I. Carusotto, “Non-local density correlations as signal of Hawking radiation in BEC acoustic black holes,” Phys. Rev. A **78**, 021603 (2008)

[114] I. Carusotto, S. Fagnocchi, A. Recati, R. Balbinot and A. Fabbri, “Numerical observation of Hawking radiation from acoustic black holes in atomic BECs,” New J. Phys. **10**, 103001 (2008)

[115] K. Fredenhagen and R. Haag, “On the Derivation of Hawking Radiation Associated With the Formation of a Black Hole,” Commun. Math. Phys. **127**, 273 (1990)

[116] A. Almheiri, D. Marolf, J. Polchinski and J. Sully, “Black Holes: Complementarity or Firewalls?,” JHEP **02**, 062 (2013)

[117] D. G. Boulware, “Quantum Field Theory in Schwarzschild and Rindler Spaces,” Phys. Rev. D **11**, 1404 (1975)

[118] T. Jacobson, “Black hole evaporation and ultrashort distances,” Phys. Rev. D **44**, 1731-1739 (1991)

[119] W. G. Unruh, “Sonic analog of black holes and the effects of high frequencies on black hole evaporation,” Phys. Rev. D **51**, 2827-2838 (1995)

[120] L. J. Garay, J. R. Anglin, J. I. Cirac and P. Zoller, “Black holes in Bose-Einstein condensates,” *Phys. Rev. Lett.* **85**, 4643-4647 (2000)

[121] S. Corley and T. Jacobson, “Hawking spectrum and high frequency dispersion,” *Phys. Rev. D* **54**, 1568-1586 (1996)

[122] W. G. Unruh and R. Schützhold, “On the universality of the Hawking effect,” *Phys. Rev. D* **71**, 024028 (2005)

[123] S. J. Robertson, “The theory of Hawking radiation in laboratory analogues,” *J. Phys. B* **45**, 163001 (2012)

[124] U. Leonhardt, “Questioning the recent observation of quantum Hawking radiation,” *Annalen Phys.* **530**, no.5, 1700114 (2018)

[125] M. K. Parikh and F. Wilczek, “Hawking radiation as tunneling,” *Phys. Rev. Lett.* **85**, 5042-5045 (2000)

[126] R. Schützhold and W. G. Unruh, “Hawking radiation with dispersion versus breakdown of the WKB approximation,” *Phys. Rev. D* **88**, no.12, 124009 (2013)

[127] F. Del Porro, S. Liberati and M. Schneider, “Tunneling method for Hawking quanta in analogue gravity,” arXiv:2406.14603

[128] W. G. Unruh, “Notes on black hole evaporation,” *Phys. Rev. D* **14**, 870 (1976)

[129] P. Chen and T. Tajima, “Testing Unruh radiation with ultraintense lasers,” *Phys. Rev. Lett.* **83**, 256-259 (1999)

[130] R. Schützhold, G. Schaller and D. Habs, “Signatures of the Unruh effect from electrons accelerated by ultra-strong laser fields,” *Phys. Rev. Lett.* **97**, 121302 (2006)

[131] R. Schützhold, G. Schaller and D. Habs, “Tabletop Creation of Entangled Multi-keV Photon Pairs and the Unruh Effect,” *Phys. Rev. Lett.* **100**, 091301 (2008)

[132] A. Recati, P. O. Fedichev, W. Zwerger, J. von Delft, and P. Zoller, “Atomic Quantum Dots Coupled to a Reservoir of a Superfluid Bose-Einstein Condensate,” *Phys. Rev. Lett.* **94**, 040404 (2005)

[133] A. Retzker, J. I. Cirac, M. B. Plenio and B. Reznik, “Methods for Detecting Acceleration Radiation in a Bose-Einstein Condensate,” *Phys. Rev. Lett.* **101**, no.11, 110402 (2008)

[134] C. Gooding, S. Biermann, S. Erne, J. Louko, W. G. Unruh, J. Schmiedmayer and S. Weinfurtner, “Interferometric Unruh detectors for Bose-Einstein condensates,” *Phys. Rev. Lett.* **125**, no.21, 213603 (2020)

[135] S. Biermann, S. Erne, C. Gooding, J. Louko, J. Schmiedmayer, W. G. Unruh and S. Weinfurtner, “Unruh and analogue Unruh temperatures for circular motion in 3+1 and 2+1 dimensions,” *Phys. Rev. D* **102**, no.8, 085006 (2020)

[136] J. Rodriguez-Laguna, L. Tarruell, M. Lewenstein and A. Celi, “Synthetic Unruh effect in cold atoms,” *Phys. Rev. A* **95**, no.1, 013627 (2017)

[137] A. Kosior, M. Lewenstein and A. Celi, “Unruh effect for interacting particles with ultracold atoms,” *SciPost Phys.* **5**, no.6, 061 (2018)

[138] E. Schrödinger, “The proper vibrations of the expanding universe,” *Physica* **6**, 899 (1939)

[139] L. Parker, “Particle creation in expanding universes,” *Phys. Rev. Lett.* **21**, 562-564 (1968)

[140] S. Lang and R. Schützhold, “Analog of cosmological particle creation in electromagnetic waveguides,” *Phys. Rev. D* **100**, no.6, 065003 (2019)

[141] U. R. Fischer and R. Schützhold, “Quantum simulation of cosmic inflation in two-component Bose-Einstein condensates,” *Phys. Rev. A* **70**, 063615 (2004)

[142] A. Chatrchyan, K. T. Geier, M. K. Oberthaler, J. Berges and P. Hauke, “Analog cosmological reheating in an ultracold Bose gas,” *Phys. Rev. A* **104**, no.2, 023302 (2021)

[143] M. Tolosa-Simeón, Á. Parra-López, N. Sánchez-Kuntz, T. Haas, C. Viermann, M. Sparn, N. Liebster, M. Hans, E. Kath and H. Strobel, et al, “Curved and expanding spacetime geometries in Bose-Einstein condensates,” *Phys. Rev. A* **106**, no.3, 033313 (2022)

[144] C. L. Hung, V. Gurarie and C. Chin, “From Cosmology to Cold Atoms: Observation of Sakharov Oscillations in Quenched Atomic Superfluids,” *Science* **341**, 1213-1215 (2013)

[145] J. Hu, L. Feng, Z. Zhang and C. Chin, “Quantum simulation of Unruh radiation,” *Nature Phys.* **15**, no.8, 785-789 (2019)

[146] J. L. Roberts, N. R. Claussen, S. L. Cornish, E. A. Donley, E. A. Cornell, and C. E. Wieman, “Controlled Collapse of a Bose-Einstein Condensate,” *Phys. Rev. Lett.* **86**, 4211 (2001)

[147] E. Donley, N. Claussen, S. Cornish, et al. “Dynamics of collapsing and exploding Bose-Einstein condensates,” *Nature* **412**, 295-299 (2001)

[148] M. Uhlmann, Y. Xu and R. Schützhold, “Aspects of cosmic inflation in expanding Bose-Einstein condensates,” *New J. Phys.* **7**, 248 (2005)

[149] R. Schützhold, “Emergent horizons in the laboratory,” *Class. Quant. Grav.* **25**, 114011 (2008)

[150] S. Eckel, A. Kumar, T. Jacobson, I. B. Spielman and G. K. Campbell, “A rapidly expanding Bose-Einstein condensate: an expanding universe in the lab,” *Phys. Rev. X* **8**, no.2, 021021 (2018)

[151] G. W. Gibbons and S. W. Hawking, “Cosmological Event Horizons, Thermodynamics, and Particle Creation,” *Phys. Rev. D* **15**, 2738-2751 (1977)

[152] P. O. Fedichev and U. R. Fischer, “Gibbons-Hawking effect in the sonic de Sitter space-time of an expanding Bose-Einstein-condensed gas,” *Phys. Rev. Lett.* **91**, 240407 (2003)

[153] V. L. Ginzburg and V. P. Frolov, “Excitation and emission of a ‘detector’ in accelerated motion in a vacuum or in uniform motion at a velocity above the velocity of light in a medium,” *Pis’Ma Zh. Eksp. Teor. Fiz.* **43**, 265 (1986); [*JETP Lett.* **43**, 339 (1986)]

[154] V. L. Ginzburg, “Radiation by uniformly moving sources (Vavilov-Cherenkov effect, transition radiation, and other phenomena),” *Phys. Usp.* **39**, 973-982 (1996)

[155] S. Lang, R. Sauerbrey, R. Schützhold and W. G. Unruh, “Ginzburg effect in a dielectric medium with dispersion and dissipation,” *Phys. Rev. Res.* **4**, no.3, 033074 (2022)

[156] J. Marino, A. Recati and I. Carusotto, “Casimir Forces and Quantum Friction from Ginzburg Radiation in Atomic Bose-Einstein Condensates,” *Phys. Rev. Lett.* **118**, no.4, 045301 (2017)

[157] R. H. Dicke, “Coherence in Spontaneous Radiation Processes,” *Phys. Rev.* **93**, 99-110 (1954)

[158] R. Schützhold and W. G. Unruh, “Gravity wave analogs of black holes,” *Phys. Rev. D* **66**, 044019 (2002)

[159] R. Penrose, “Gravitational collapse: The role of general relativity,” *Riv. Nuovo Cim.* **1**, 252-276 (1969)

[160] Y. B. Zeldovich, “Generation of waves by a rotating body,” *JETP Lett.* **14**, 180 (1971)

[161] T. Torres, S. Patrick, A. Coutant, M. Richartz, E. W. Tedford and S. Weinfurtner, “Rotational superradiant scattering in a vortex flow,” *Nature Phys.* **13**, 833-836 (2017)

[162] M. C. Braidotti, R. Prizia, C. Maitland, F. Marino, A. Prain, I. Starshynov, N. Westerberg, E. M. Wright and D. Faccio, “Measurement of Penrose Superradiance in a Photon Superfluid,” *Phys. Rev. Lett.* **128**, no.1, 013901 (2022)

[163] M. C. Braidotti, A. Vinante, M. Cromb, et al, “Amplification of electromagnetic fields by a rotating body,” *Nat. Commun.* **15**, 5453 (2024)

[164] T. Boulier, M. J. Jacquet, et al, “Microcavity Polaritons for Quantum Simulation,” *Adv. Quantum Technol.* **3**, 2000052 (2020)

[165] W. G. Unruh, “Quantum Noise in Amplifiers and Hawking/Dumb-Hole Radiation as Amplifier Noise,” arXiv:1107.2669

[166] F. Federici, C. Cherubini, S. Succi, and M. P. Tosi, “Superradiance from hydrodynamic vortices: A numerical study,” *Phys. Rev. A* **73**, 033604 (2006)

[167] U. R. Fischer and G. Baym, “Vortex states of rapidly rotating dilute Bose-Einstein condensates,” *Phys. Rev. Lett.* **90**, 140402 (2003)

[168] P. Švančara, P. Smaniotto, L. Solidoro, J. F. MacDonald, S. Patrick, R. Gregory, C. F. Barenghi and S. Weinfurtner, “Rotating curved spacetime signatures from a giant quantum vortex,” *Nature* **628**, no.8006, 66-70 (2024)

[169] S. Patrick, A. Gupta, R. Gregory, and C. F. Barenghi, “Stability of quantized vortices in two-component condensates,” *Phys. Rev. Research* **5**, 033201 (2023)

[170] L. Giacomelli and I. Carusotto, “Ergoregion instabilities in rotating two-dimensional Bose-Einstein condensates: Perspectives on the stability of quantized vortices,” *Phys. Rev. Res.* **2**, no.3, 033139 (2020)

[171] S. Patrick, A. Geelmuyden, S. Erne, C. F. Barenghi and S. Weinfurtner, “Quantum vortex instability and black hole superradiance,” *Phys. Rev. Res.* **4**, no.3, 033117 (2022)

[172] S. Patrick, A. Geelmuyden, S. Erne, C. F. Barenghi and S. Weinfurtner, “Origin and evolution of the multiply quantized vortex instability,” *Phys. Rev. Res.* **4**, no.4, 043104 (2022)

[173] A. Berti, L. Giacomelli, I. Carusotto, “Superradiant phononic emission from the analog spin ergoregion in a two-component Bose–Einstein condensate,” *Comptes Rendus Physique* **24**, no.S3, 1-20 (2023)

[174] L. Giacomelli and I. Carusotto, “Understanding superradiant phenomena with synthetic vector potentials in atomic Bose–Einstein condensates,” *Phys. Rev. A* **103**, no.4, 043309 (2021)

[175] L. Giacomelli and I. Carusotto, “Spontaneous quantum superradiant emission in atomic Bose–Einstein condensates subject to a synthetic vector potential,” *Phys. Rev. A* **104**, no.1, 013313 (2021)

[176] G. E. Volovik, “Classical and quantum regimes of the superfluid turbulence,” *Pisma Zh. Eksp. Teor. Fiz.* **78**, 1021-1025 (2003)

[177] B. Nowak, D. Sexty and T. Gasenzer, “Superfluid Turbulence: Nonthermal Fixed Point in an Ultracold Bose Gas,” *Phys. Rev. B* **84**, 020506 (2011)

[178] M. Tsubota, K. Fujimoto and S. Yui, “Numerical Studies of Quantum Turbulence,” *J. Low Temp. Phys.* **188**, no.5-6, 119-189 (2017)

[179] L. Madeira, A. Cidrim, M. Hemmerling, M. A. Caracanhas, F. E. A. dos Santos and V. S. Bagnato, “Quantum turbulence in Bose–Einstein condensates: Present status and new challenges ahead,” *AVS Quantum Sci.* **2**, no.3, 035901 (2020)

[180] C. F. Barenghi, H. A. J. Middleton-Spencer, L. Galantucci and N. G. Parker, “Types of quantum turbulence,” *AVS Quantum Sci.* **5**, no.2, 025601 (2023)

[181] C. F. Barenghi, L. Skrbek, K. R. Sreenivasan, “Quantum Turbulence” (Cambridge University Press 2023)

[182] B. P. Abbott, et al [LIGO Scientific and Virgo], “Observation of Gravitational Waves from a Binary Black Hole Merger,” *Phys. Rev. Lett.* **116**, no.6, 061102 (2016)

[183] S. Hod, “Bohr’s correspondence principle and the area spectrum of quantum black holes,” *Phys. Rev. Lett.* **81**, 4293 (1998)

[184] E. Berti, V. Cardoso and J. P. S. Lemos, “Quasinormal modes and classical wave propagation in analogue black holes,” *Phys. Rev. D* **70**, 124006 (2004)

[185] C. Barcelo, A. Cano, L. J. Garay and G. Jannes, “Quasi-normal mode analysis in BEC acoustic black holes,” *Phys. Rev. D* **75**, 084024 (2007)

[186] T. Torres, S. Patrick, M. Richartz and S. Weinfurtner, “Quasinormal Mode Oscillations in an Analogue Black Hole Experiment,” *Phys. Rev. Lett.* **125**, no.1, 011301 (2020)

[187] M. J. Jacquet, L. Giacomelli, Q. Valnais, M. Joly, F. Claude, E. Giacobino, Q. Glorieux, I. Carusotto and A. Bramati, “Quantum Vacuum Excitation of a Quasinormal Mode in an Analog Model of Black Hole Spacetime,” *Phys. Rev. Lett.* **130**, no.11, 111501 (2023)

[188] H. S. Vieira, K. Destounis and K. D. Kokkotas, “Analog Schwarzschild black holes of Bose–Einstein condensates in a cavity: Quasinormal modes and quasibound states,” *Phys. Rev. D* **107**, no.10, 104038 (2023)

[189] P. Marecki, R. Schützhold, “Whispering gallery like modes along pinned vortices,” *JETP Lett.* **96**, 674-680 (2013)

[190] F. Sauter, “Über das Verhalten eines Elektrons im homogenen elektrischen Feld nach der relativistischen Theorie Diracs,” *Z. Phys.* **69**, 742-764 (1931)

[191] J. S. Schwinger, “On gauge invariance and vacuum polarization,” *Phys. Rev.* **82**, 664-679 (1951)

[192] G. Breit and J. A. Wheeler, “Collision of two light quanta,” *Phys. Rev.* **46**, no.12, 1087-1091 (1934)

[193] R. Schützhold, H. Gies and G. Dunne, “Dynamically assisted Schwinger mechanism,” *Phys. Rev. Lett.* **101**, 130404 (2008)

[194] C. Kohlfürst, N. Ahmadianiaz, J. Oertel and R. Schützhold, “Sauter-Schwinger Effect for Colliding Laser Pulses,” *Phys. Rev. Lett.* **129**, no.24, 241801 (2022)

[195] A. M. Piñeiro, D. Genkina, M. Lu and I. B. Spielman, “Sauter-Schwinger effect with a quantum gas,” *New J. Phys.* **21**, no.8, 083035 (2019)

[196] M. F. Linder, A. Lorke and R. Schützhold, “Analog Sauter-Schwinger effect in semiconductors for spacetime-dependent fields,” *Phys. Rev. B* **97**, no.3, 035203 (2018)

[197] V. Kasper, F. Hebenstreit, M. Oberthaler and J. Berges, “Schwinger pair production with ultracold atoms,” *Phys. Lett. B* **760**, 742-746 (2016)

[198] V. Kasper, F. Hebenstreit, F. Jendrzejewski, M. K. Oberthaler and J. Berges, “Implementing quantum electrodynamics with ultracold atomic systems,” *New J. Phys.* **19**, no.2, 023030 (2017)

[199] T. V. Zache, F. Hebenstreit, F. Jendrzejewski, M. K. Oberthaler, J. Berges and P. Hauke, “Quantum simulation of lattice gauge theories using Wilson fermions,” *Quantum Sci. Technol.* **3**, no.3, 034010 (2018)

[200] M. Aidelsburger, L. Barbiero, A. Bermudez, T. Chanda, A. Dauphin, D. González-Cuadra, P. R. Grzybowski, S. Hands, F. Jendrzejewski and J. Jünemann, et al, “Cold atoms meet lattice gauge theory,” *Phil. Trans. Roy. Soc. Lond. A* **380**, 20210064 (2021)

[201] F. Queisser, P. Navez and R. Schützhold, “Sauter-Schwinger-like tunneling in tilted Bose-Hubbard lattices in the Mott phase,” *Phys. Rev. A* **85**, 033625 (2012)

[202] F. Queisser, K. Krutitsky, P. Navez and R. Schützhold, “Doublon-holon pair creation in Mott-Hubbard systems in analogy to QED,” arXiv:2305.04895

[203] V. V. Dodonov, “Fifty Years of the Dynamical Casimir Effect,” *MDPI Physics* **2**, no.1, 67-104 (2020)

[204] H. B. G. Casimir, “On the attraction between two perfectly conducting plates,” *Indag. Math.* **10**, no.4, 261-263 (1948)

[205] G. T. Moore, “Quantum Theory of the Electromagnetic Field in a Variable-Length One-Dimensional Cavity,” *J. Math. Phys.* **11**, no.9, 2679 (1970)

[206] R. Schützhold, G. Plunien and G. Soff, “Trembling cavities in the canonical approach,” *Phys. Rev. A* **57**, 2311 (1998)

[207] S. K. Lamoreaux, "Demonstration of the Casimir force in the 0.6 to 6 micrometers range," *Phys. Rev. Lett.* **78**, 5-8 (1997) [erratum: *Phys. Rev. Lett.* **81**, 5475-5476 (1998)]

[208] C. M. Wilson, G. Johansson, A. Pourkabirian, M. Simoen, J. R. Johansson, T. Duty, F. Nori and P. Delsing, "Observation of the dynamical Casimir effect in a superconducting circuit," *Nature* **479**, 376-379 (2011)

[209] P. Lähteenmäki, G. S. Paraoanu, J. Hassel and P. J. Hakonen, "Dynamical Casimir effect in a Josephson metamaterial," *Proc. Nat. Acad. Sci.* **110**, 4234-4238 (2013)

[210] R. Schützhold and W. G. Unruh, "Hawking radiation in an electro-magnetic wave-guide?," *Phys. Rev. Lett.* **95**, 031301 (2005)

[211] U. Leonhardt and P. Piwnicki, "Relativistic effects of light in moving media with extremely low group velocity," *Phys. Rev. Lett.* **84**, 822-825 (2000)

[212] M. Visser, "Comment on 'Relativistic effects of light in moving media with extremely low group velocity,'" *Phys. Rev. Lett.* **85**, 5252 (2000)

[213] U. Leonhardt and P. Piwnicki, "U. Leonhardt and P. Piwnicki reply to the 'Comment on 'Relativistic effects of light in moving media with extremely low group velocity' by M. Visser,'" *Phys. Rev. Lett.* **85**, 5253 (2000)

[214] R. Schützhold, G. Plunien and G. Soff, "Dielectric black hole analogs," *Phys. Rev. Lett.* **88**, 061101 (2002)

[215] T. G. Philbin, C. Kuklewicz, S. Robertson, S. Hill, F. Konig and U. Leonhardt, "Fiber-optical analogue of the event horizon," *Science* **319**, 1367-1370 (2008)

[216] R. Schützhold, "Refractive index perturbations: Unruh effect, Hawking radiation or dynamical Casimir effect?," arXiv:1110.6064, in the Proceedings of the II Amazonian Symposium on Physics - Analogue Models of Gravity 30 Years Celebration

[217] S. Lang, R. Schützhold and W. G. Unruh, "Quantum radiation in dielectric media with dispersion and dissipation," *Phys. Rev. D* **102**, no.12, 125020 (2020)

[218] M. F. Linder, R. Schützhold and W. G. Unruh, "Derivation of Hawking radiation in dispersive dielectric media," *Phys. Rev. D* **93**, no.10, 104010 (2016)

[219] S. R. Coleman, "The Quantum Sine-Gordon Equation as the Massive Thirring Model," *Phys. Rev. D* **11**, 2088 (1975)

[220] W. E. Thirring, "A Soluble relativistic field theory?," *Annals Phys.* **3**, 91-112 (1958)

[221] D. J. Gross and A. Neveu, "Dynamical Symmetry Breaking in Asymptotically Free Field Theories," *Phys. Rev. D* **10**, 3235 (1974)

[222] T. Schweigler, V. Kasper, S. Erne, et al, "Experimental characterization of a quantum many-body system via higher-order correlations," *Nature* **545**, 323-326 (2017)

[223] T. V. Zache, T. Schweigler, S. Erne, J. Schmiedmayer and J. Berges, "Extracting the field theory description of a quantum many-body system from experimental data," *Phys. Rev. X* **10**, no.1, 011020 (2020)

[224] T. Schweigler, M. Gluza, M. Tajik, et al, “Decay and recurrence of non-Gaussian correlations in a quantum many-body system,” *Nat. Phys.* **17**, 559-563 (2021)

[225] M. Tajik, I. Kukuljan, S. Sotiriadis, B. Rauer, T. Schweigler, F. Cataldini, J. Sabino, F. Møller, P. Schüttelkopf and S. C. Ji, et al, “Verification of the area law of mutual information in a quantum field simulator,” *Nature Phys.* **19**, no.7, 1022-1026 (2023)

[226] T. Kinoshita, T. Wenger and D. S. Weiss, “A quantum Newton’s cradle,” *Nature* **440**, no.7086, 900-903 (2006)

[227] E. Haller, R. Hart, M. Mark, et al, “Pinning quantum phase transition for a Luttinger liquid of strongly interacting bosons,” *Nature* **466**, 597-600 (2010)

[228] T. W. B. Kibble, “Topology of Cosmic Domains and Strings,” *J. Phys. A* **9**, 1387-1398 (1976)

[229] T. W. B. Kibble, “Some Implications of a Cosmological Phase Transition,” *Phys. Rept.* **67**, 183 (1980)

[230] W. H. Zurek, “Cosmological Experiments in Superfluid Helium?,” *Nature* **317**, 505-508 (1985)

[231] W. H. Zurek, “Cosmological experiments in condensed matter systems,” *Phys. Rept.* **276**, 177-221 (1996)

[232] N. D. Mermin and H. Wagner, “Absence of ferromagnetism or antiferromagnetism in one-dimensional or two-dimensional isotropic Heisenberg models,” *Phys. Rev. Lett.* **17**, 1133-1136 (1966)

[233] C. Bäuerle, Y. Bunkov, S. Fisher, et al, “Laboratory simulation of cosmic string formation in the early Universe using superfluid ^3He ,” *Nature* **382**, 332-334 (1996)

[234] V. Ruutu, V. Eltsov, A. Gill, et al, “Vortex formation in neutron-irradiated superfluid ^3He as an analogue of cosmological defect formation,” *Nature* **382**, 334-336 (1996)

[235] T. Kibble, “Phase-transition dynamics in the lab and the universe,” *Phys. Today* **60N9**, 47-52 (2007)

[236] C. Weiler, T. Neely, D. Scherer, et al, “Spontaneous vortices in the formation of Bose-Einstein condensates,” *Nature* **455**, 948-951 (2008)

[237] J. Beugnon and N. Navon, “Exploring the Kibble-Zurek mechanism with homogeneous Bose gases,” *J. Phys. B* **50**, no.2, 022002 (2017)

[238] G. Lamporesi, S. Donadello, S. Serafini, et al, “Spontaneous creation of Kibble-Zurek solitons in a Bose-Einstein condensate,” *Nature Phys.* **9**, 656-660 (2013)

[239] L. E. Sadler, J. M. Higbie, S. R. Leslie, M. Vengalattore and D. M. Stamper-Kurn, “Spontaneous symmetry breaking in a quenched ferromagnetic spinor Bose-Einstein condensate,” *Nature* **443**, no.7109, 312-315 (2006)

[240] M. Anquez, B. A. Robbins, H. M. Bharath, M. Boguslawski, T. M. Hoang, and M. S. Chapman, “Quantum Kibble-Zurek Mechanism in a Spin-1 Bose-Einstein Condensate,” *Phys. Rev. Lett.* **116**, 155301 (2016)

[241] B. Ko, J. W. Park and Y. Shin, “Kibble-Zurek universality in a strongly interacting Fermi superfluid,” *Nature Phys.* **15**, no.12, 1227-1231 (2019)

[242] K. Lee, S. Kim, T. Kim and Y. Shin, “Universal Kibble–Zurek scaling in an atomic Fermi superfluid,” *Nature Phys.* **20**, no.10, 1570-1574 (2024)

[243] G. Schaller, F. Queisser, S. P. Katoorani, et al, “Kibble-Zurek dynamics in the anisotropic Ising model of the Si(001) surface,” arXiv:2310.18216

[244] M. Uhlmann, R. Schützhold, and U. R. Fischer, “Vortex Quantum Creation and Winding Number Scaling in a Quenched Spinor Bose Gas,” *Phys. Rev. Lett.* **99**, 120407 (2007)

[245] M. Uhlmann, R. Schützhold and U. R. Fischer, “System size scaling of topological defect creation in a second-order dynamical quantum phase transition,” *New J. Phys.* **12**, 095020 (2010)

[246] M. Uhlmann, R. Schützhold and U. R. Fischer, “ $O(N)$ symmetry-breaking quantum quench: Topological defects versus quasiparticles,” *Phys. Rev. D* **81**, 025017 (2010)

[247] S. R. Coleman, “The Fate of the False Vacuum. 1. Semiclassical Theory,” *Phys. Rev. D* **15**, 2929-2936 (1977) [erratum: *Phys. Rev. D* **16**, 1248 (1977)]

[248] C. G. Callan, Jr. and S. R. Coleman, “The Fate of the False Vacuum. 2. First Quantum Corrections,” *Phys. Rev. D* **16**, 1762-1768 (1977)

[249] O. Fialko, B. Opanchuk, A. I. Sidorov, P. D. Drummond and J. Brand, “Fate of the false vacuum: towards realization with ultra-cold atoms,” *EPL* **110**, no.5, 56001 (2015)

[250] J. Braden, M. C. Johnson, H. V. Peiris and S. Weinfurtner, “Towards the cold atom analog false vacuum,” *JHEP* **07**, 014 (2018)

[251] J. Braden, M. C. Johnson, H. V. Peiris, A. Pontzen and S. Weinfurtner, “Nonlinear Dynamics of the Cold Atom Analog False Vacuum,” *JHEP* **10**, 174 (2019)

[252] T. P. Billam, K. Brown and I. G. Moss, “Simulating cosmological supercooling with a cold atom system,” *Phys. Rev. A* **102**, no.4, 043324 (2020)

[253] T. P. Billam, K. Brown, A. J. Groszek and I. G. Moss, “Simulating cosmological supercooling with a cold atom system. II. Thermal damping and parametric instability,” *Phys. Rev. A* **104**, no.5, 053309 (2021)

[254] K. L. Ng, B. Opanchuk, M. Thenabadu, M. Reid and P. D. Drummond, “Fate of the False Vacuum: Finite Temperature, Entropy, and Topological Phase in Quantum Simulations of the Early Universe,” *PRX Quantum* **2**, no.1, 010350 (2021)

[255] T. P. Billam, K. Brown and I. G. Moss, “False-vacuum decay in an ultracold spin-1 Bose gas,” *Phys. Rev. A* **105**, no.4, L041301 (2022)

[256] T. P. Billam, K. Brown and I. G. Moss, “Bubble nucleation in a cold spin 1 gas,” *New J. Phys.* **25**, no.4, 043028 (2023)

[257] A. C. Jenkins, J. Braden, H. V. Peiris, A. Pontzen, M. C. Johnson and S. Weinfurtner, “Analog vacuum decay from vacuum initial conditions,” *Phys. Rev. D* **109**, no.2, 023506 (2024)

[258] A. C. Jenkins, I. G. Moss, T. P. Billam, Z. Hadzibabic, H. V. Peiris and A. Pontzen, “Generalized cold-atom simulators for vacuum decay,” *Phys. Rev. A* **110**, no.3, L031301 (2024)

[259] T. P. Billam, R. Gregory, F. Michel and I. G. Moss, “Simulating seeded vacuum decay in a cold atom system,” *Phys. Rev. D* **100**, no.6, 065016 (2019)

[260] S. Darbha, M. Kornjača, F. Liu, J. Balewski, M. R. Hirsbrunner, P. L. S. Lopes, S. T. Wang, R. Van Beeumen, D. Camps and K. Klymko, “False vacuum decay and nucleation dynamics in neutral atom systems,” *Phys. Rev. B* **110**, no.15, 155103 (2024)

[261] A. Zenesini, A. Berti, R. Cominotti, C. Rogora, I. G. Moss, T. P. Billam, I. Carusotto, G. Lamporesi, A. Recati and G. Ferrari, “False vacuum decay via bubble formation in ferromagnetic superfluids,” *Nature Phys.* **20**, no.4, 558-563 (2024)

[262] B. Song, S. Dutta, S. Bhave, J. C. Yu, E. Carter, N. Cooper and U. Schneider, “Realizing discontinuous quantum phase transitions in a strongly correlated driven optical lattice,” *Nature Phys.* **18**, no.3, 259-264 (2022)

[263] R. Schützhold, M. Uhlmann, and U. R. Fischer, “Effect of fluctuations on the superfluid-supersolid phase transition on the lattice,” *Phys. Rev. A* **78**, 033604 (2008)

[264] D. Pirvu, J. Braden and M. C. Johnson, “Bubble clustering in cosmological first order phase transitions,” *Phys. Rev. D* **105**, no.4, 043510 (2022)

[265] J. Braden, M. C. Johnson, H. V. Peiris, A. Pontzen and S. Weinfurtner, “Mass renormalization in lattice simulations of false vacuum decay,” *Phys. Rev. D* **107**, no.8, 083509 (2023)

[266] C. Kohlfürst, F. Queisser and R. Schützhold, “Dynamically assisted tunneling in the impulse regime,” *Phys. Rev. Res.* **3**, no.3, 033153 (2021)

[267] D. Ryndyk, C. Kohlfürst, F. Queisser and R. Schützhold, “Dynamically assisted tunneling in the Floquet picture,” *Phys. Rev. Res.* **6**, no.2, 023056 (2024)

[268] B. Misra and E. C. G. Sudarshan, “The Zeno’s Paradox in Quantum Theory,” *J. Math. Phys.* **18**, 756 (1977)

[269] C. Maia and R. Schützhold, “Quantum toy model for black-hole back-reaction,” *Phys. Rev. D* **76**, 101502 (2007)

[270] G. Plunien, M. Ruser and R. Schützhold, “A Relativistic toy model for back-reaction,” *Class. Quant. Grav.* **24**, 4361-4376 (2007)

[271] R. Schützhold and C. Maia, “Black-hole back-reaction: A toy model,” *J. Phys. A* **41**, 164065 (2008)

[272] R. Balbinot, S. Fagnocchi, A. Fabbri and G. P. Procopio, “Backreaction in acoustic black holes,” *Phys. Rev. Lett.* **94**, 161302 (2005)

[273] R. Balbinot, S. Fagnocchi and A. Fabbri, “Quantum effects in acoustic black holes: The Backreaction,” *Phys. Rev. D* **71**, 064019 (2005)

[274] R. Schützhold, M. Uhlmann, Y. Xu and U. R. Fischer, “Quantum back-reaction in dilute Bose-Einstein condensates,” *Phys. Rev. D* **72**, 105005 (2005)

[275] R. Balbinot, A. Fabbri, S. Fagnocchi and R. Parentani, “Hawking radiation from acoustic black holes, short distance and back-reaction effects,” *Riv. Nuovo Cim.* **28**, no.3, 1-55 (2005)

[276] S. Fagnocchi, “Back-reaction effects in acoustic black holes,” *J. Phys. Conf. Ser.* **33**, 445-450 (2006)

[277] R. Schützhold, “Quantum back-reaction problems,” *PoS QG-PH*, 036 (2007)

[278] S. Liberati, G. Tricella and A. Trombettoni, “Back-reaction in canonical analogue black holes,” *Appl. Sciences* **10**, no.24, 8868 (2020)

[279] S. Patrick, H. Goodhew, C. Gooding and S. Weinfurtner, “Backreaction in an analogue black hole experiment,” *Phys. Rev. Lett.* **126**, no.4, 041105 (2021)

[280] G. Jannes and G. E. Volovik, “The cosmological constant: A lesson from the effective gravity of topological Weyl media,” *JETP Lett.* **96**, 215-221 (2012)

[281] S. Finazzi, S. Liberati and L. Sindoni, “Cosmological Constant: A Lesson from Bose-Einstein Condensates,” *Phys. Rev. Lett.* **108**, 071101 (2012)

[282] G. E. Volovik, “The Superfluid Universe,” *Int. Ser. Monogr. Phys.* **156**, 570-618 (2013)

[283] R. Schützhold, “Small cosmological constant from the QCD trace anomaly?,” *Phys. Rev. Lett.* **89**, 081302 (2002)

[284] K. Xu, Y. Liu, D. E. Miller, J. K. Chin, W. Setiawan, and W. Ketterle, “Observation of Strong Quantum Depletion in a Gaseous Bose-Einstein Condensate,” *Phys. Rev. Lett.* **96**, 180405 (2006)

[285] R. Lopes, C. Eigen, N. Navon, D. Clément, R. P. Smith, and Z. Hadzibabic, “Quantum Depletion of a Homogeneous Bose-Einstein Condensate,” *Phys. Rev. Lett.* **119**, 190404 (2017)

[286] R. Schützhold and W. G. Unruh, “Origin of the particles in black hole evaporation,” *Phys. Rev. D* **78**, 041504 (2008)

[287] M. Visser, “Essential and inessential features of Hawking radiation,” *Int. J. Mod. Phys. D* **12**, 649-661 (2003)

[288] R. Schützhold, “Dynamical zero-temperature phase transitions and cosmic inflation/deflation,” *Phys. Rev. Lett.* **95**, 135703 (2005)

[289] N. Ahmadiniaz, M. Geller, J. König, P. Kratzer, A. Lorke, G. Schaller and R. Schützhold, “Quantum Zeno manipulation of quantum dots,” *Phys. Rev. Res.* **4**, no.3, L032045 (2022)

[290] E. Poli, T. Bland, S. J. M. White, M. J. Mark, F. Ferlaino, S. Trabucco and M. Mannarelli, “Glitches in Rotating Supersolids,” *Phys. Rev. Lett.* **131**, no.22, 223401 (2023)